Neodymium isotopic composition of conodonts as a palaeoceanographic proxy in the Variscan oceanic system

Dissertation

zur Erlangung des naturwissenschaftlichen Doktorgrades
der Justus-Liebig-Universität Gießen

vorgelegt von
Jolanta Dopieralska

Institut für Geowissenschaften und Lithosphärenforschung
Justus-Liebig-Universität Gießen (Mai 2003)

Acknowledgments

First and foremost, I am grateful to Prof. Dr. Zdzislaw Belka (Tübingen, Halle) who supervised this thesis and whose inspirational thinking stimulated various aspects of this project. He supported me with advice, constructive discussion, comment and suggestion during the course of this work. I want also to thank him for his invaluable assistance in the field where I profited from his knowledge on the Devonian and Moroccan geology. Most of the stratigraphic data, which are of great importance for this thesis, were provided by him. His time and work invested in this task and finally his conviction about my scientific potential is much appreciated.

Special thanks are to Prof. Dr. Udo Haack (Giessen) who co-promoted this thesis, offered me to use the laboratory facilities for Nd, Sm and Sr analyses, and provided invaluable assistance during my stay in Giessen. His stimulating discussions and constructive critical review significantly improved the manuscript.

Financial support for this study was provided by the Deutsche Forschungsgemeinschaft and is gratefully acknowledged. This is a contribution to the priority programme “SPP 1054 - Evolution of the Earth System during the Palaeozoic ...” funded by the DFG.

Dr. Jens Schneider (Giessen) is gratefully acknowledged for his help and advice on construction of the laboratory equipment and development of analytical procedures for separation and mass spectrometric measurements of Sm and Nd at Giessen. His constructive criticism helped to improve the English of the manuscript. I would like also to thank him for his help in organizing my stay in Giessen.

I thank Prof. Dr. Ernst Hegner (Munich) for introducing me to chemical separation and mass spectrometric measurements of Nd, Sm and Sr.

Dr. Michael Brauns (Giessen) helped to gain the laboratory equipment and provided several conodont samples. Acknowledgements are extended to Janina Schastok (Giessen) who helped with a good grace by every technical problem in the laboratory and outside. Several staff members of the Institute of Geosciences at Giessen have assisted with the technical work. Their help is also appreciated.

I wish to thank Dr. Wouter Heijlen (Leuven) who carried out ICP-MS analysis of conodont samples.

I am indebted to M. Bensaid and M. Dahmani (Ministère de l'Energie et des Mines, Rabat) for the permission to carry out the fieldwork and export the samples. I would like to express my gratitude also to Christine Schubert, Mark Exner, Mirko Heckner and Mike Härtel (all at Halle) who processed all rock samples. Thanks are also to Prof. Dr. Stanislaw Skompski (Warsow), Dr. Blazej Berkowski (Poznan) and Philipp Eisenmann (Halle) for their assistance in the field.

Special thanks are due to my friend Sylwia Krolikowska-Ciaglo (Kiel) for sharing her “isotopic experience”, supporting with advice and practical help in “hard times” or just being there whenever needed.

Finally, I wish to thank my family for their moral support and trust that I will overcome all difficulties.

Contents

Zusammenfassung

Die lateralen und zeitlichen Variationen der Neodym-Isotopie im Meerwasser spiegeln die Dynamik geologischer Prozesse auf der Erdoberfläche. Die Nd-Isotopenzusammensetzung des Meerwassers reflektiert u.a. das Ausmaß der Erosion der exhumierten Kruste und deren Alter auf den umliegenden festländischen Gebieten. Die kontinentale Kruste mit schwach radiogenen Isotopensignaturen (ε_{Nd} zwischen -10 und -30) ist die Hauptquelle des Nd im Meerwasser. Der Nd-Eintrag aus der ozeanischen Kruste (ε_{Nd} von etwa +8) ist dagegen sehr gering, weil sie kaum erodiert wird (nur im Bereich der vulkanischen Inselbögen und ozeanischen Inseln). Die Information über die Isotopenzusammensetzung der Paläo-Ozeane ist in Fossilien, chemischen Sedimenten und authigenen Mineralen archiviert. Im Rahmen dieser Arbeit wurde versucht, anhand der Nd-Isotopie von Conodonten (phosphatische Reste der ältesten marinen Vertebraten, $\leq$ 2 mm groß) unterschiedliche Wassermassen (Aquafazies) im Ozeansystem der Varisziden während der Devon-Zeit zu identifizieren. Das weitere Ziel der Untersuchungen bestand darin, die gewonnen Daten als Hilfe für die Rekostruktion der temporären Zirkulationsmuster sowie die Bewegung der Wassermassen in der zeitlichen Dimension zu benutzen. Außerdem wurde ein Versuch unternommen, auf der Basis der Nd-Isotopie von Conodonten auch Aussagen über die Hebung der Landmassen und das durschnittliche Alter der exhumierten Kruste zu treffen.

Als Untersuchsgebiet wurde ein Meeresbereich ausgewählt, der während des Devons und Karbons zwischen Euramerika und Gondwana existierte. Er stellte eine Verbindung zwischen dem riesigen Panthalassia-Ozean und der Paläotethys dar und bestand aus kleineren ozeanischen Einheiten (Rheischer Ozean, Rhenoherzynischer Ozean, Variszisches Meer) und flankierenden Schelfgebieten. Dieser Meeresbereich wurde während des Devons, als Folge des nördlichen Drifts von Gondwana, immer enger, was letztlich im Laufe des Unterkarbons zu seiner Schließung und zur Bildung des variszischen Orogens führte. Das Probenmaterial für die systematische isotopengeochemische, geochemische, stratigraphische und sedimentologische Untersuchungen wurde hauptsächlich in Marokko (östliches Anti-Atlas, Meseta) und in Südfrankreich (Montagne Noire) gesammelt. Die sedimentolgischen Abfolgen des Frasnes und des Famennes sind dort sehr reich an Conodonten, was eine sehr präzise Datierung und Korrelation ermöglicht hat. Dieses reiche Conodonten-Material wurde detailliert isotopen-geochemisch untersucht, um die elementare und isotopische Systematik des Neodyms und des Samariums in den Conodonten zu entziffern. Weitere Proben kamen aus dem Devon von Polen (Heiligkreuz-Gebirge, Krakauer Paläozoikum, Sudeten), das durch sehr niedrige thermische Überprägung charakterisiert ist. Damit konnte der Einfluss der diagenetischen bzw. epigenetischen Prozesse (z.B. thermische Überprägung) auf die Nd-Isotopie der Conodonten untersucht werden. Während der gesamten Untersuchungen wurden

fast 300 Condonten-Proben gemessen und ausgewertet.

Nd-Systematik der Conodonten

Die phosphatischen Knochen der rezenten Fische zeigen *in vivo* äußerst niedrige Nd-Gehalte (SHAW & WASSERBURG, 1985; ELDERFIELD & PAGETT, 1986). Das Neodym wird erst *post-mortem* eingebaut, so dass fossiles Material sehr hohe Nd-Konzentrationen aufweist (bis 5000 ppm). Aufgrund rezenter Beobachtungen (BERNAT, 1975) wird angenommen, dass die Anreicherung etwa eintausend Jahre dauert und hauptsächlich direkt auf der Sedimentoberfläche (SHAW & WASSERBURG, 1985) erfolgt. Diese Erkenntnisse lassen vermuten, dass ähnliche Anreicherung auch beim fossilen phosphatischen Material (Conodonten) stattgefunden haben müßte.

Die Untersuchungen während dieser Arbeit haben ergeben, dass alle Conodonten innerhalb einer Probe die gleiche Nd-Isotopenzusammensetzung haben, obwohl sie oft recht unterschiedliche Nd-Gehalte aufweisen. Die Conodonten-Kronen zeigen Nd-Konzentrationen von 25 bis 280 ppm, die Conodonten mit den Basen dagegen Konzentrationen von 200 bis 820 ppm. Die Konzentrationsunterschiede in den Kronen sind vor allem auf die unterschiedliche Morphologie der Conodonten zurückzuführen. Sowohl kleine als auch große Exemplare eines bestimmten Typs sind durch ähnliche Nd-Konzentrationen charakterisiert. Dies zeigt, dass nicht die absolute Größe der Conodonten eine entscheidende Rolle beim Nd-Einbau spielte sondern das Verhältnis zwischen ihrer Oberfläche und Masse. Einen geringen Einfluss hatte auch die Dauer des Kontaktes mit dem Meereswasser, bevor die Sedimentbedeckung die Aufnahme von Nd aus dem Meerwasser beendete. Entsprechend weisen Conodonten aus den Sedimenten mit hohen Sedimentationsraten generell niedrigere Nd-Gehalte als die des gleichen Typs aus den kondensierten Profilen. Diese Tatsache beweist, dass der Einbau von Nd in das Phosphat von Conodonten während der Phase des direkten Kontaktes mit dem Meerwasser erfolge. Nach der Einbettung in die Sedimente wurde offensichtlich kein zusätzliches Neodym in die Conodonten eingebaut.

Die Abhängigkeit der Nd-Konzentrationen in Conodonten von deren Form stellt einen großen praktischen Vorteil für die Isotopen-Analytik dar. Die Isotopenverdünnungsmethode, die zur Messung der Nd-Isotopenkonzentrationen oft angewandt wird, kann sehr genau sein, erfordert aber vorab eine ungefähre Kenntnis der Nd-Konzentration in der Probe. Damit kann die optimale Menge des Spikes, der mit der Probe gemischt wird, abgeschätzt werden. Bei einer zu großen oder zu kleinen Menge des Spikes ist die Messung ungenau und muss wiederholt werden. Im Falle der Conodonten ist es jetzt sehr leicht, die ungefähre Nd-Konzentration anhand ihrer Morphologie abzuschätzen. Dabei sind keine besonderen taxonomischen Kenntnisse der Conodonten notwendig.

An ausgewählten Proben wurde auch die Verteilung der SEE analysiert. Trotz der großen Unterschiede in den absoluten Konzentrationen zeigen alle Proben ein sehr ähnliches SEE-Muster,

das durch eine Anreicherung der mittleren Seltenen Erden charakterisiert ist. Dieses Muster wird in der Literatur als “bell-shaped” bezeichnet und als typisch für die paläozoischen biogenen Phosphate betrachtet.

Das Sm-Nd-System der Conodonten scheint weitgehend unempfindlich für spätere, diagenetische Einflüsse zu sein. Bei der Auswertung der untersuchten Conodonten-Proben, wurde keine Korrelation zwischen den Nd-Isotopensignaturen und der thermischen Überprägung der Conodonten festgestellt. Als deren indirektes Maß gelten die CAI-Werte (Farbveränderungswerte) die beim untersuchten Material zwischen 1 und 4 schwankten.

Conodonten im Vergleich zu anderen biogenen Phosphaten

In den marinen Ablagerungen des Devons kommen neben Conodonten auch andere Fossilien vor, die aus phosphatischem Material aufgebaut sind. Das sind vor allem Knochen von Placodermen (Panzerfische) und Zähne von Haifischen. Anders als die Conodonten werden diese Fossilien relativ selten gefunden und eignen sich deswegen kaum für systematische geochemische Studien. Außerdem macht die chemische Zusammensetzung des Knochenmaterials von Fischen, d.h. der höhere Anteil an Kalziumkarbonat als beim Conodonten-Fluorapatit, diese Fossilien anfälliger für chemische und strukturelle Veränderungen während der Diagenese. Das Knochenmaterial wird allerdings im Mesozoikum und Känozoikum oft zur Ermittlung der Zusammensetzung des Meerwassers verwendet, da Conodonten-Elemente nicht zur Verfügung stehen (die Conodonten-Tiere sind am Ende der Trias-Zeit ausgestorben). Da in einigen Gesteinsproben neben Conodonten auch Haifischzähne und Placodermenreste gefunden wurden, konnte getestet werden, ob die Nd-Isotopenzusammensetzung und die Sm/Nd Fraktionierung in diesen verschiedenen biogenen Apatiten innerhalb einer Probe homogen sind. Die Analysen ergaben in der ersten Linie, dass die Haifischzähne und die Plakodermenreste Konzentrationen aufweisen, die um eine Größenordnung höher sind als die der Conodonten. Außerdem konnten auch Unterschiede in den Isotopensignturen und Sm/Nd-Verhältnissen festgestellt werden, die zum Teil infolge der thermischen Überprägung der Sedimente entstanden sind. In dem relativ wenig erhitzten Probenmaterial (CAI-Werte 1 bis 3) sind sowohl die ε_{Nd}-Werte der Haifischzähne als auch der Placodermenreste systematisch weniger radiogen als die der Conodonten. In den Proben mit hohen CAI-Werten von 4 (Proben aus dem östlichen Anti-Atlas) sind die Isotopensignaturen der anderen biogenen Apatite deutlich radiogener als die der Conodonten. Ähnlich gestört ist auch das Sm/Nd-Verhältnis; erhitztes Knochenmaterial zeigt niedrigere Werte als die der Conodonten. In den Proben mit geringer thermischer Überprägung sind die Sm/Nd-Verhältnisse in allen biogenen Apatiten identisch. Parallele Sr-Isotopenuntersuchungen der gleichen Proben ergaben, dass nur Conodonten-Material Sr-Werte aufweist, die den ozeanischen Sr-Isotopenverhältnissen entsprechen. Demzufolge erscheinen die Conodonten verglichen mit den Haifischzähnen und den

Placodermenresten als besser für die Untersuchungen der Zusammensetzung des Meerwassers geeignet. Die Haifischzähne und Placodermenreste können allerdings für paläozeanographische Untersuchungen dort eingesetzt werden, wo die Conodonten fehlen, wie zum Beispiel in den Flachwasser-Sedimenten.

Nd-Isotopie der Conodonten: lokale Variationen

Die meisten Untersuchungen in Rahmen dieser Arbeit wurden im östlichen Anti-Atlas durchgeführt. Bei dem Versuch die Zirkulationsmuster des Meerwassers zu rekonstruieren, wurde diese Region als Testgebiet betrachtet, da dort die devonischen Ablagerungen großflächig aufgeschlossen sind und ein breites Spektrum von Sedimentstrukturen, darunter auch verschiedene Strömungsmarker enthalten. Es wurden Proben aus zwei Zeitscheiben analysiert, nämlich aus der Basis und aus dem Top der Kellwasser-Fazies. Anders als in vielen europäischen Profilen bildet die Kellwasser-Fazies im südlichen Marokko ein mehrere Meter mächtiges Intervall.

Beim Einsetzen der Kellwasser-Fazies (während der Conodonten-Zone 11) zeigen sich große Unterschiede in den ε_{Nd}-Werten zwischen –6 und –11. Die niedrigsten ε_{Nd}-Werte resultierten vom starken terrigenen Eintrag. Dieser erfolgte sowohl aus südlicher Richtung, aus dem Westafrikanischen Kraton, und aus dem Westen, aus dem präkambrischen Grundgebirge des Jebel Ougnate. Die mehr radiogenen Nd-Signaturen des Meerwassers auf der Mader Plattform deuten auf eine Verbindung mit dem Rheischen Ozean. Eine Verbindung zum offenen Meer existierte auch in die nördliche Richtung. Die ε_{Nd}-Gradienten stimmen in der Regel sehr gut mit den Strömungsmarken (hier die Orientierung der orthoconen Nautiloiden) überein. Ausgehend von den lateralen Trends der ε_{Nd}-Werte wurde ein Zirkulationsmuster entworfen. Dieses zeigt eine generelle Meerwasserzirkulation von Südwesten nach Osten. Sie änderte sich noch während des Frasnes, gleich nach der Regression während der Zone 12. Die Gradienten in den Nd-Isotopensignaturen wurden deutlich geringer, was wahrscheinlich auf einen Meeresspiegelhochstand zurückzuführen ist, der höchstwahrscheinlich eine bessere Zirkulation des Meerwassers und Homogenisierung der Nd-Isotopenzusammensetzung verursachte. Die Hauptströmung kam damals aus östlicher Richtung und kehrte teilweise im Bereich der zentralen Tafilalt Plattform zurück. Dieses komplexe Zirkulationssystem herrschte bis zum späteren Famenne. Charakteristisch für diese Phase ist relativ schwacher terrigener Eintrag aus dem Westafrikanischen Kraton.

Nd-Isotopie der Conodonten: regionale Variationen

Die regionalen Unterschiede in der geochemischen Zusammensetzung des Meerwassers im variszischen Raum während des Oberdevons werden sichtbar, wenn man die ε_{Nd}-Werte und die Sm/Nd-Verhältnisse der Conodonten gegeneinander aufträgt. Besonders deutlich sind die

unterschiedlichen Sm/Nd-Verhältnisse der Wassermassen auf dem baltischen Schelf von Euramerika (Südpolen) im Vergleich zu den Wassermassen auf dem marokkanischen Schelf von Gondwana (Anti-Atlas). Das Meerwasser in Südpolen war durch niedrige Sm/Nd-Verhältnisse (0,16 bis 0,29) charakterisiert, wie sie auch heute typisch für ozeanische Bereiche sind. Das deutet darauf hin, dass das Wasser am Rande des baltischen Schelfs von Euramerika stark mit ozeanischem Wasser vermischt war. Dabei spielte der Nd-Eintrag aus dem fast 300 km weit entfernten Landgebiet (Weißrussisches Land) offensichtlich nur eine untergeordnete Rolle. Im Gegensatz dazu war das Meerwasser auf dem marokkanischen Schelf von Gondwana stark durch den terrestrischen Eintrag des Nd geprägt. Die Sm/Nd-Verhältnisse waren hoch, zwischen 0,21 und 0,85. Diese Spanne ist wesentlich breiter als die auf den rezenten Schelfgebieten beobachteten Werte, die kleiner als 0,44 sind. Es ist hier allerdings zu betonen, dass der Datensatz aus den rezenten Schelfgebieten bisher sehr klein ist und nur aus einer Studie im südost-asiatischen Raum stammt (AMAKAWA et al., 2000). Für die hohen Sm/Nd-Verhältnisse in östlichem Anti-Atlas können Fraktionierungsprozesse, ähnlich denen in rezenten Estuarien verantwortlich sein. Während der Mischung des Flusswassers mit dem Meerwasser werden die gelösten SEE gefällt, was in der Regel mehr die leichten, an die Kolloide gebunden, SEE betrifft. Paläoozeanographisch noch signifikanter als die regionalen Unterschiede in der SEE-Fraktionierung auf den spätdevonischen Schelfgebieten sind die Variationen in der Nd-Isotopenzusammensetzung der Conodonten. Die ε_{Nd}-Werte schwanken zwischen -2 und -12 und belegen Anwesenheit von zwei unterschiedlichen Aquafazies. Eine hatte ein stark radiogenes Wasser, mit ε_{Nd}-Werten von -2 bis -5, und repräsentierte das ozeanische Wasser, das sporadisch, während der Episoden des Meeresspiegelanstiegs die Schelfgebiete teilweise überflutete. Die Schelf-Aquafazies war dagegen durch ε_{Nd}-Werte zwischen etwa -6 und -12 gekennzeichnet. Die Daten aus der Meseta belegen außerdem, dass der Wasseraustausch zwischen den beiden Aquafazies sehr eingeschränkt war. Beide zeigen nicht nur unterschiedliche Nd-Isotopenentwicklung sondern auch eine unterschiedliche Kohlenstoff-Isotopie und SEE-Fraktionierung. Die Entkopplung der geochemischen Evolution zwischen den beiden Wasserreservoiren hat sehr wichtige Konsequenzen für die Interpretation der Kohlenstoffisotopendaten. In einem globalen ozeanischen System mit lokal individueller geochemischen Entwicklung des Meerwassers kann nämlich schnell eine Anomalie in der C-Isotopie entstehen, wenn sich die Meerwasserzirkulation ändert und zum Vermischen von zwei Aquafazies führt.

Die stark radiogenen Nd-Isotopensignaturen der ozeanischen Aquafazies (ε_{Nd}-Werte bis -2,6) ähneln sehr stark den Signaturen des rezenten Pazifiks, der im Durchschnitt ε_{Nd}-Werte von -3,5 zeigt (BERTRAM & ELDERFIELD, 1993). Das Wasser im Atlantischen und Indischen Ozean ist dagegen mehr kontinental geprägt und daher weniger radiogen, mit durchschnittlichen ε_{Nd}-Werten von etwa -12 und -8. Die isotopengeochemische Ähnlichkeit des Wassers im Pazifik und der

ozeanischen Aquafazies des Variszikums zeugt von ähnlichem geotektonischen Regime der beiden ozeanischen Systeme. Wie heute im Pazifik kamen auch im variszischen Raum während des Oberdevons zahlreiche Subduktionszonen und vulkanischen Inselbögen vor.

Meeresspiegelschwankungen

Die Analyse der temporären Variationen der Nd-Isotopensignaturen in mehreren Profilen Marokkos und Frankreichs hat gezeigt, dass die stärksten Fluktuationen weniger durch lokale und viel mehr durch globale Faktoren verursacht wurden. Besonders deutlich wird dies im östlichen Anti-Atlas, wo die stärksten Schwankungen der ε_{Nd}-Werte perfekt mit dem Auftreten von stratigraphischen Lücken korrelieren. Da diese Lücken infolge der Meeresregressionen entstanden sind, werden eustatische Meeresspiegelschwankungen als Hauptfaktor angesehen, der die temporären Variationen der Nd-Signaturen des Meerwassers am stärksten beeinflusste. Diese Tatsache ermöglicht die temporären Nd-Isotopentrends für die Rekonstruktion der Meeresspiegelschwankungen zu benutzen. Diese Methode stellt einen Durchbruch in der paläoozeanographischen Forschung im Paläozoikum dar. Sie hat den großen Vorteil, dass die Meeresspiegelschwankungen auch in lithologisch monotonen Folgen sehr gut lesbar sein können. Die Daten zeigen außerdem, dass die Nd-Isotopie viel präziser als die Lithologie die eustatischen Meeresspiegelschwankungen nachzeichnet. Der Einfluss von lokalen Faktoren kann leicht durch den Vergleich von mehreren lokalen Nd-Isotopenkurven eliminiert werden.

Auf der Basis der Nd-Daten aus Marokko und Frankreich wurde eine, auf Isotopen basierte Kurve der eustatischen Meeresspiegelschwankungen für das Oberfrasne und Unterfamenne erstellt. Diese wurde mit der klassischen, auf der Basis von faziellen Daten konstruierten Meeresspiegelschwankungskurve verglichen (JOHNSON et al., 1985; JOHNSON & SANDBERG, 1988; SANDBERG et al., 1992). Die neue Kurve weist eine relativ große Übereinstimmung mit der bisherigen Schema auf. Der größte Unterschied besteht darin, dass die Isotopendaten zwei markante Regressionsereignisse während des späteren Frasnes dokumentieren. Während dieser Phasen sind die beiden Kellwasser-Einheiten, der Untere Kellwasserkalk und der Obere Kellwasserkalk, in Europa und in der marokkanischen Meseta abgelagert worden. Diese wurden bisher fast immer als Transgressionen aufgefasst. Die Nd-Untersuchungen haben gezeigt, dass das Gegenteil richtig ist. Als Folge der beiden Regressionen kommen im östlichen Anti-Atlas signifikante stratigraphische Lücken vor. Eine weitere wichtige Beobachtung im östlichen Anti-Atlas ist, dass dort kein nennenswerter Meerwasser-Austausch am Anfang der Kellwasserkrise während der Zone 11 aufgetreten ist. Die Eutrophierung wurde also nicht durch das Eindringen von kaltem, nährstoffreichen Wasser aus dem Ozean verursacht. Das ozeanische Wasser hat den marokkanischen Schelf erst während der *semichatovae*-Transgression überflutet und führte in Beckenbereichen zur Bildung von hellen, oxidierten Karbonaten.

1 Introduction

The world ocean constitutes a complex system that mirrors the dynamics of the Earth's surface. This is because geochemical properties of seawater depend on a variety of endogenic and exogenic factors, such as variations in the lithologic composition of the crust exposed to weathering, configuration and topographic relief of continents, extent of continental inundation by epeiric seas, extent of volcanic activity, variation in climate, changes in biological activity and carbon dioxide level. In addition, there are interactions between the ocean and the seafloor, the ocean and the biosphere, and the ocean and the atmosphere. During Earth's history, processes involved in the evolution of the Earth's surface varied and thus changed the composition of the oceans. In turn, the chemical composition of seawater influenced the chemistry of marine sedimentary precipitates and controlled processes of biomineralisation (e.g. SANDBERG, 1983; VEIZER, 1985; MACKENZIE & AGEGIAN, 1989). Although the evolutionary changes in seawater chemistry were presumably rather small during the last 600 million years (e.g. KASTING, 1989, KUMP, 1989; MORSE & MACKENZIE, 1990), geochemical properties of seawater in the ancient oceans form a fundamental basis for understanding the geological history of the Earth.

Geochemical properties of seawater are recorded in sediments and biogenic skeletal precipitates. But original seawater signatures are preserved only in marine phases that precipitated in equilibrium with seawater. One of the primary difficulties of using isotopes as a proxy for past seawater composition is the identification of a common, datable, marine phase that incorporates significant concentrations of a given element and remains chemically inert during burial and diagenesis. Biogenic phosphates meet these requirements better than any other geological material and are therefore regarded as very suitable for palaeoceanographic studies (e.g. WRIGHT *et al.*, 1987; GRANDJEAN *et al.*, 1987; SCHMITZ *et al.*, 1991; MORAD & FELITSYN, 2001). In the Palaeozoic sediments, conodont elements are particularly useful because they are ubiquitous, biostratigraphically important and their apatite exhibits a high thermal and chemical stability (e.g. WRIGHT *et al.*, 1984; WRIGHT, 1990; EBNETH *et al.*, 1997; FELITSYN *et al.*, 1998; HOLMDEN *et al.*, 1998; JOACHIMSKI & BUGGISCH, 2002).

Numerous studies have shown that the Nd isotopic composition of modern seawater varies both within and between different parts of the oceans (e.g. PIEPGRAS &WASSERBURG, 1980; BERTRAM & ELDERFIELD, 1993). This led to the idea that Nd isotope signals recorded in marine precipitates can be used as a tool for distinguishing between different water masses. Moreover, because the main input of Nd to the ocean is from continental weathering through riverine transport, the Nd isotopic signatures of ancient seawater are useful tracers of changes in continental runoff and seawater circulation (e.g. PIEPGRAS *et al.*, 1979; KETO & JACOBSEN, 1987, 1988; STILLE *et al.*, 1996; VANCE & BURTON, 1999).

Most of the Nd data obtained from conodonts are records of REE distribution patterns, or simply, measurements of Nd concentrations (e.g. WRIGHT *et al.*, 1987; GRANDJEAN & ALBARÈDE, 1989; GRANDJEAN *et al.*, 1993; GIRARD & ALBARÈDE, 1996; BRUHN *et al.*, 1997; HAUNOLD *et al.*, 1999; ARMSTRONG *et al.*, 2001). Nd isotopic signatures of conodonts were published in several papers but, in fact, only very few samples were analysed (WRIGHT *et al.*, 1984; SHAW & WASSERBURG, 1985; KETO & JACOBSEN, 1987, 1988; BERTRAM *et al.*, 1992; HOLMDEN *et al.*, 1996, 1998; FELITSYN *et al.*, 1998). The published Devonian data set, for instance, comprises only six Nd isotope ratios.

The present study deals with Nd isotopic data obtained from a large number (more than 300) of Devonian conodont samples. The primary purpose of this research was to recognize lateral and temporal variations in the Nd isotopic composition of seawater in the western part of the Variscan Sea. Upper Devonian deposits exposed in Morocco (eastern Anti-Atlas, Meseta) and in southern France (Montagne Noire) were selected for a detailed investigation (Fig. 1). The study focuses primarily on the late Frasnian and the early Famennian successions, known to bear an extremely rich conodont fauna that permits a high-resolution stratigraphic correlation and dating. Late Devonian time has been targeted because of its crucial importance for the evolution of the biosphere. Several global events and turning points occurred during this time, such as development of organic-rich facies (Kellwasser), reef decline, significant mass extinction, origin of earliest forests and onset of dramatic climatic fluctuations (glaciations). The palaeogeography of the Late

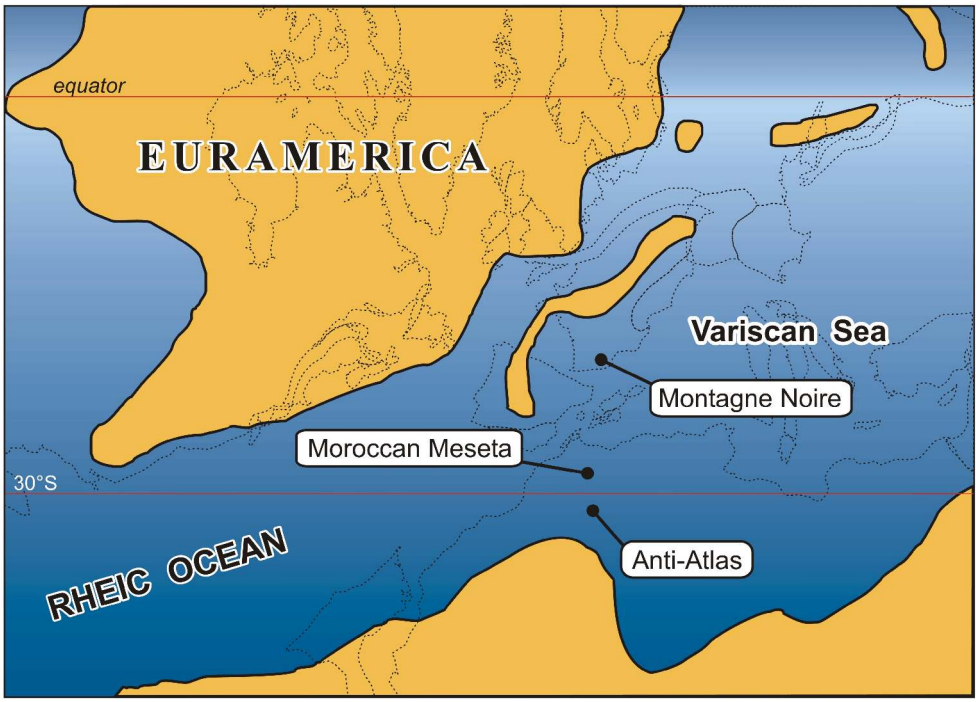

Fig. 1. Palaeogeographic location of the studied areas during the Late Devonian. The palaeogeographic reconstruction is taken from Atlas (Version 3.2), an interactive software developed for the PC by Cambridge Paleomap Services Limited.

Devonian is still a matter of debate. It is likely that Gondwana approached Euramerica during this time and thus the Variscan oceanic system has substantially been modified. In order to provide additional constraints for the Devonian palaeogeography this treatise includes an attempt to reconstruct seawater circulation on the Gondwana shelf. Finally, the study concerns also the Nd elemental and isotopic systematics in Devonian conodonts and compares it to that of fish remains.

This work is a contribution to the priority programme "SPP 1054 - *Evolution des Systems Erde während des jüngeren Paläozoikms im Spiegel der Sediment-Geochemie*" funded by the Deutsche Forschungsgemeinschaft (DFG) and it constitutes part of the project *Neodym-Isotopie von Conodonten als paläoozeanographische Proxies im Ozeansystem der Varisciden* (grants Be 1296/8-1, Ha 1207/26-1).

2 Conodonts and their applications

Conodonts are small (≤2 mm) skeletal remains of an extinct group of nektonic marine animals. Being a long time enigmatic, conodont animals are now regarded as the earliest jawless vertebrates (e.g. SWEET, 1988; ALDRIDGE *et al.*, 1993; DONOGHUE *et al.*, 2000). Conodont animals had slender, eel-like and most frequently only 40 mm long bodies. Their only hard skeletal parts were conodont elements assemblaged into a feeding apparatus, which was positioned in the head region of the animal.

The apparatuses included elements of several different morphologies but the composition and architecture of apparatuses is known for a few conodont species only. Conodont elements are phosphatic and constructed from two distinct parts, the upper crown and the lower basal filling. Both are mostly internally laminated, but laminae of the basal tissue are thicker and less densely packed than those of the crown. In addition, the basal filling contains significantly more organic matter than the crowns and consequently, it is more susceptible to postdepositional alteration. This is why in the majority of conodont samples the less resistant basal bodies are lacking. The conodont crowns occur in a wide variety of shapes subdivided into three major groups of single cones, ramiforms, and platform elements. The lamellar crown tissue is composed of crystallites that typically range in length from 1-30 µm and can display an individual arrangement within different laminae. The structure of basal bodies, however, is highly variable including both lamellar, spherulitic and tubular patterns.

According to PIETZNER *et al.* (1968), the mineral phase of conodonts [$Ca_5Na_{0.14}(PO_4)_{3.01}(CO_3)_{0.16}\ F_{0.73}(H_2O)_{0.85}$] approximates the mineral francolite. BELKA (1993), however, noticed that the crystallographic properties of the conodont phosphate indicate that the conodont crowns are essentially fluorapatit rather than francolite. Due to its low CO_2 content and

high unit cell *a*-value of 9.37 Å the conodont fluorapatite exhibits a very high thermal and chemical stability under the conditions prevailing at the earth's surface. The conodont fluorapatite represents a stable mineral phase already during the growth of conodont elements, almost immune to oxidation, and thus, not susceptible to weathering (BELKA, 1993).

Conodont elements occur frequently in marine sedimentary rocks of Late Cambrian through Triassic age. They have several important applications in geological studies. Firstly, their rapid evolution combined with worldwide distribution makes these microfossils a very effective stratigraphic tool, providing high-resolution biostratigraphic data. Secondly, conodonts are widely applied in the analysis of the thermal history of sedimentary sequences. This method is based on the irreversible change in conodont colour in response to heating (EPSTEIN *et al.*, 1977). The conodont Colour Alteration Index (CAI) has been calibrated with temperature ranges and is complementary to other organic maturity indices. Thirdly, conodont species frequently seem to show an affinity for particular environments and display limits in their ecological occurrence. Therefore, conodont records constitute useful biofacies indices that permit identification of various sedimentary environments (e.g. SWEET, 1988). Because conodonts were remarkably cosmopolitan in their paleogeographic distribution and displayed only a distinct provincial occurrence during the Ordovician and the Triassic, they generally play a subordinate role in palaeogeographical reconstructions (e.g. SWEET & BERGSTRÖM, 1974; CHARPENTIER, 1984). Finally, conodont elements received much attention during the last two decades because they contain trace elements reflecting the chemical and isotopic composition of seawater in which the conodont elements were deposited (for review, see WRIGHT, 1990). More than forty trace elements have been recognized in the conodont tissue. Numerous stable isotopic studies revealed that in many cases isotopic ratios of strontium, uranium, neodymium, samarium, and oxygen in conodont fluorapatite may represent the original imprint of seawater (e.g. KOVACH & ZARTMAN, 1981; WRIGHT & HOLSER, 1981; LUZ *et al.*, 1984; BERTRAM *et al.*, 1992; GRANDJEAN-LECUYER *et al.*, 1993; EBNETH *et al.*, 1997; VEIZER *et al.*, 1997; HOLMDEN *et al.*, 1998; WENZEL *et al.*, 2000; JOACHIMSKI & BUGGISCH, 2002). Recently, BRAUNS & HAACK (2001) tested conodonts for the first time as a potential tracer for the osmium isotopic composition of ancient seawater.

3 Marine geochemistry of neodymium and samarium

Neodymium and samarium belong to the group of rare earth elements (REE). Both have seven naturally occurring isotopes. Three Sm isotopes are radioactive, ^{147}Sm, ^{148}Sm, and ^{149}Sm, but the latter two, because of their extremely long half-lives (~ 10^{16} yr), produce non-measurable variations in their daughter isotopes, ^{144}Nd and ^{145}Nd. The ^{147}Sm decays to the stable isotope ^{143}Nd

with a half-live of 1.06×10^{11} years, which is also relatively long but makes these isotopes useful for dating, especially in the Precambrian. Both Nd and Sm are light rare earths and their position within the group is that the REE abundance pattern is usually accurately reflected by the Sm/Nd ratio. Low Sm/Nd ratios are characteristic of a light REE-enriched pattern, whereas high Sm/Nd ratios reflect a depletion of light REEs. Thus, the Sm-Nd system provides useful information on the overall REE chemistry and therefore, it is preferentially investigated compared to other REEs. The characteristics and applications of the Sm-Nd system to geology, geochemistry and cosmochemistry have comprehensively been summarized by DEPAOLO (1988).

The Sm/Nd ratio varies in the terrestrial materials due to the fractionation of REE between the mantle and the crust during differentiation processes. Therefore, the Nd isotopic composition of rocks (their $^{143}Nd/^{144}Nd$ ratio) depends on their ages and their initial $^{143}Nd/^{144}Nd$ and $^{147}Sm/^{144}Nd$ ratios. Because the radioactive parent ^{147}Sm is concentrated in the mantle and depleted in the continental crust, ancient continental crust shows the lowest $^{143}Nd/^{144}Nd$ ratios, whereas rocks recently extracted from the mantle display high $^{143}Nd/^{144}Nd$ ratios. Nd isotope ratios are commonly expressed by the parameter $\varepsilon_{Nd(t)}$, which is defined as the relative deviation from a chondritic $^{143}Nd/^{144}Nd$ ratio at a given time *t*:

$$\varepsilon Nd\,(t) = \left[\frac{(^{143}Nd/^{144}Nd)_{sample}(t)}{(^{143}Nd/^{144}Nd)_{CHUR}(t)} - 1 \right] x\,10^4$$

The continental crust is characterized by enrichment of light REE and hence low Sm/Nd ratios, and negative ε_{Nd} values (Fig. 2) ranging from -10 to -30 on average (DEPAOLO, 1988). However, volcanic rocks occurring within active continental margins, as those in the Andes and in California (Fig. 3), show much higher ε_{Nd} values from -13 to + 6 (e.g. JAMES, 1982; FARMER & DEPAOLO, 1984). In contrast to the continental settings, rocks of the oceanic crust, which are derived from the depleted upper mantle, generally yield high Sm/Nd ratios and positive ε_{Nd} values (Fig. 2). The present-day MORB displays a uniform ε_{Nd} value of +10 and ε_{Nd} values for Phanerozoic ophiolite complexes are about 2 units lower, usually +8 (DEPAOLO, 1988). The data from oceanic volcanic arcs lie within a small range from about +6.5 to +10, with ε_{Nd} value of +8 on average (e.g. DEPAOLO & WASSERBURG, 1977; WHITE & PATCHETT, 1984; KAY *et al.*, 1986).

Modern seawater shows a wide range of ε_{Nd} values from -18 to +3 (e.g. PIEPGRAS *et al.*, 1979; SHAW & WASSERBURG, 1985; BERTRAM & ELDERFIELD, 1993) but particular oceans have a distinct range in ε_{Nd}. In addition, there is a difference between surface and deep waters; the former is predominantly more radiogenic (Fig. 4). The Atlantic Ocean has the most negative ε_{Nd}

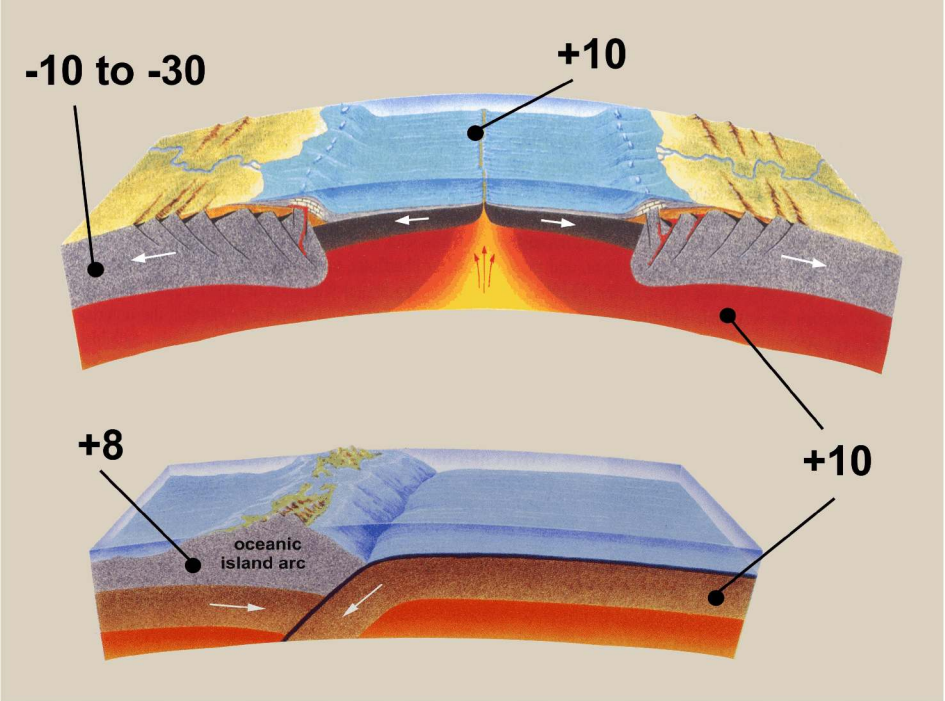

Fig. 2. Scheme of neodymium isotopic composition of the earth crust and upper mantle. Numbers are typical ε_{Nd} values in the indicated tectonic settings (data from DePaolo, 1988).

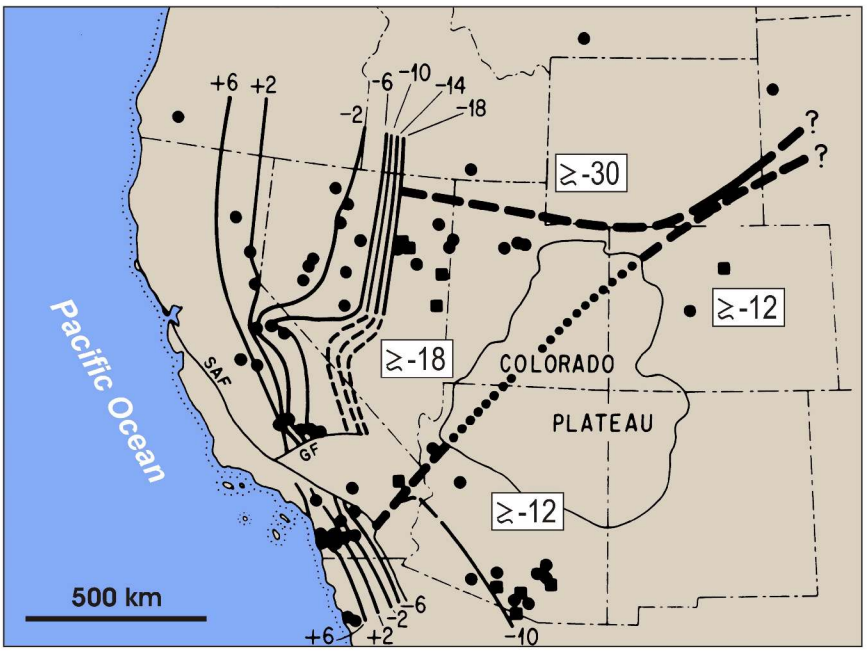

Fig. 3. Map of the southwestern US showing the ε_{Nd} values of granitoid rocks. Note the trend to more radiogenic ε_{Nd} values toward the continental margin and the relative consistency of the Nd isotopic composition of basement rocks over large geographic areas (from DePaolo, 1988).

values (average ε_{Nd} = -12.1), whereas the Pacific Ocean shows the most radiogenic signatures (average ε_{Nd} = -3.5). The Indian Ocean exhibits a relatively small range of ε_{Nd} values that are intermediate (average ε_{Nd} = -8.3) between those of the Pacific and Atlantic oceans. The range of Nd isotopic signatures of modern seawater suggests that the dominant source for Nd is continental (e.g. ELDERFIELD & GREAVES, 1982; GOLDSTEIN & JACOBSEN, 1988a; ELDERFIELD *et al.*, 1990; JEANDEL *et al.*, 1995). In fact, only continental crust and volcanic island arcs constitute sources of Nd that is supplied to the seawater in the dissolved load of rivers. Because of the relative small area occupied by island arcs, the Nd isotopic composition of seawater is controlled by the weathering flux of Nd from surrounding continents. Unlike the Sr system, the contribution from hydrothermal fluids within the mid ocean ridges appears to be negligible (e.g. PIEPGRAS & WASSERBURG, 1985; BERTRAM & ELDERFIELD, 1993). The aeolian sources are also relatively unimportant (JONES *et al.*, 1994).

The low ε_{Nd} values in the Atlantic Ocean are because rivers entering this ocean bear a strong imprint of Nd from the old continental crust. In addition, a contribution from volcanic arcs is insignificant. In fact, there is only one such system in the Caribbean. The Pacific waters, although still strongly dominated by Nd input from the continental crust, contain more radiogenic components from the abundant island arc systems, oceanic islands and active continental margins. The ε_{Nd} values reported for recent oceans are based mainly on measurements of deep water (> few hundred metres) from broadly dispersed locations (PIEPGRAS & WASSERBURG, 1980; PIEPGRAS & WASSERBURG, 1987, BERTRAM & ELDERFIELD, 1993; JEANDEL, 1993). Few studies focussed on surface

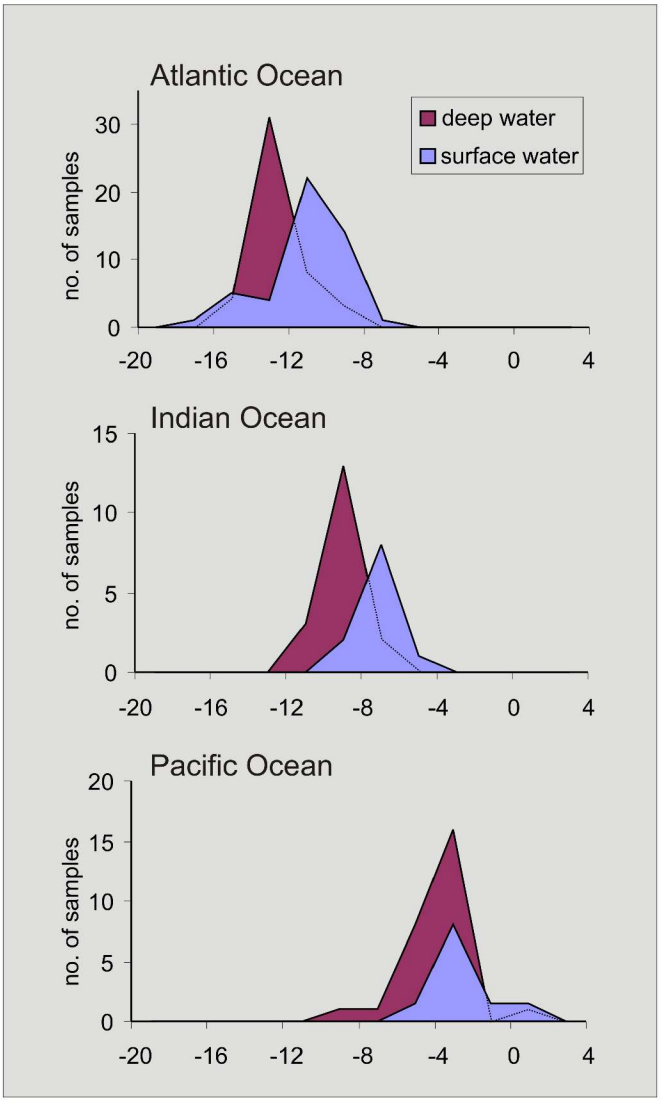

Fig. 4. Histograms of neodymium isotopic compositions of surface (< 1 km) and deep waters (> 1 km) in the modern oceans (modified from Bertram & Elderfield, 1993).

waters and smaller areas with a net of sample sites sufficiently dense to recognize local variations in the isotopic composition of Nd in seawater. AMAKAWA *et al.* (2000) presented Nd isotopic data for the eastern part of the Indian Ocean and seas between southeastern Asia and Australia (Fig. 5). In these areas, ε_{Nd} values range from -1.3 to -11.6 and their distribution corresponds well with that of local Nd sources. The high values of -1.3 and -1.5 from locations close to the Philippines and the Indonesian Archipelago suggest that Nd is supplied from these young oceanic island arcs. Moreover, the relatively high Nd concentrations compared with those of the North Pacific waters point to Nd contribution from local sources. The high Nd concentrations with non-radiogenic ε_{Nd} values of –11.2 and -11.4, measured in samples of the Bay of Bengal and Andaman Sea indicate that Nd is supplied from the Asian continent by the Ganges-Brahmaputra river system.

The remarkable variation of the Nd isotopic composition in modern seawater provides crucial evidence for an apparently short oceanic residence time of neodymium. Several authors proposed various estimates for this value between a few hundreds and ~10^3 years (ELDERFIELD

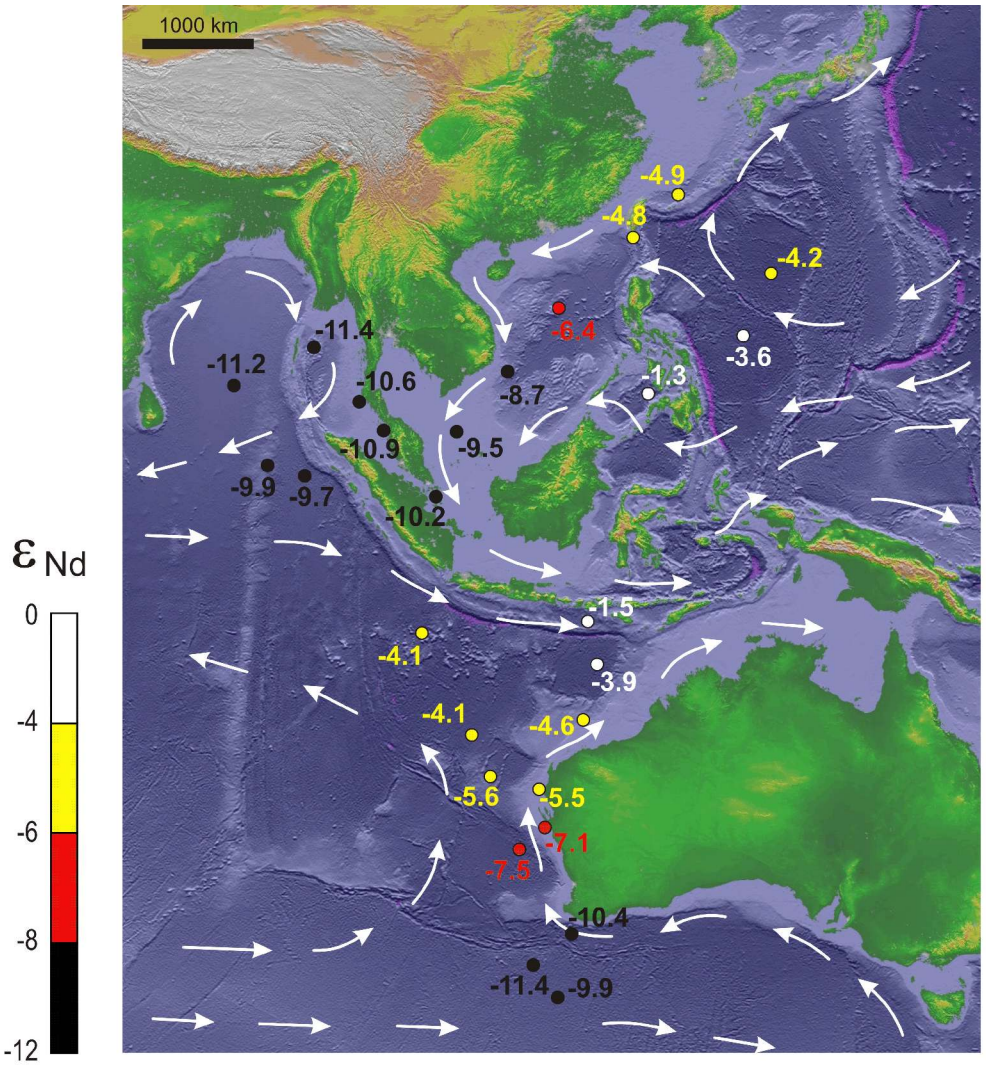

Fig. 5. Distribution of ε_{Nd} values in surface waters of the eastern Indian Ocean and adjacent seas (data from Amakawa et al., 2000).

& GREAVES, 1982; PIEPGRAS & WASSERBURG, 1985; JEANDEL *et al.*, 1995; TACHIKAWA *et al.*, 1999; ALIBO & NOZAKI, 1999). The absolute value cannot be precisely defined, but the variations in Nd isotopic composition of seawater indicate that the residence time of Nd must by shorter than the time required to mix the oceans, which is about 1-2 x 10^3. However, the Nd residence time is sufficiently long that deep water masses, as for example the North Atlantic Deep Water, can retain their isotopic identity over considerable distances (PIEPGRAS & WASSERBURG, 1987). In such cases, the neodymium signatures do not reflect local or even regional fluvial inputs, but rather fluvial inputs to the source areas of deep water masses.

The short oceanic residence time and the lateral variations in the Nd isotopic composition of seawater are prime advantages of the Sm-Nd system that plays an important role in defining the water masses and tracing the seawater circulation. Moreover, several studies showed that the Nd isotopic signatures of modern seawater are accurately recorded in marine precipitates (ferromanganese nodules, sedimentary phosphates) and in biogenic apatites and carbonates (e.g. ELDERFIELD *et al.*, 1981; GOLDSTEIN & O'NIONS, 1981; SHAW & WASSERBURG, 1985; ALBARÈDE & GOLDSTEIN, 1992). This allows to use the neodymium isotopes as a palaeoceanographic tool for reconstructing of temporal and lateral variations of seawater in ancient oceans. The record of the Nd isotopic composition of seawater over time can also approximate the history of Nd isotopic variations within exposed crust on surrounding continents and delineate the possible provenance pathways. There are already several studies documenting the Nd isotopic composition of seawater and oceanic palaeocirculation patterns during the past 200 Ma (e.g. GRANDJEAN *et al.*, 1988; STILLE, 1992; STILLE *et al.*, 1996), however, reports from the Palaeozoic are still rare (e.g. HOLMDEN *et al.*, 1996, 1998; FANTON *et al.*, 2002).

4 Neodymium in biogenic apatites

Fossil biogenic apatites, such as conodonts, fish bones and shark teeth, are characterized by a very high content of rare earth elements (~10^2-10^3 ppm) which appear to be derived from seawater. In contrast, apatites of marine vertebrates yield *in vivo* extremely low concentrations, only a few parts per billion of Nd, for example (SHAW & WASSERBURG, 1985; ELDERFIELD & PAGETT, 1986). Analyses of modern fish debris taken from bottom sediments reveal that the bulk of neodymium is acquired *post mortem*, very quickly (~1000 y), at or very near the seawater-sediment interface (BERNAT, 1975; SHAW & WASSERBURG, 1985; TOYODA & TOKONAMI, 1990). Moreover, there is almost no fractionation during the REE uptake indicating that biogenic apatites acquire the REE signature of overlying bottom water (BERNAT, 1975; WRIGHT, 1984; STAUDIGEL, 1985; MARTIN & HALEY, 2000).

The rare earth elements are incorporated into the biogenic apatites through a process that is not fully understood as yet. Different models of REE uptake have been proposed: adsorption, substitution, diffusion, percolation, and recrystallization (BERNAT, 1975; WRIGHT *et al.*, 1987; GRANDJEAN *et al.*, 1987, 1988; SHOLKOVITZ *et al.*, 1989; GRANDJEAN-LECUYER *et al.*, 1993; REYNARD *et al.*, 1999). It is likely that the rapid, postdepositional increase in REE concentration coincides with the transformation of hydroxy-apatite of the living animal to the more stable francolite of the fossil specimen (WRIGHT *et al.*, 1984; SHAW & WASSERBURG, 1985; STAUDIGEL *et al.*, 1985; ARMSTRONG, 2001). Some authors imply, however, that sediment pore water can also contribute REE to biogenic apatites (ELDERFIELD & PAGETT, 1986; TOYODA & TOKONAMI, 1990).

It is informative to compare the Nd isotopic composition of fish material with that of manganese nodules (STAUDIGEL, 1985) and ferromanganese crusts (MARTIN & HALEY, 2000), because all these materials exhibit very similar ε_{Nd} values at similar depths in the modern oceans. Manganese nodules, which are known to form at the sediment-water interface, record the Nd isotopic values of seawater and not the values of surrounding pelagic clays (PIEPGRAS & WASSERBURG, 1979; ELDERFIELD et al., 1981; GOLDSTEIN & O´NIONS, 1981). Moreover, an examination of a single manganese nodule showed that Nd isotopic ratio at the top of the nodule, which was in contact with seawater, was identical with that of the lower part of the nodule, which was in contact with sediment (PIEPGRAS, 1979). However, the Nd concentration in the upper part was much higher than in the lower one. Thus, the contribution of REE from sediment pore fluids seems to be negligible, both in the case of manganese nodules and biogenic apatites. Moreover, because Nd signatures of pore waters in well ventilated, bioturbated sediment layers are identical with those of bottom waters (PIEPGRAS, 1979), the Nd contribution from pore waters cannot change the original isotopic signature of seawater. According to STAUDIGEL (1985), most bottom sediments, in particular in the Pacific and Indian oceans, have lower $^{143}Nd/^{144}Nd$ ratios than manganese nodules. Thus, if the REEs in the sediment really affected the composition of pore water in the uppermost part of sediment, fish teeth from the Pacific should display lower $^{143}Nd/^{144}Nd$ ratios than those of ambient seawater and manganese nodules. This phenomenon, however, has not yet been observed.

Neodymium exchange during burial and extensive diagenesis was also considered as process that can alter the original seawater isotopic signature preserved in biogenic apatites. Numerous case studies have demonstrated, however, that very high Nd concentrations in fish remains, acquired within the top few mm of the sediment-water interface, show no systematic variations with burial depth or age (BERNAT, 1974; STAUDIGEL et al., 1985; ELDERFIELD & PAGETT, 1986; WRIGHT et al., 1987; GRANDJEAN, 1987; MARTIN & HALEY, 2000). The lack of systematic enrichment or depletion of the REE with burial depth indicates that progressive diagenesis does not influence Nd isotopic signatures in biogenic apatites. A similar conclusion

arises from the study of ARMSTRONG *et al.* (2001), who tested the effects of a thermal metamorphism on REE systematics in conodonts. They investigated samples from a single bed in which conodonts show laterally progressively higher CAI values from 2 to 6, resulting from the contact metamorphism of a basalt dyke. Regardless of their thermal alteration level, the conodonts yielded homogeneous, "bell-shaped" shale-normalized REE patterns.

Variations in REE abundance recognized in biogenic apatites were interpreted by ELDERFIELD & PAGETT (1986) as related to exposure time and redox conditions at the sea bottom, prior to burial. They observed that fish debris from deep-ocean sediments, deposited at a slow sedimentation rate, had high concentrations of REE, whereas fish debris from continental margins, where sedimentation rates are generally higher, revealed low REE concentrations. Data of WRIGHT *et al.* (1987), however, suggest that this relationship is not linear, and that other factors must influence the enrichment process.

5 Marine geochemistry of strontium

Strontium has four naturally occurring isotopes ^{84}Sr, ^{86}Sr, ^{87}Sr, and ^{88}Sr, of which only ^{87}Sr is partly radiogenic. This isotope is a product of radioactive decay of ^{87}Rb. Fractionation during early separation of the continental crust and the earth's mantle has resulted in the former having higher Rb/Sr ratios. In consequence, continental rocks exhibit higher (more radiogenic) $^{87}Sr/^{86}Sr$ ratios than mantle rocks. The sources of strontium in the oceans are both the continental crust and sea-floor hydrothermal fluids. PALMER & EDMOND (1989) calculated the marine Sr budget and showed that the global fluvial input of Sr, with $^{87}Sr/^{86}Sr$ of 0.7119, is twice as much as the hydrothermal Sr flux, with $^{87}Sr/^{86}Sr$ of 0.7035. Another, less significant, contribution represents Sr released from marine carbonates by diagenetic recrystallization (ELDERFIELD & GIESKES, 1982). Although the fluvial input of Sr is the most substantial, rivers are not able to affect noticeably the marine $^{87}Sr/^{86}Sr$ ratio, even locally in estuaries (ELDERFIELD, 1986; VEIZER, 1989), because the concentration of Sr in rivers is often less than 1 percent of the Sr concentration in seawater (GOLDSTEIN & JACOBSEN, 1987; PALMER & EDMOND, 1989). A very long residence time of Sr in the oceans (~ 10^6 yr), which significantly exceeds the mixing time of seawater (~ 10^3 yr), is responsible for a worldwide uniform $^{87}Sr/^{86}Sr$ ratio of about 0.7092 in present-day seawater (ELDERFIELD, 1986). This $^{87}Sr/^{86}Sr$ ratio is accurately recorded by calcium-bearing minerals precipitated from seawater (e.g. BURKE *et al.*, 1982; ELDERFIELD, 1986; VEIZER, 1989).

Measurements on ancient marine carbonates revealed fluctuations of the Sr isotope ratio throughout geological time (PETERMAN *et al.*, 1970; DASH & BISCAYE, 1971; VEIZER & COMPSTON, 1974). Archaean carbonates yield strongly non-radiogenic Sr isotope ratios (~ 0.7010)

but during the Precambrian there was a significant increase of the Sr isotope ratio, so that the isotopic composition of the Cambrian seawater was similar to that of the present time (VEIZER & COMPSTON, 1976). The first seawater Sr isotope evolution curve for the Phanerozoic was published by BURKE *et al.* (1982), but it was predominantly based on whole-rock carbonates, which are usually contaminated by radiogenic Sr from diagenetic fluids. Because postdepositional exchange of Sr causes an increase of the $^{87}Sr/^{86}Sr$ ratio (VEIZER & COMPSTON, 1974), a minimum Sr isotope ratio measured at any given time is the most reliable value reflecting the contemporaneous seawater composition. A careful diagenetic screening of investigated skeletal material in the last two decades allowed assembling of a huge data set for the construction of high-resolution strontium-isotope curves for most periods in the Phanerozoic (e.g. HESS *et al.*, 1986; VEIZER *et al.*, 1999; JENKYNS *et al.*, 2002).

Devonian strontium isotope data include predominantly measurements on brachiopods and conodonts that represent the most suitable study material from the Palaeozoic (DIENER *et al.*, 1996). Conodonts, however, often provide slightly more radiogenic $^{87}Sr/^{86}Sr$ values than coeval brachiopods (EBNETH *et al.*, 1997). This is chiefly because of significant isotopic heterogeneity within single conodont elements (TROTTER *et al.*, 1999). The lowest, and perhaps primary, $^{87}Sr/^{86}Sr$ ratio is mostly retained in the cusp tissue, along the growth axis of the conodont element. Therefore, in most cases, a physical separation of cusp tissue is required to obtain $^{87}Sr/^{86}Sr$ ratios approaching primary seawater values. The majority of data used for construction of the high-resolution strontium-isotope curve for the Devonian was produced by Veizer and co-workers (see VEIZER *et al.*, 1999 and references therein). The curve displays a well-defined structure (Fig.6) but the precision of the biostratigraphical assignment of the majority of samples is rather low and thus unsatisfying. In fact, sample correlations within a single conodont zone constituted the most crucial problem during the curve construction (VEIZER *et al.*, 1997). Nevertheless, this curve is better constrained than that of BURKE *et al.* (1982). It shows a very uniform $^{87}Sr/^{86}Sr$ ratios of about 0.7087 in Lochkovian time followed by a steep decline to 0.7080 across the Pragian and the Emsian. The latter interval potentially permits dating of Early Devonian pristine carbonates to the stage level. The Middle Devonian interval of the curve is relatively flat. High frequency oscillations in the $^{87}Sr/^{86}Sr$ ratio as recognized in the Middle Devonian of the Eifel region in Germany are interpreted as resulting from slow accumulation rates and local hiatuses that are below the level of biostratigraphical resolution (DIENER *et al.*, 1996; EBNETH *et al.*, 1997). From late Givetian into Late Devonian time, a continuous increase in $^{87}Sr/^{86}Sr$ ratio can be observed (Fig. 6). This trend, however, is poorly constrained, particularly for the Famennian (VEIZER *et al.*, 1999). Data from the lowest Mississippian suggest a ratio between 0.7081 and 0.7082 at the Devonian-Carboniferous boundary (DENISON *et al.*, 1994; VEIZER *et al.*, 1997).

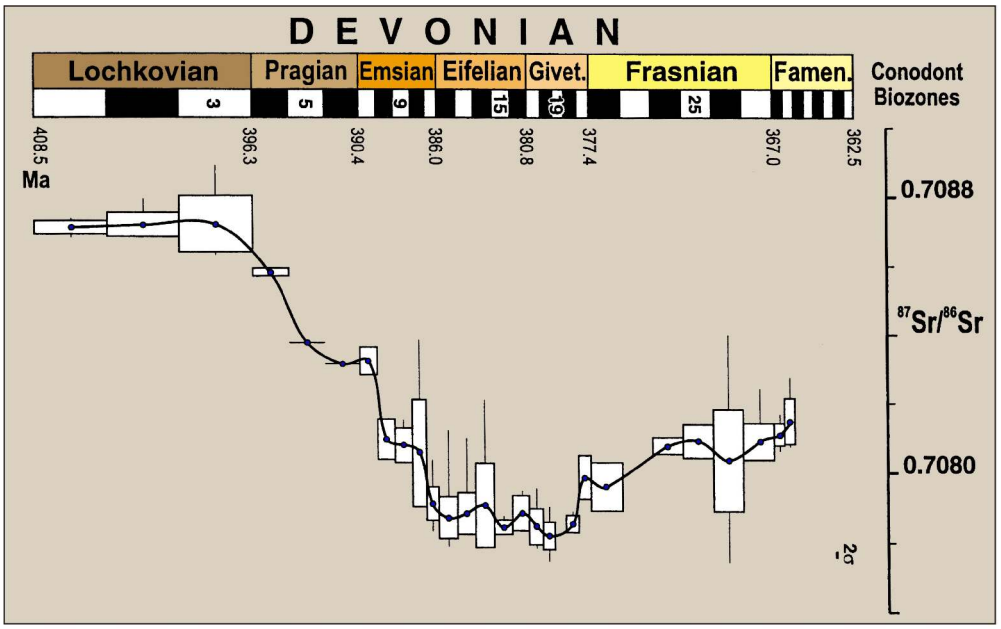

Fig. 6. $^{87}Sr/^{86}Sr$ variations during the Devonian showed in the resolution of conodont zonation (adopted from Veizer et al. (1999). Explanations; circle= mean; box = $\pm 1\sigma$; vertical line = minimum and maximum; the conodont zones are indicated by black-white bands.

6 Palaeogeography

Palaeogeographical reconstructions are based mainly on palaeomagnetic, palaeobiogeographic and lithological data. These three types of evidence, however, can provide basically contrasting models of the configuration of continents in the past, especially for pre-Mesozoic times. This is because each method has some limitations and generally provides a different kind of data. None of the methods involved in the palaeogeographical synthesis is capable of determining the relative palaeolongitudes for the investigated areas. The palaeomagnetic method is generally regarded as the most useful and accurate, because it provides quantitative information for the latitude position at which measured rocks were formed. The disadvantage, however, is that the primary magnetisation of rocks can be easily changed due to thermal overprint during burial or orogenic processes. This is mostly why palaeomagnetic data obtained from Lower Palaeozoic and older rocks are sometimes inconsistent and suggest contrasting models of the drift histories of palaeocontinents (for examples, see e.g. TORSVIK *et al.*, 1996; TAIT *et al.*, 2000). Erroneous palaeomagnetic reconstructions can also result from incorrect age determinations of magmatic rocks used for the studies. In addition, the palaeomagnetic method provides latitudinal data points with a resolution that is generally lower than ± 500 km, and therefore only wide separation of plates and continents can be credibly shown. The distribution patterns of fauna and flora, which are the basis of the biogeographical method, are not only dependent on the configuration of continents. They can be strongly influenced by various external factors, such as climatic

conditions, sea-level oscillations, or seawater circulation. Although isolated continents usually produce distinctive and often endemic biota, similar fauna or flora can be widely dispersed throughout the world. This makes an interpretation of biogeographic data quite difficult and requires a thorough knowledge of taxonomy and ecology of organisms, which are mostly extinct. The most crucial problem in the interpretation of biogeographic data for the Palaeozoic is the fact that all available information is from the epeiric seas and terrestrial areas. Almost nothing is known about the ancient oceanic realms and their oceanographic characteristics. Lithology and sedimentary features related to particular climatic conditions (e.g. warm-water reefs, evaporates, karst, or tillites) constitute an important evidence in palaeogeographical reconstructions. The method, however, can only provide rough estimates for palaeogeographic positions. By comparison with the modern zonation of climatic belts, potential errors can arise for periods in which asymmetric climatic zones may have existed due to the distribution of land masses, monsoonal effects or orographic factors.

Two large palaeocontinents, Gondwana and Euramerica, existed during the Late Devonian (Fig. 7). Gondwana, which included South America, Africa, Antarctica, Australia, India, Arabia and Iran, was located in the Southern hemisphere at intermediate to high latitudes. It formed the largest land mass of the Devonian world and only its margins were covered by epeiric seas. The palaeocontinent of Euramerica, termed also as Laurussia or the Old Red Continent, originated by amalgamation of Laurentia, Baltica and Avalonia during late Ordovician to Silurian times, as a result of the Caledonian orogenic events (TORSVIK *et al.*, 1996; MCKERROW *et al.*, 2000). Euramerica was positioned in equatorial latitudes during the Late Devonian and possessed extremely wide shelf areas along its western and eastern margins (Fig. 7). Other smaller

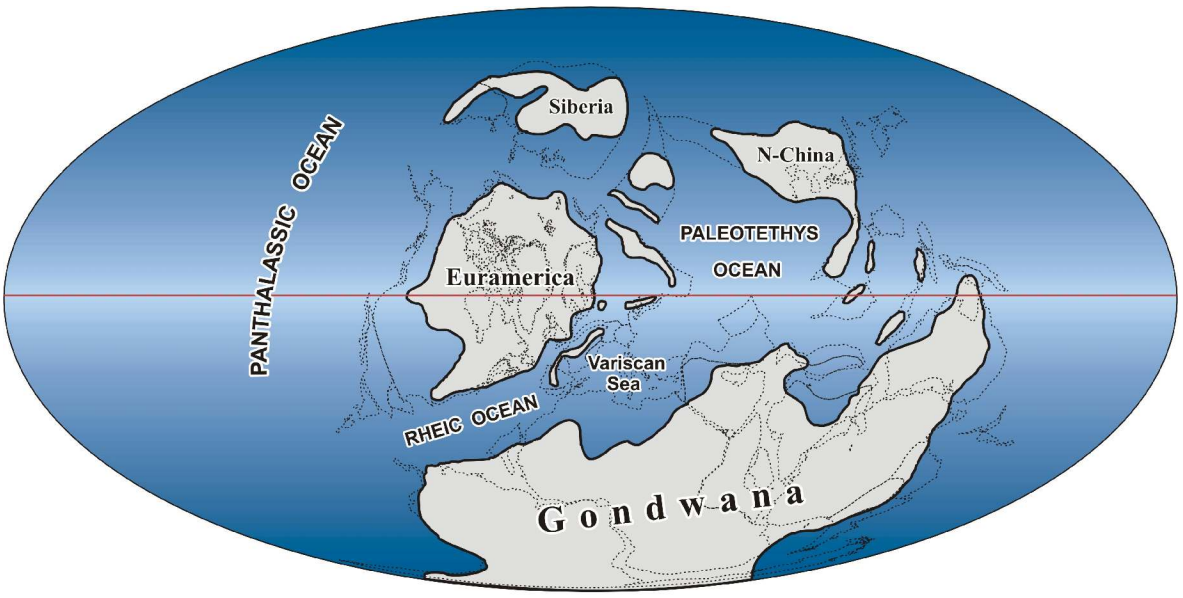

Fig. 7. Late Devonian paleogeographic reconstruction with paleogeographic terminology used in this study (taken from Atlas, Version 3.2, an interactive software developed for the PC by Cambridge Paleomap Services Limited).

continents, i.e. Siberia, Kazakhstan, North and South China, were located in the Northern hemisphere and mostly covered by shallow seas. Palaeomagnetic data show that several small Variscan terranes occurred between Gondwana and Euramerica. There is still a debate whether some of these Gondwana-derived crustal blocks, i.e. Saxo-Thuringia, Bohemia, Moldanubia, Iberia, and Armorican Massif, constituted individual terranes or they formed a coherent microplate termed the Armorican Terrane Assemblage (TAIT *et al.*, 1997). STAMPFLI & BOREL (2002) suggested a more radical scenario and merged all crustal blocks between Gondwana and Euramerica into one large superterrane, the European Hunic Terrane.

The boundaries of continents are relatively well defined whereas the outlines of the oceans are rather roughly recognized. In the present study, the terminology of oceanic spaces in the Late Devonian (Fig. 7) follows that of SCOTESE (in http://www.scotese.com) with a huge Panthalassic Ocean outside the assemblage of continental blocks and two relatively small oceans separating the continents. These are the Palaeotethys Ocean between eastern Gondwana, North China and Euramerica, and the Rheic Ocean separating the northwestern margin of Gondwana from the southern margin of Euramerica. The Rheic Ocean has been originally defined to describe only the space between Avalonia and Armorica, which has already been closed during Emsian time (FRANKE, 2000). The palaeogeographic space separating the Armorican Terrane Assemblage (ATA) from the Gondwana margin is termed here as the Variscan Sea following the scenario of NEUGEBAUER (1988).

In the last two decades, several paleogeographical reconstructions for the Late Devonian were presented. Because of different projections used for the reconstructions, it is difficult to compare them to see differences in the positions of continents. Therefore, six of them have been redrawn using the Schmidt's projection and are presented in Figures 8 and 9. Most of these models (i.e. SCOTESE & MCKERROW, 1990; MCKERROW et al., 2000; TAIT et al., 2000; LEWANDOWSKI, 2002) are in good agreement with regard to the equatorial position of Euramerica during Late Devonian time. Palaeomagnetic and palaeoclimatic data show that Gondwana continued its northward movement during the Devonian, but its palaeogeographic position is palaeomagnetically poorly constrained (for review, see TAIT et al., 2000). This is why the paleogeographical reconstructions for the Late Devonian differ first of all in the position of Gondwana and, hence, they show a quite narrow or a very wide ocean between Gondwana and Euramerica. The first scenario is suggested in the reconstruction based predominantly on biogeographic data (DALZIEL et al. 1994; MCKERROW et al. 2000), whereas palaeomagnetism provides rather evidence for the second one (TAIT et al., 2002; STAMPFLI & BOREL, 2002; LEWANDOWSKI, 2002). The palaeoclimatic model of WITZKE & HECKEL (1988), which is based on lithological and facies data only, shows Gondwana and Euramerica in relatively close position (Fig.8).

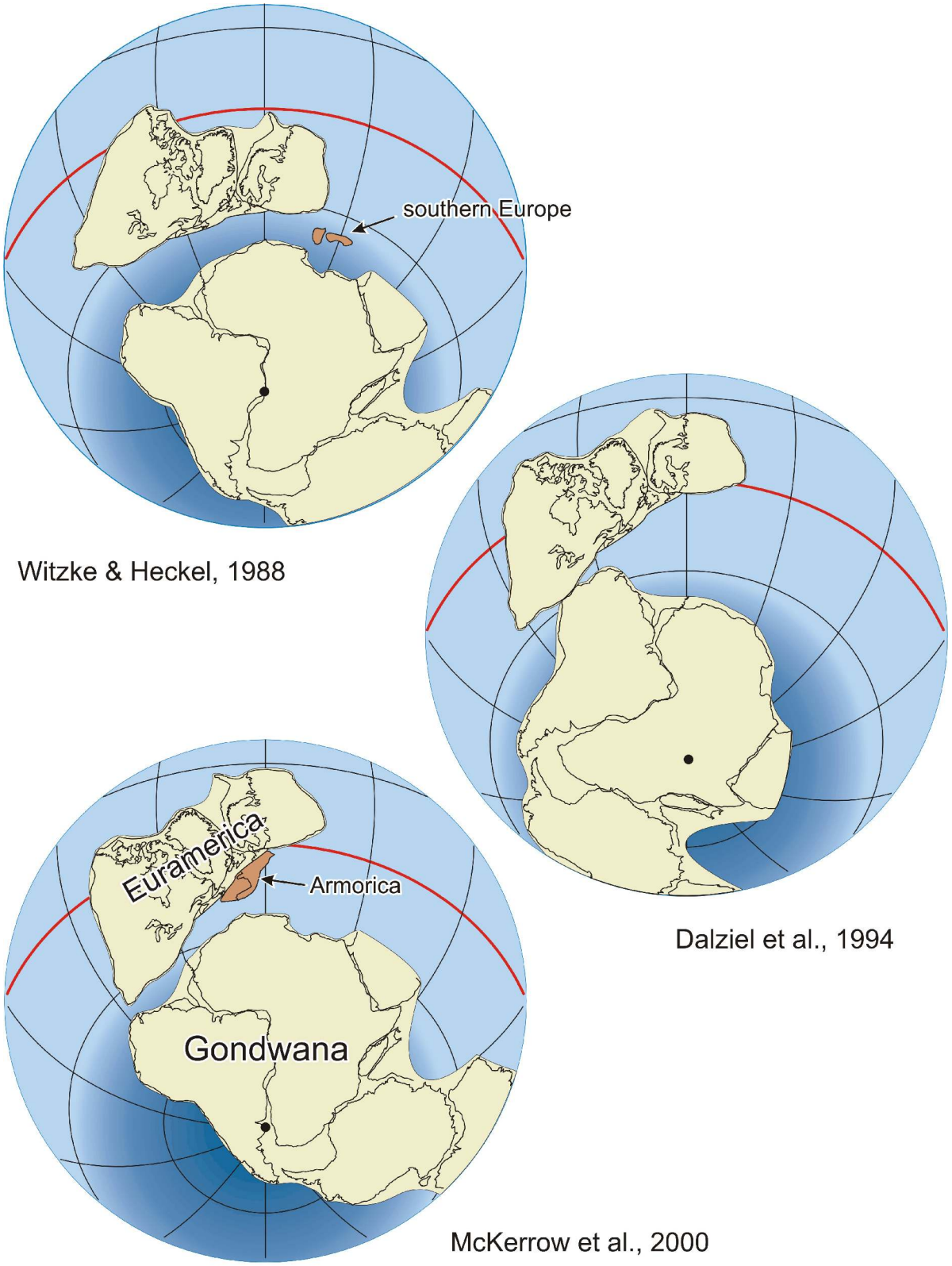

Fig. 8. Alternative reconstructions of continental disposition in Late Devonian time after Witzke & Heckel (1988), Dalziel et al. (1994) and McKerrow et al. (2000). In order to reveal differences in the position of Gondwana and Euramerica palaeocontinents the reconstructions are presented in the same projection (Schmidt projection; grid every 30°; red circle - equator; black spot - south pole). The reconstructions were plotted using the GMAP32 software package (Torsvik & Smethurst 1989-1997).

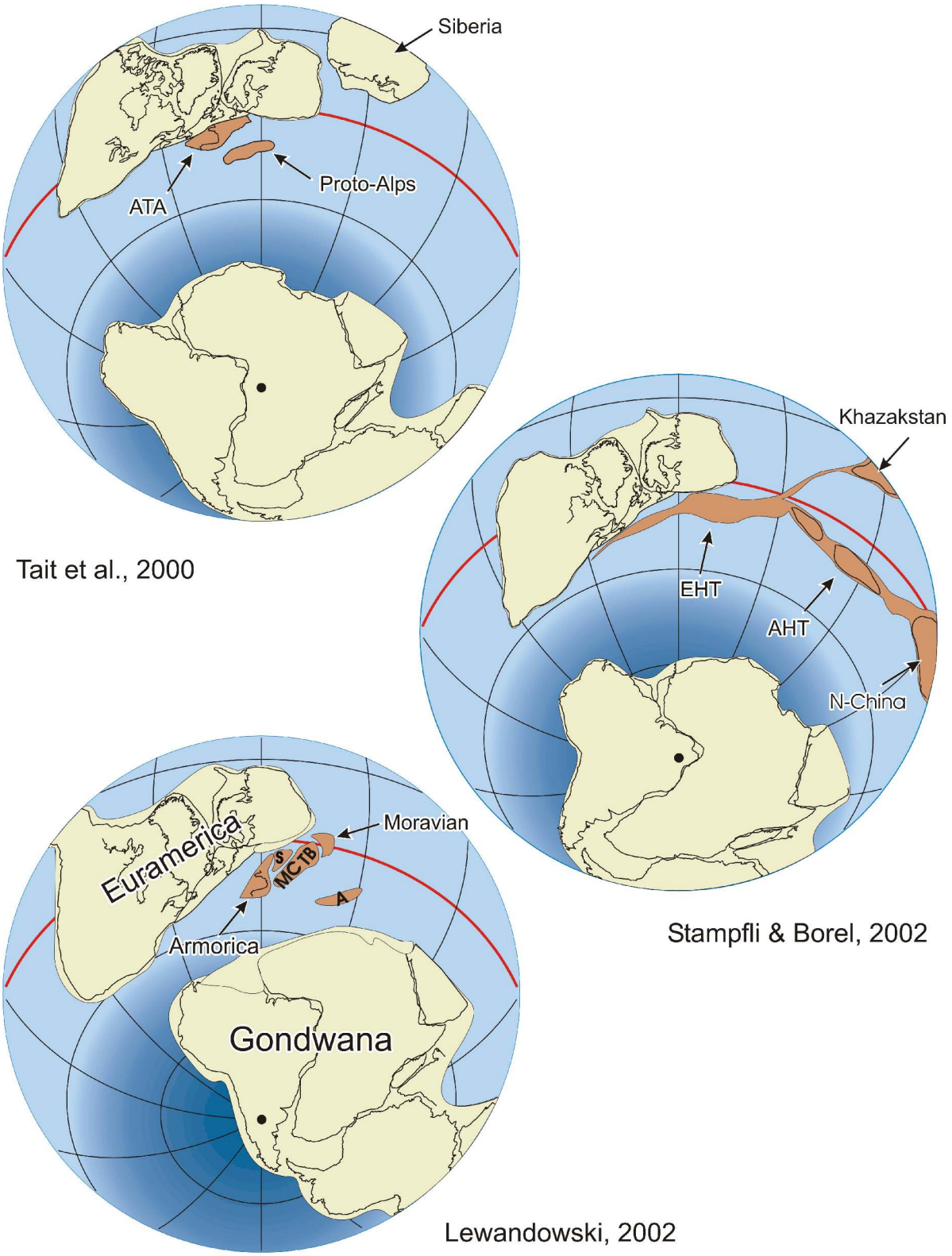

Fig. 9. Alternative reconstructions of continental disposition in Late Devonian time after Tait et al. (2000), Stampfli & Borel (2002) and Lewandowski (2002). In order to reveal differences in the position of Gondwana and Euramerica palaeocontinents the reconstructions are presented in the same projection (Schmidt projection, ; grid every 30°; red circle - equator; black spot - south pole). The reconstructions were plotted using the GMAP32 software package (Torsvik & Smethurst 1989-1997). Abbreviations used in this figure are: A - Alpine basement units, AHT - Asiatic Hunic Terrane, ATA - Armorica Terrane Assemblage, EHT - European Hunic Terrane, MC - Massif Central-Moldanubian, S - Saxothuringia, TB - Tepla-Barrandian.

McKERROW et al. (2000) postulate that the connection between the African margin of Gondwana and Euramerica was already achieved in mid-Devonian time (Fig. 8). Similar fish fauna in Northern Australia and Euramerica, and also similar ostracods in the Emsian of Algeria and Baltica exclude the existence of wide ocean between Gondwana and Euramerica after Early Devonian time. According to this model, the northern margin of Africa was positioned at the palaeolatitude of 20˚ S in the Late Devonian and the distance between the margins of Euramerica and Gondwana was 300 to 500 km, which is comparable with the present-day latitudinal extent of the Mediterranean Sea. The final collision of Gondwana and Euramerica, which resulted in formation of the supercontinent Pangea, took place in the Late Carboniferous. In fact, the most recent palaeogeographical reconstruction of SCOTESE (http://www.scotese.com) is very similar to that of McKERROW et al. (2000).

TAIT et al. (2000), who used only paleomagnetic data, favoured a position of Gondwana at high latitudes in Late Devonian time, with the North African margin at ~ 50˚S. This implies that the European margin of Euramerica was separated from Gondwana by an ocean of at least 3000 km width (Fig.9). They argued that, in southern Europe, there is no tectonic or magmatic evidence for a Devonian collision between Gondwana and Euramerica. According to STAMPFLI (1996), continuous sedimentation in the passive margin environment lasted in the European Alpine realm until Late Carboniferous time. Much more controversial paleomagnetic data were presented by CHEN et al. (1993), who postulated an ~ 4500 km wide ocean between Gondwana and Euramerica during the Early Carboniferous.

DALZIEL et al. (1994) have interpreted the Early Devonian deformation in the Appalachians and Britain (Acadian Orogeny) as a result of local collision between this segment of Euramerica and Gondwana (Fig 8). This scenario can explain faunal affinities between both continents. In this model the final closure of the ocean and formation of Pangea involved a massive dextral movement accompanied by clockwise rotation of Euramerica. The concept of the Early Emsian proximity of the northwestern margin of Gondwana and the southwestern margin of Euramerica is favoured by LEWANDOWSKI (2002), who postulates only a narrow oceanic domain (~ 400 km) between both margins. He suggested, however, that the northward drift of Euramerica during the Givetian resulted in reopening of the ocean in the late Famennian to a width of ~ 2000 km (Fig. 9). Despite such separation, fauna from both continents could potentially mix across the archipelago of dispersed, small terranes of the ATA and Alpine realm. In this reconstruction, the drift history of Baltica, Laurentia and Avalonia is based on paleomagnetic data, whereas paleoclimatic data were applied to constrain the position of Gondwana. The palaeogeographical model of STAMPFLI & BOREL (2002) arises from the concept of dynamic plate boundaries and is supported by geological, paleomagnetic and paleobiogeographic information. It suggests a scenario with a large ocean between Gondwana and Euramerica in Devonian time (Fig. 9), similar

to that of TAIT et al. (2000).

Unfortunately, little is known about outline and position of the small terranes which were separated from the Gondwana margin during the Early Palaeozoic and drifted northwards. The proposed drift history of the Armorican Terrane Assemblage differs strongly in various palaeogeographical models. According to MCKERROW *et al.* (2000) and Scotese (http://www.scotese.com), the ATA remained adjacent to the northern Gondwana margin until its final collision with Euramerica (Fig. 8). In contrast, TAIT *et al.* (2000) postulated a detachment of the ATA from Gondwana already in Ordovician times. Consequently, the ATA was situated in the proximity of the southern Euramerica margin during the Late Devonian and was separated from Gondwana by at least 3000 km wide oceanic spaces. Most palaeogeographical reconstructions agree that some terrains forming the ATA were individual plates and moved more or less individually. A contrasting scenario was proposed by STAMPFLI & BOREL (2002), who suggested the existence of the Hun superterrane that comprised all Variscan and Avalonian crustal units (Fig. 9) coalescing in a long, narrow band, which has been detached from Gondwana in Silurian time. Subsequently, it moved northwards as a coherent unit and collided with Euramerica in mid to Late Devonian time.

7 Seawater circulation during the Devonian

As outlined in the previous chapter, palaeogeographical reconstructions for the Late Devonian differ primarily with respect to the width of the ocean that separated Gondwana and Euramerica. There is general agreement that at least some narrow seaways, if not a wide ocean, existed between both palaeocontinents at that time. However, advanced models of oceanic circulation for one or another palaeogeographical scenario are lacking. A first attempt to reconstruct seawater circulation in the Devonian was made by HECKEL & WITZKE (1979), who deduced an oceanic circulation pattern from the distribution of facies belts, interpreted in terms of climatic conditions. In this reconstruction, which concerns only Early Devonian time, a generally westward flow splits east of Euramerica into two masses that move along the northern and southeastern margins of this continent (Fig. 10). A counterclockwise rotation can be inferred for the Variscan realm because HECKEL & WITZKE (1979) postulated a local junction of Gondwana with Euramerica and, in consequence, an eastward current along the northern margin of Gondwana. Along its western margin, however, water masses flowed up northwards. A circulation pattern for the Middle Devonian has been presented by OCZLON (1990), who reconstructed current directions from palaeogeographical distribution of various sedimentary features such as contourites, condensation and non-deposition phenomena, and erosional surfaces. His model shows, in fact, similar

circulation system to that of HECKEL & WITZKE (1979). The seawater moved along the southern margin of Euramerica in the westerly direction as the South Equatorial Current, approached the western part of the Variscan realm, and turned southeast to form the eastward North Gondwana Current (Fig. 11). Biogeographical data provide an additional information on the surface circulation during the Devonian. PEDDER (1999) compared corals from the Devonian of Morocco with those of other regions in the world and found indication that coral fauna started to migrate from the Appalachian towards the eastern Anti-Atlas already during the Early Devonian. By early Givetian time, the eastward transport of coral larvae across the Rheic Ocean had ceased or was strongly reduced. The South Equatorial Current, however, contributed to the migration of corals in the southwesterly direction (PEDDER, 1999). A reverse flow direction, as suggested by JOSEPH & TSIEN (1977), is rather unlikely (PEDDER, 1999). The South Equatorial Current facilitated a transfer of coral larvae from the southeastern margin of Euramerica (Rhenohercynian Zone, Moravia) across the Variscan terranes of Spain and France to at least as far as the Anti-Atlas area. During the late Famennian, the eastern part of the South Equatorial Current was responsible for migration of

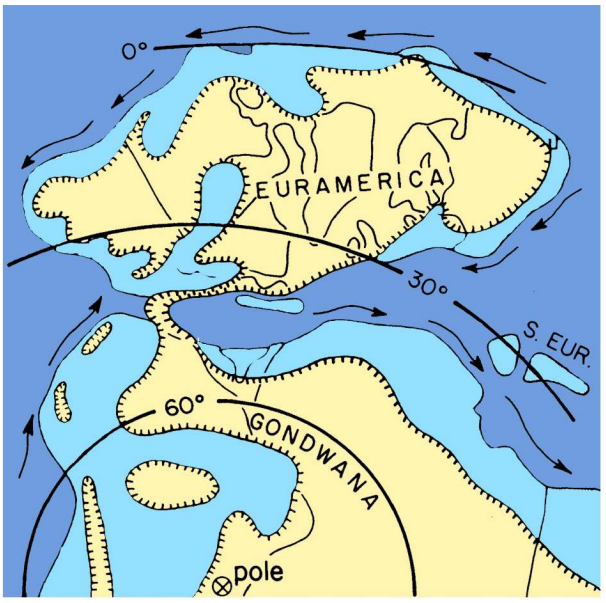

Fig. 10. Early Devonian paleogeography with general land areas and postulated ocean currents (from Witzke & Heckel, 1988; simplified and coloured). Note the presence of a land barrier connecting northwestern Gondwana and southwestern Euramerica.

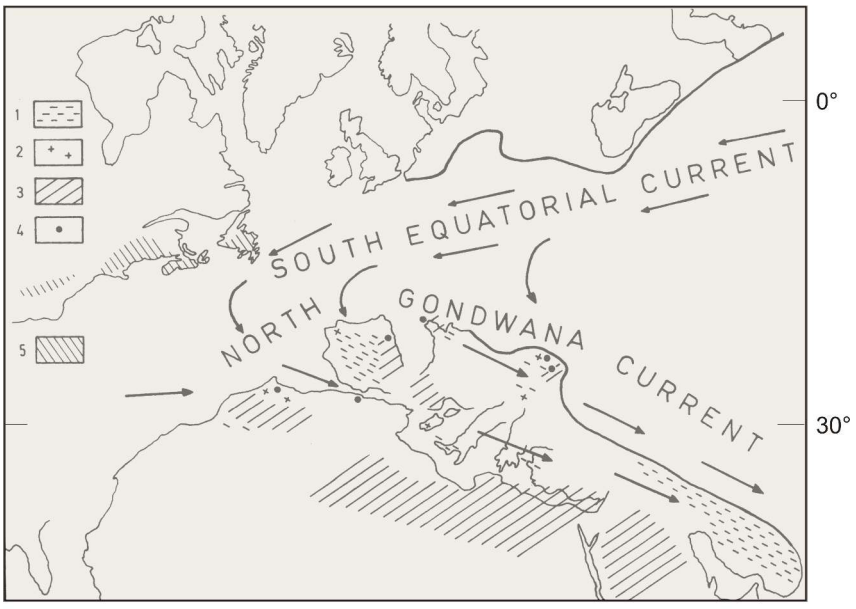

Fig. 11. Reconstruction of northern Gondwana and southern Euramerica during Middle Devonian time (from Oczlon, 1990). 1-sections with sedimentary gaps; 2 - condensations; 3 - mainly complete and uncondensed sections; 4 - contourites; 5 - zone of Acadian orogeny.

conodonts and corals from Russia (from areas on both sides of the Ural fold system) to the Bruno-Silesian unit, an outboard terrane at the southeastern margin of Euramerica (BELKA, 1998; BERKOWSKI, 1999).

8 Materials and methods

8.1 Field work

Conodont samples used in this study were collected in the eastern Anti-Atlas (Morocco), Moroccan Meseta and in the Montagne Noire (southern France) (Fig. 1). Additional conodont material was provided by Z. Belka (University of Halle) from Devonian outcrops and boreholes located in southern Poland (Sudetes, Holy Cross, vicinity of Cracow) and in southern Algeria (Ahnet Basin). Detailed information on localities, stratigraphy of samples, and their other characteristics are presented in the Appendix.

In order to reconstruct the temporal Nd isotopic evolution of seawater on the Gondwana shelf during the Late Devonian, three sections were sampled in the Anti-Atlas area. They were selected as representative for different depositional settings. These are: the Ait ou Nebgui section from the shallow-water Mader Platform, the Mech Irdane section from the pelagic Tafilalt Platform, and the Lahmida section from the Rheris Basin (Fig.12). The sections were densely sampled (Mech Irdane - 26 samples, Ait ou Nebgui - 20 samples and Lahmida - 61 samples) and also investigated in detail with respect to lithology and sedimentary content. Their conodont stratigraphy has already been presented by BELKA et al. (2002). To recognize the lateral pattern in the Nd isotopic composition of conodonts, samples were also systematically taken from two distinct stratigraphic horizons across the Anti-Atlas area: the base and the top of the Kellwasser facies. However, stratigraphic examination of the recovered conodont fauna revealed that both selected horizons are significantly diachronous (see also WENDT & BELKA, 1991). This required additional sampling to receive material from more synchronous levels: the lower part of the Frasnian Zone 11 (*jamieae*) and the upper part of the Famennian Uppermost *crepida* Zone. In total, 142 samples from 27 Anti-Atlas localities were examined in the present study.

Field work in the Moroccan Meseta focussed on the Upper Devonian succession exposed east of Mrirt (Fig. 13). A total of 17 samples was collected from the Frasnian and the lower Famennian part of the succession, including both the lower and the upper Kellwasser units.

In the Montagne Noire, the famous Upper Devonian carbonate sequence of Coumiac (see chapter 9.3) was selected for sampling. This section has often been studied in the past and extensive palaeontological, stratigraphical and geochemical data are already available. Conodont

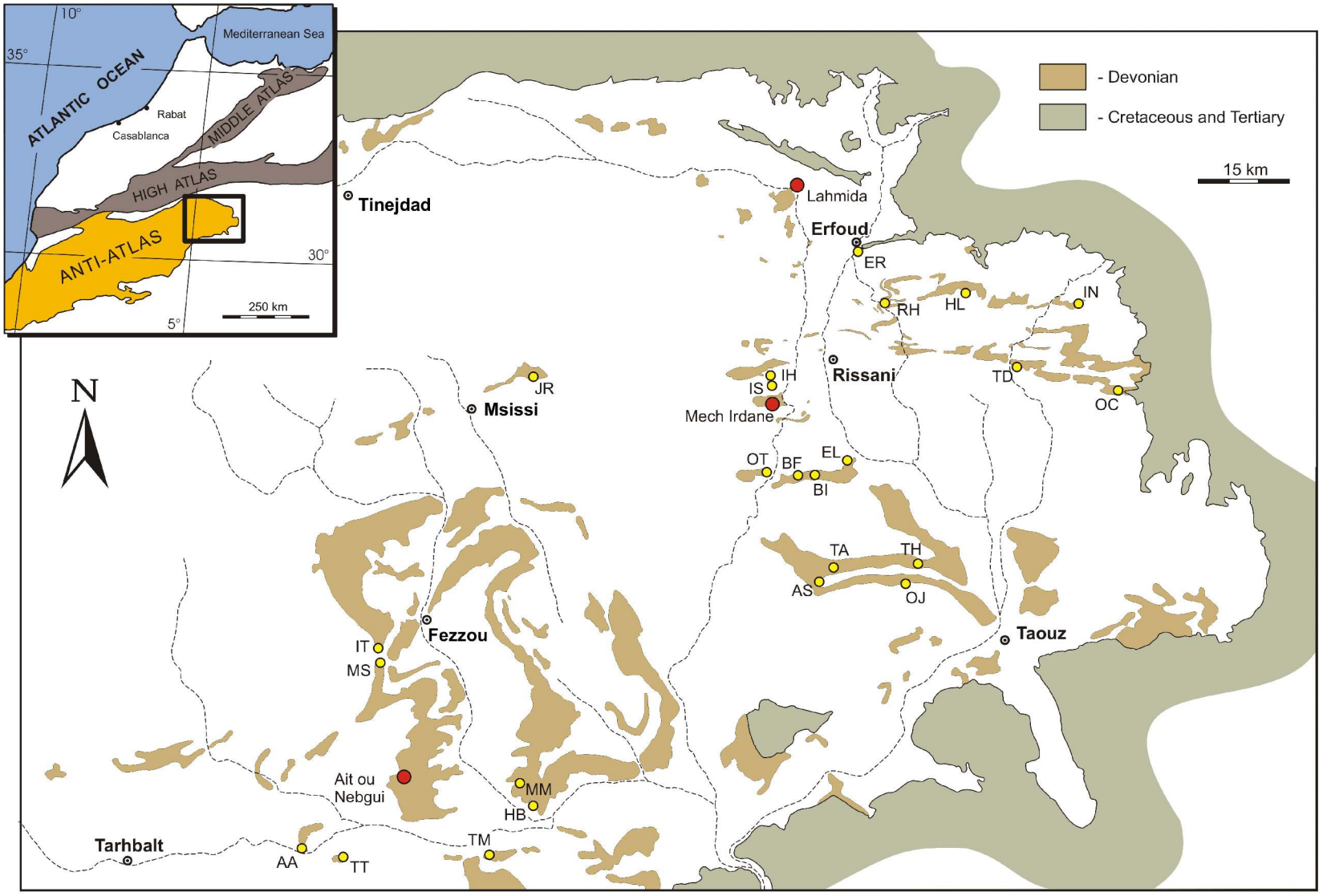

Fig. 12. Map of the eastern Anti-Atlas with location of outcrops from which conodont samples used in this study were recovered. Initials refer to sample localities listed in the Tab. 1.

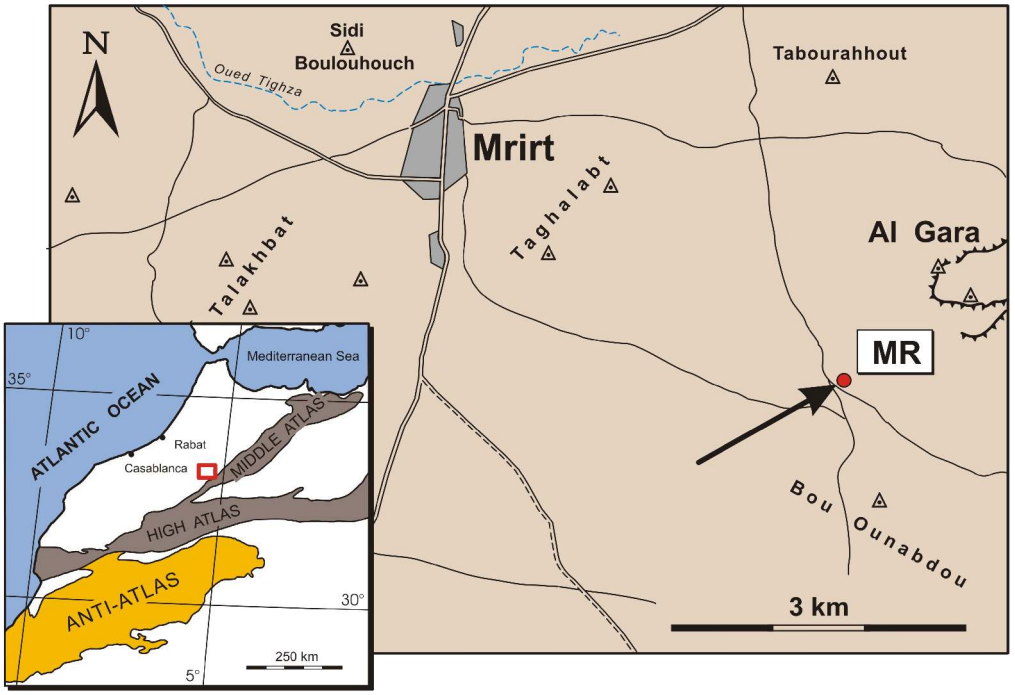

Fig. 13. Map showing the location of the section Gara de Mrirt (MR) in the eastern part of the Western Meseta.

samples (46) were collected from the section exposed in the Upper Quarry at Coumiac. The lithological column of the Frasnian and the lower Famennian and its conodont stratigraphy was adopted from Klapper (in FEIST, 1990). The upper portion of the section, however, that comprises the middle Famennian has been described and analysed in terms of stratigraphy in the course of the present study.

8.2 Processing of rock samples

Rock samples, each between 1-2 kg, were predominantly limestones and marly limestones; only a few samples were taken from shales. They have been processed in the micropalaeontological laboratory of the University of Halle. Conodont elements and fish material were recovered from the host rock by dissolution in 10% acetic acid followed by wet-sieving. To avoid input of additional, unknown chemical components, a pure (99.7-100%) acetic acid was used and diluted. The biogenic fluorapatites were separated from the insoluble residue with a Frantz isodynamic magnetic separator. Although this method did not yield satisfactory results in every case, heavy liquids were not used for conodont separation, because they remove a part of rare earth elements from conodonts (SHAW, 1984; WRIGHT, 1985). Such a diminution of REE content, however, is not accompanied by fractionation. Final selection of conodont elements and fish remains was accomplished by handpicking under a binocular microscope. In order to remove any adhering

mineral detritus from the conodont surface, the samples were shortly (~ 2 min.) treated with 1% HCl, washed with deionised water and repeatedly handpicked. Conodont sample weights used for Nd isotope analysis averaged 1 to 5 mg (see Tab.s 3 and 4), i.e. the samples contained from 10 to 120 conodont elements. This conodont material displayed CAI values of 1 to 5. The isotopic composition of Sr, however, was determined only on samples yielding CAI values of 2.5 or lower.

Because fish remains are characterized by a very high Nd content (usually 1000 to 2000 ppm), weights of fish samples were generally much lower than those of conodonts. The average weight of analysed fish material was about 0.5 mg (Tab. 5).

8.3 Analytical procedure

The analytical part of this work, including chemical separation of Nd, Sm and Sr and measurements of their isotopic composition, were carried out by author at the University of Munich, Department of Earth and Environmental Sciences (from September 1999 to August 2001) and at the University of Giessen, Institute of Geosciences (from September 2001 to November 2002). Rare earth elements analyses were carried out by Dr. W. Heijlen at the Katholieke Universiteit Leuven, Fysico-chemische Geologie.

The sample weights used for Nd isotope analyses depend on the Nd concentrations. In the case of conodonts, the advantage is that their Nd content can roughly be estimated from the general morphology of conodont elements (for more details, see chapter 10.1.2). The predicted Nd content permits calculation of the final weight of conodont samples required for optimal measurement parameters. The required amount of Nd in the sample is about 0.5 to 1 µ g. The isotopic composition and concentrations of Nd and Sm were determined by isotope dilution. Sr isotope analysis was performed on the same sample as Nd and Sm. The samples were spiked with a ^{150}Nd–^{149}Sm tracer solution and dissolved on a hot plate (~100˚C, overnight) in closed PFA vials using concentrated nitric acid (~ 14 N). In the next step, the solutions were evaporated to dryness, re-wetted with in 1 ml of 2.5 N HCl, and centrifugated.

Two slightly different techniques were applied in the laboratories at Munich and Giessen for separation of Nd, Sm and Sr from geological materials. In both cases, the procedure consisted of two stages. In the first stage, the REEs as a group and Sr were separated from matrix elements. In the laboratory at Munich, quartz columns filled with a 5 ml resin bed of AG 50W-X12, 200-400 mesh were used for separation. Columns were washed with 45 ml 6 N HCl and preconditioned with three 5 ml portions of 2.5 N HCl. The centrifugated samples were loaded onto the columns and rinsed twice with 1 ml of 2.5 N HCl. All major elements were eluted with the same acid in the first fraction of 38 ml followed by an 8 ml fraction containing Sr.

Subsequently, the eluent was switched to 6 N HCl and the first 5 ml were discarded. The next 15 ml fraction, enriched in LREE, was collected. In the laboratory at Giessen, miniaturized chromatographic techniques described by PIN et. al. (1994) were applied for REE and Sr separation. However, some modifications in the column size and concentration of reagents were introduced. Two sets of 50 µl polyethylene columns were filled with EICHROM *Sr* and *TRU* resins, respectively and washed with 0.5 ml H_2O. After preconditioning with 0.3 ml 2 N HNO_3 the columns were coupled (Fig. 14). The sample was loaded onto the upper column with 0.3 ml 2 N HNO_3 and rinsed with 0.25 ml of the same acid. The columns were then decoupled and subjected to separate elution schemes for the isolation of Sr and recovery of light REE from the Sr and TRU columns, respectively. The Sr column was washed with two 0.2 ml portions of 2 N HNO_3, and subsequently, the Sr was eluted with 1 ml H_2O. The TRU column was washed with two 0.2 ml portions of 2 N HNO_3 prior to elution of the LREE with 1.25 ml H_2O. The second stage of the procedure, during which Nd and Sm are separated from other REEs, was identical in both laboratories. Because the chemical properties of individual REEs are very similar, more refined techniques must be used for separations within the REE group. This is necessary because there are several isobaric interferences (e.g. ^{144}Sm interferes onto ^{144}Nd), and Ce, for instance, suppresses the ionisation of other REEs. Ba has similar negative effects on ionisation. Separation of Nd and Sm from other REEs was achieved by reverse-phase ion-exchange chromatography. Samples containing REEs

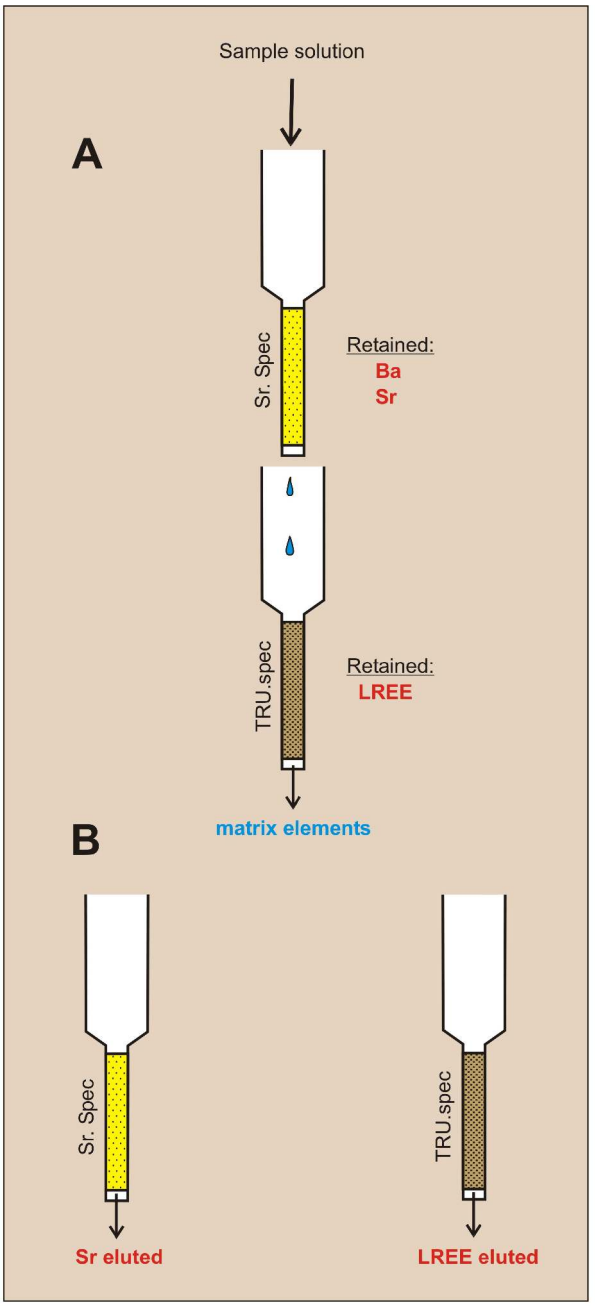

Fig. 14. Scheme of extraction chromatographic procedure to separate Sr and light REEs using *Sr.Spec* and *TRU.Spec* resins.
A - Loading of sample and extraction step
B - elution step

obtained during the first stage of separation were evaporated to dryness and redissolved in 0.3 ml 0.18 N HCl. The quartz columns packed with 2 ml Teflon powder coated with HDEHP (Hexyl di-ethyl hydrogen phosphate) were washed with 45 ml 6 N HCL and preconditioned with three 2 ml portions of 0.18 N HCl. The samples were loaded in 0.3 ml and rinsed four times with 0.2 ml of the same acid. The first 10 ml fraction of 0.18 N HCl containing La, Ce and Pr was discarded and Nd was eluted with the next 7 ml of the same acid. Afterwards, the eluent was switched to 0.4 N HCl; Sm appeared after 4 ml and was collected in a 4 ml fraction.

After separation, 2-3 drops of H_3PO_4 were added to Sr, Nd and Sm fractions, and each of them was evaporated to dryness for subsequent mass spectrometric analysis. Strontium was loaded with a Ta-HF activator on a single W filament, whereas Nd and Sm (loaded as phosphate) were measured in a Re double filament configuration. Sr and Sm measurements were carried out in static collection mode on a Finnigan MAT 261 mass spectrometer and Nd was measured using both static and dynamic modes on the same mass spectrometer.

Total procedure blanks were ~ 24 pg for Nd and ~ 75 pg for Sr. The $^{87}Sr/^{86}Sr$ ratios were normalized to $^{86}Sr/^{88}Sr = 0.1194$, $^{143}Nd/^{144}Nd$ ratios to $^{146}Nd/^{144}Nd = 0.7219$, and Sm isotopic ratios to $^{147}Sm/^{152}Sm = 0.56081$. Repeated measurements of the AMES standard yielded in Munich $^{143}Nd/^{144}Nd = 0.512073 \pm 10$ (2σ, n = 31) in static collection mode and 0.512135 ± 11 (2σ, n = 23) in dynamic collection mode, and in Giessen - 0.512135 ± 8 (2σ, n = 27) in static collection mode. The NBS 987 Sr standard measured in Giessen gave $^{87}Sr/^{86}Sr$ of 0.710231 ± 16 (2σ, n =31). Nd isotopic analyses are reported in the standard epsilon notation calculated using the $^{143}Nd/^{144}Nd$ ratio of CHUR that corresponds to a present-day value of 0.512638 (HAMILTON et al., 1983). All ε_{Nd} values are recalculated according to the measured $^{147}Sm/^{144}Nd$ ratios for the time of deposition (365 Ma). Although the stratigraphic age of the measured samples spans approximately 8 Ma, the maximum error introduced by using a single age for all samples is 0.1 epsilon units only.

9 Geological background

9.1 Eastern Anti-Atlas

The Anti-Atlas of southern Morocco is a broad, NE-SW trending Variscan anticlinorium developed at the northern margin of the West African Craton (PIQUÉ & MICHARD, 1989). To the north, east and south, it is surrounded by flat-lying Upper Cretaceous to Quaternary deposits of the Hamada (Fig. 12). The contact with the structures of the Variscan Belt is supposed to occur along the Tizi n´Test fault and the Tinerhir-Bechar thrusts, which form the southern border the

High-Atlas Chain. The basement of the Anti-Atlas consists of Precambrian granitic plutons that are exposed in the mountain belt stretching from the Atlantic coast in the west, to the Tafilalt area in the east. A weakly folded and very thick (more than 10 km) sedimentary sequence, ranging from the Late Proterozoic to the Namurian in age, covers the crystalline rocks in the north and particularly in the south, where it continues into the Tindouf Basin. The lithology and facies content of this sequence reveals a depositional and climatic evolution on the passive margin of Gondwana in the course of northward drift of this paleocontinent during the Paleozoic. The depositional and tectonic development of the eastern Anti-Atlas was controlled by regional, E-W trending strike-slip faults. Two main fault systems representing a part of the pre-existing Precambrian network have been recognized (BELKA et al., 1997). They were reactivated several times during the Paleozoic and provoked local volcanic activity in the Middle Cambrian and the Early Devonian. The Lower Paleozoic sequence is dominated by clastic deposits. Among these, the Ordovician ones are mainly of glacial origin. Records of a post-glacial transgression are pronounced in the Silurian to Lower Devonian facies sequence from littoral clastic deposits to open-marine graptolite-bearing shales and pelagic carbonates. During the Early to Middle Devonian, the strike-slip faults became active. In response to regional transtension, differential subsidence led to formation of carbonate platforms and small basins in this intracratonic setting (WENDT, 1985; WENDT, 1988; BELKA et al., 1997; KAUFMANN, 1998). Devonian sediments, perfectly exposed over an area of about 20000 km^2 (Fig. 12), reach a maximum thickness of 2000 m. They are represented by extremely fossiliferous carbonates on the shallow-water platforms and by monotonous shales in the basins. For several decades, these carbonates have attracted interest of geologists and paleontologists. Studies on the Devonian stratigraphy and lithology were initiated by MASSA (1965) and HOLLARD (1967, 1974, 1981). Most of the investigations focussed on fossiliferous carbonates and facies development (see for review WENDT, 1988, 1995; BRACHERT et al., 1992; BELKA, 1998; KAUFMANN, 1998). Stratigraphical work has been carried out by using primarily conodonts and ammonoids (e.g. BUGGISCH & CLAUSEN, 1972; BULTYNCK & HOLLARD, 1980; BULTYNCK, 1985; BELKA et al., 1997, 1999). The thermal and burial history of Devonian rocks was reconstructed using conodont CAI data (BELKA, 1991). This study showed that the sea-floor relief with carbonate platforms and intracratonic basins has been levelled during Early Carboniferous time, with deposition of the thick clastic succession interrupted occasionally by the development of mud-mound complexes (WENDT et al., 2001). As a result of final closure of the Variscan space due to the Gondwana-Euramerica collision, the sedimentary cover of the Anti-Atlas was folded (PIQUÉ & MICHARD, 1989). Subsequent uplift and erosion took place very early during the Late Carboniferous (BELKA, 1991).

9.1.1 Facies pattern

The Late Devonian sedimentary pattern of the eastern Anti-Atlas has been presented by WENDT (1988, 1991). He distinguished four depositional realms on this shelf area: the Mader Basin, the Tafilalt Basin, the Mader Platform and the Tafilalt Platform (Fig. 15). Later on, WENDT & BELKA (1991) recognized an additional basinal realm, the Rheris Basin, in the northernmost part of the Tafilalt region. North of Erfoud, only a small fragment of this basin is exposed. Its shape and extent remain unknown because of the Cretaceous-Quaternary cover. In general, the platform-to-basin configuration of the shelf was stable during the Late Devonian (WENDT 1988, BELKA & WENDT, 1992). Remarkable changes, chiefly promoted by sea-level fluctuations, resulted in expansion of carbonate production or even emersion of platforms during sea-level lowstands, and in drowning of carbonate platforms during sea-level highstands. Because the platform slopes were gently dipping and formed long ramps as a rule, there was only an insignificant transfer of detrital carbonate material from the platforms into the basins. WENDT (1988) characterized the Tafilalt and the Mader platforms as situated in a pelagic position but the clastic input from the south and northwest indicates that, in fact, the shelf of the eastern Anti-Atlas was located between two land areas. In the northwest, between Msissi and Tinejdad (Fig. 15), the Precambrian basement of the Jebel Ougnate was at least episodically exposed and it supplied clastic material into the northern margin of the Mader Basin. In the south, clastic input, particularly pronounced during the

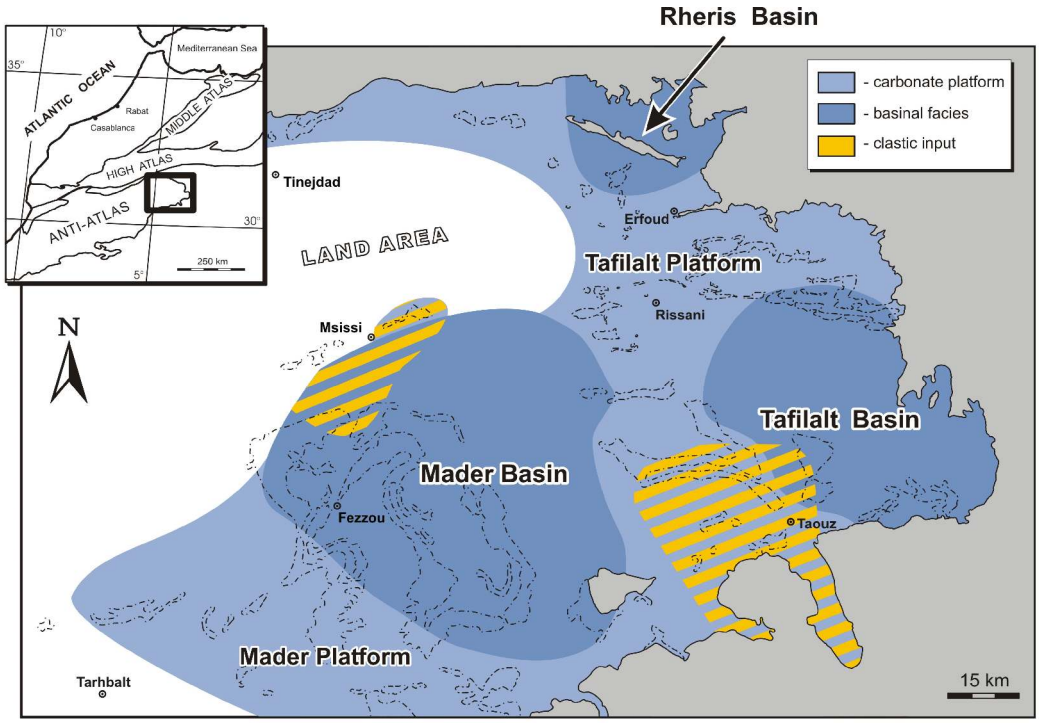

Fig. 15. Depostional environments on the shelf area of the eastern Anti-Atlas during the Late Devonian (modified from Belka & Wendt, 1992). The map shows the shelf configuration during the time of the Frasnian conodont Zone 11 (*jamieae*).

Frasnian, came from the basement of the West African Craton.

The thickness of the Upper Devonian varies strongly depending on the depositional setting. On the platforms, it ranges from only a few metres to 50 m. Much more sediment accumulated in the basinal realms. In the central part of the Mader Basin, the Upper Devonian attains a maximum thickness of 1200 m (BELKA, 1991). Facies trends follow the platform-basin configuration, with fossiliferous wackestones and packstones on the platforms, whereas monotonous, organic-rich shales occur in the basins. On the slopes, the sequences are predominantly shaly and contain levels of marly concretions and limestone interbeds. The latter, however, are only occasionally of turbiditic origin.

The most conspicuous part of the Upper Devonian sequence of the Anti-Atlas is a black, organic-rich facies, which constitutes an equivalent to the Kellwasser sediments of the Rhenohercynian Zone in Germany. In contrast to the German counterparts, the Kellwasser deposits in the Anti-Atlas contain a more extensive spectrum of lithology and represent a much longer stratigraphic interval that comprises the upper Frasnian and the lower Famennian (WENDT & BELKA, 1991; BELKA & WENDT 1992). On the platforms, the Kellwasser deposits are usually developed as an extremely fossiliferous cephalopod packstone with predominantly nektonic and planktonic fauna. Only in the Taouz area, where fine-grained clastic material was transported from the south into the littoral zone (Fig. 15), black bioclastic, sandy packstones interfinger with siltstones and fine-grained sandstones. In the basins, the Kellwasser facies is represented by monotonous black shales devoid of any fossils.

9.1.2 Lithology and stratigraphy

Mech-Irdane

This section is located in the western part of the Tafilalt Platform, about 12 km southwest of Rissani, where Devonian rocks crop out in the flanks of the small, E-W trending Jebel Mech Irdane syncline (Fig. 12). The sampled interval is situated in the central part of the southern flank (Loc. MI in Tab. 1 and Loc. 40 in WENDT & BELKA, 1991), close to a synsedimentary transverse fault described by WENDT & BELKA (1991). The exposed Upper Devonian succession is condensed, about 12 m thick and consists of bioclastic limestones (Fig. 16). It begins within the conodont Zone 8 of the Frasnian and ranges up to the Lower *postera* Zone of the Famennian (BELKA et al., 2002). The succession rests on the Givetian shales with some carbonate interbeds. The stratigraphic gap comprises a half of the Givetian stage and the first seven conodont zones of the Frasnian. Because the conodont fauna recovered from the first Frasnian layer includes also reworked specimens from the Frasnian Zone 2 (*rotundiloba*) and Zone 3 (*rugosa*), both lacking

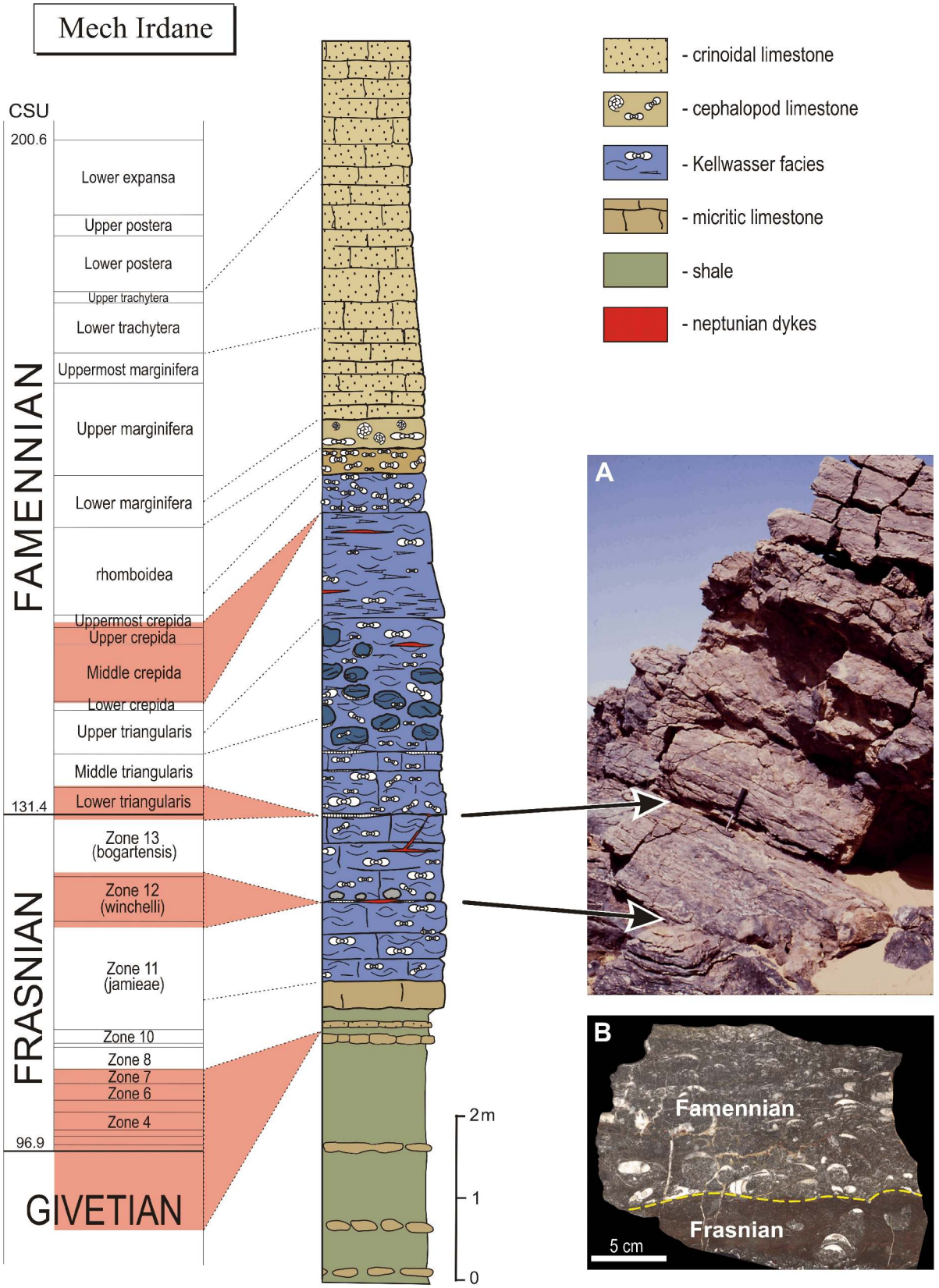

Fig. 16. Lithology and stratigraphy of the Upper Devonian at Mech Irdane. Note the occurrence of significant stratigraphic gaps and the long range of the Kellwasser facies. **A** - Photograph of the Kellwasser carbonates showing the position of erosional surfaces within the Frasnian sequence. **B** - Polished slab showing the erosional contact between the Frasnian and the Famennian.

in the section, the contact between the Givetian and the Frasnian appears to be sedimentary in character. The Frasnian part of the section is about 2.5 m thick and starts with light bioclastic wackestone followed by ca. 6.5 m thick, organic-rich Kellwasser deposits. As in other platform sections, the Kellwasser limestone is developed as an extremely fossiliferous cephalopod packstone. The abundant nektonic and planktonic fauna includes orthoconic nautiloids and ammonoids associated with conodonts, tentaculitids, styliolinids and fish remains. There is an apparent dominance of nektonic and planktonic fossils. The only benthic organism occurring commonly in the Kellwasser carbonates at Mech Irdane is *Buchiola* (bivalve). The scarcity of benthic organisms and black colouration of sediments are typical features of the Kellwasser lithology and indicate a presence of anoxic or dysaerobic conditions on the sea floor. The middle part of the Kellwasser unit contains abundant, large nodules (up to 30 cm) that do not show any remarkable difference in microfacies and biota from the surrounding matrix (Fig. 16). They represent fragments of semi-lithified carbonate sediment, redeposited from the adjacent upthrown side of the synsedimentary fault.

Three stratigraphic gaps have been documented within the Kellwasser unit (BELKA et al., 2002). The conodont fauna shows that the first gap comprises the entire Zone 12 of the Frasnian, whereas the second one comprises the Frasnian/Famennian boundary interval (Fig. 16). In consequence, the Middle *triangularis* Zone overlies directly the uppermost Frasnian. The third gap comprises the Middle and the Upper *crepida* zones. Each gap surface is associated with a system of dykes and irregular cavities filled with very peculiar black megacements. The origin and diagenetic history of these calcite cements were described by WENDT & BELKA (1991), who interpreted them as possible primary aragonite crystals that were transformed into calcite and partly dissolved in the vadose zone. The cements thus provide clear evidence for subaerial exposure episodes, during which also solution cavities and dykes were formed. Their infill is composed predominantly of marine sediment of the same age as the first layer above the gap surface.

The deposition of the Kellwasser facies terminates within the lower part of *rhomboidea* Zone. In fact, there is only a change in colour at the top of the Kellwasser limestone (Fig. 16). The overlying light-brown cephalopod packstone with very abundant cheiloceratids exhibits the same microfacies and faunal content as the black, organic-rich Kellwasser limestone below, but it was deposited under oxidizing conditions. A significant change in the composition of bioclastic material took place within the Lower *marginifera* Zone. The wackestone bears abundant cephalopods but the medium-grained biodetritus is predominantly from skeletons of benthic organisms. Such material built up the sequence of coarse-grained crinoidal limestones, packstone to grainstone in texture, that constitute the last Famennian lithological unit.

Ait ou Nebgui

The section Ait ou Nebgui is located in the central part of the Mader Platform, about 22 km south of Fezzou (Fig. 12). The Upper Devonian rocks are exposed within a small, E-W trending tectonic graben (Loc. AN in Tab. 1 and Loc. 27 in WENDT & BELKA, 1991). The sequence is only about 5 m thick and shows a peculiar lithological succession. This exposure is the only one locality in the Anti-Atlas (Fig.17) where the Kellwasser unit is composed of three complexes of black carbonates separated by two shale intervals. The lowest part of the exposed succession, below the Kellwasser deposits, consists of shales with some interbeds of yellowish crinoidal limestones (Fig. 18). Their conodont fauna is indicative of the interval from the Zone 7 to the lower part of the Zone 11 (*jamieae*). The crinoidal limestones are overlain by carbonates of the Kellwasser facies. The contact is sharp and displays some erosional features; such as clasts of reworked micritic limestone embedded in the black Kellwasser matrix. The conodont fauna recovered from the first Kellwasser layer is characteristic for the middle part of the Frasnian Zone 11. Thus, there is no evidence for any stratigraphic gap at the base of the Kellwasser sequence. The lower carbonate complex of the Kellwasser facies is represented by black bioclastic limestones that are packstone

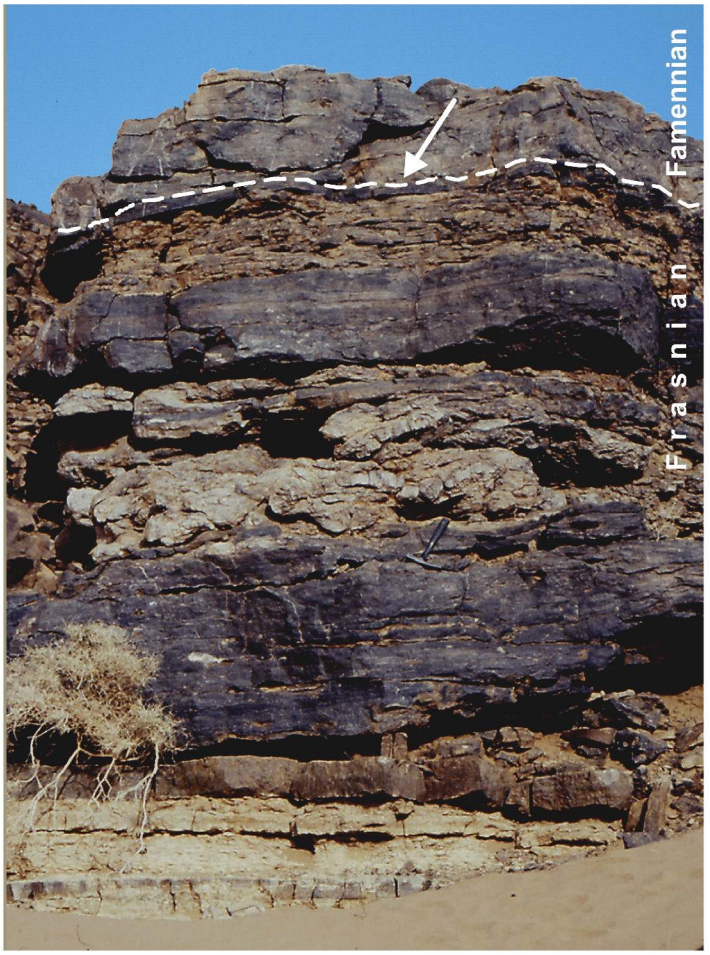

Fig. 17. Upper Devonian sequence at Ait ou Nebgui. Note the presence of three complexes of the Kellwasser facies. The position of the Frasnian-Famennian boundary is arrowed.

to grainstone in texture. Allochems include predominantly debris of cephalopods but remains of bivalves can also be found. Overlying is strongly weathered shale with conspicuous calcite megacements. Macrofossils are rare but a rich conodont fauna has been recovered. The second Kellwasser carbonate complex is composed of bioclastic packstone with a large amount of cephalopod debris and *in situ* reworked fragments of semi-lithified Kellwasser sediment. In its lower portion, the complex is interrupted by a thin layer of white crinoidal grainstone that bears calcite megacements identical to those occurring in the shales. The upper shales are separated from the middle Kellwasser member by a significant stratigraphic gap comprising an interval from the uppermost part of the Zone 11 up to the lowest part of the Frasnian Zone 13 (Fig. 18). They are extremely rich in conodonts indicative of the Zone 13. The shales are topped by the third Kellwasser carbonate unit, which is, however, stratigraphically composed of two parts. The lower and only 15 cm thick limestone layer belongs to the Frasnian, whereas the remaining part is Famennian in age (Fig. 18). The erosional contact can be clearly observed in the field (Fig. 19). The stratigraphic gap is here significantly longer than the equivalent sedimentary break on the Tafilalt Platform (see the Mech Irdane section). Because both stratigraphic gaps recognized at Ait ou Nebgui have a regional character and, in addition, carbon isotopic data suggest that the calcite megacements are products of meteoric diagenesis (Z. BELKA, pers. comm.), it seems that the gaps reflect two episodes of subaerial exposure. The Famennian part of the Kellwasser facies is

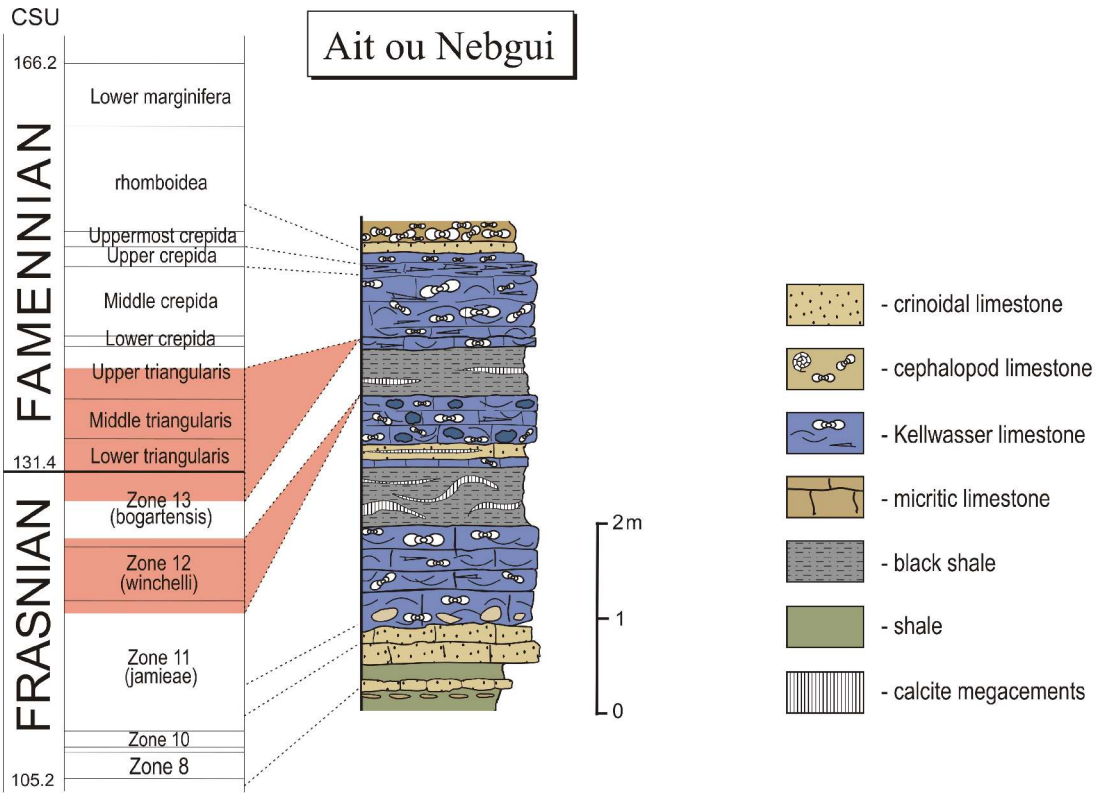

Fig. 18. Lithology and stratigraphy of the Upper Devonian at Ait ou Nebgui. Note the occurrence of white calcite megacements that are probably related to subaerial exposure during the late Frasnian and the early Famennian.

Fig. 19. Details of the Frasnian-Famennian contact (arrowed) in the Ait ou Nebgui section. The stratigraphic gap comprises an interval of four conodont zones.

represented by cephalopod packstone with very abundant, well-preserved ammonoids and orthoconic nautiloids. Deposition of black, organic-rich sediments terminated within the *rhomboidea* Zone, with a layer of cephalopod packstone bearing very abundant cheiloceratids. Overlying is a thin layer of red crinoidal packstone, followed by brown-coloured cephalopod wackestone. The latter is extremely rich in cheiloceratids and form a characteristic unit occurring consistently above the Kellwasser sediments in the Anti-Atlas (BELKA et al., 1999).

Lahmida

The section is situated in the southern part of the Rheris Basin, about 12 km northwest of Erfoud (Fig.12). The Upper Devonian succession crops out along the dry river bed of Rheris, south of the Lahmida Barrage (Loc. LH in Tab. 1 and Loc. 14 in WENDT & BELKA, 1991). The strata dip monoclinal to the SE (Fig. 20). The succession is represented by basinal deposits and differs strongly in stratigraphy, lithology and biota from those of the carbonate platforms in the Anti-Atlas. It is about 65 m thick and consists mainly of monotonous shales with numerous marly interbeds and concretion horizons. In the upper part, a thick complex of yellow-coloured nodular limestones occurs. Black shales, which constitute the major part of the shaly succession, start in the lowest Frasnian (conodont Zone 1) and range up to the *rhomboidea* Zone of the Famennian (Fig. 21). According to WENDT & BELKA (1991), these shales represent the Kellwasser facies in the Rheris Basin. In the Frasnian part, they are interrupted by three intervals with yellowish micritic limestones and/or greenish shales. Black marly interbeds and concretions, chiefly

mudstones in texture and mostly diagenetic in origin, are finely laminated and do not show any traces of bioturbation. In some levels, especially in the Famennian, discoidal concretions attain considerable dimensions, with more than one m in diameter and up to 50 cm in height (Fig.22). Macrofossils, which are extremely frequent in the Kellwasser deposits on the carbonate platforms in the Anti-Atlas, are very rare. They are represented by small-sized cephalopods (ammonoids and orthoconic nautiloids) that are restricted to the marly interbeds and concretions. Sporadically, they are accompanied by small brachiopods. Less abundant and poorly preserved but generally larger in size are ammonoids, occurring in the light-coloured carbonate complexes. A very rich macrofauna occurs in the section only within two concretionary horizons of the Uppermost *crepida* Zone and the lowest marly interbed of the *rhomboidea* Zone. These three levels are also

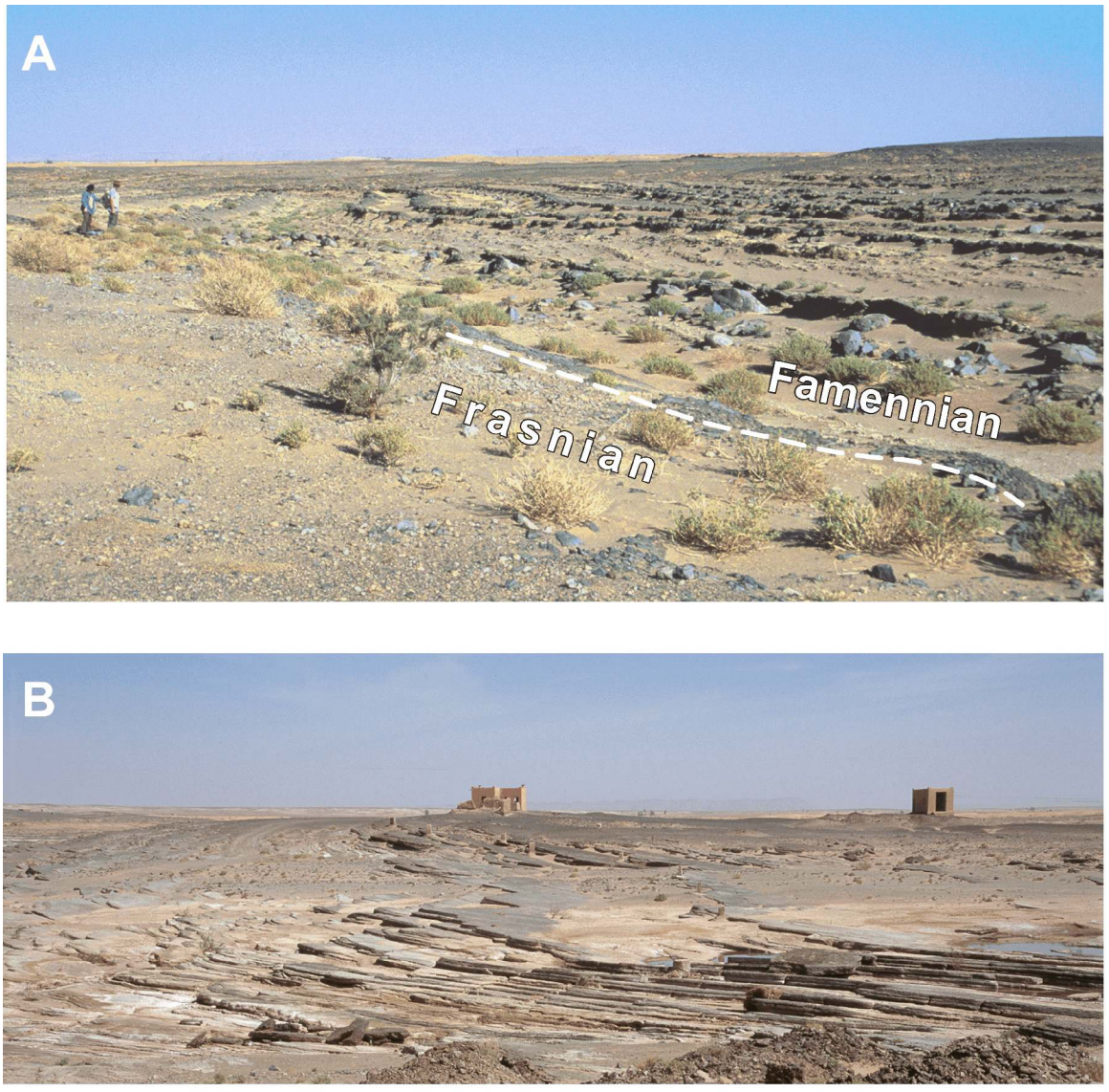

Fig. 20. Exposures of the Upper Devonian at Lahmida. **A** - Photograph showing the lower Famennian shaly sequence and the position of the Frasnian/Famennian boundary. **B** - Photograph showing the thick complex of the Famennian nodular limestones.

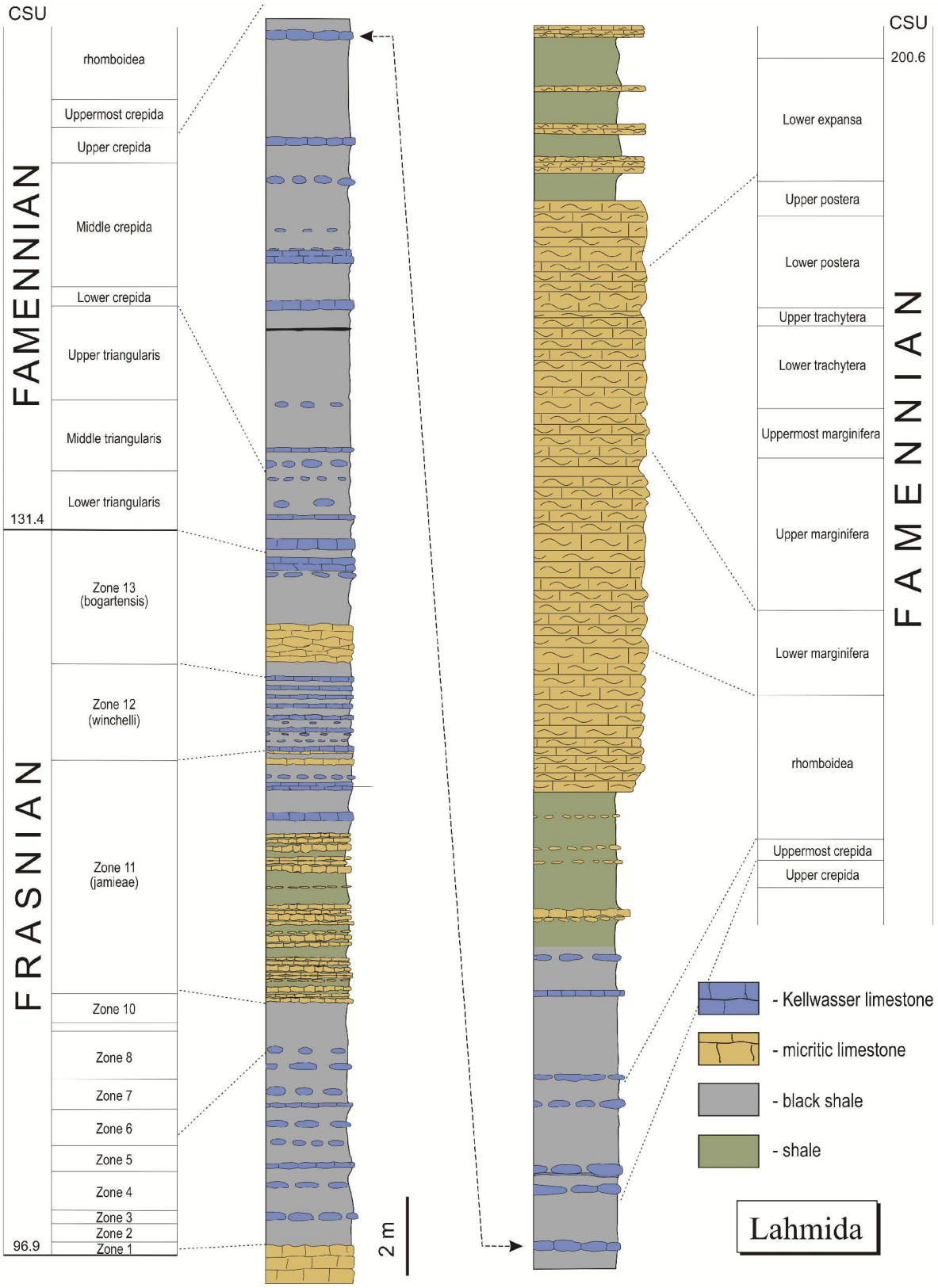

Fig. 21. Lithology and conodont stratigraphy of the Upper Devonian succession at Lahmida.

Fig. 22. Upper view of marly interbed with large concretions within the shaly Kellwasser facies (Uppermost *crepida* Zone) at Lahmida.

very productive for fish remains and conodonts. The latter are also frequent in the Frasnian light-coloured carbonates but significantly less abundant in the black Kellwasser facies. It is remarkable that conodonts are virtually absent in the interval from the base of the Famennian up to the Upper *crepida* Zone as well as in the uppermost part of the succession, above the Upper *marginifera* Zone. Other microfossils are represented by styliolinids, very abundant in particular within the lowest Frasnian black shale interval, and ostracods distributed throughout the whole section.

9.2 Moroccan Meseta

The Moroccan Meseta forms the westernmost termination of the Variscan Belt. It is bordered by the High Atlas chain in the south and the Rif Mountain in the north. The NE-SW trending Tertiary fold belt of the Middle Atlas subdivides the Meseta into a western and an eastern (Oran) part (Fig. 13). The Western Meseta is composed of three major Paleozoic massifs: the Massif Central, Rehamna and Jbilete, whereas numerous smaller units, such as the Jerada, Debdou, Mekkam and the Midelt Massif are located in the Eastern Meseta (PIQUÉ & MICHARD, 1989). The exposed Paleozoic succession ranges in age from the Cambrian to the Westphalian. It is strongly deformed due to a NW-SE compression, resulting from the collision of Gondwana with Euramerica during Late Carboniferous time. The numerous NE-SW trending folds have been thrusted predominantly in the NW direction and intruded by Carboniferous granitic plutons. The Paleozoic rocks display a thermal overprint that ranges from supramature level to metamorphic amphibolite facies. In general, the older the rocks the higher is the level of thermal maturation. There is also a regional trend of increasing of deformation and metamorphism towards the west.

Devonian rocks investigated during the present study have been collected in the Mrirt nappe, which is a part of the Kenifra-Azrou tectonic unit located at the eastern margin of the Moroccan Massif Central. The Mrirt nappe includes an Ordovician to Carboniferous sedimentary sequence overthrusted on the autochthonous unit of Tandara-Bou Tazart (HUVELIN, 1970, 1973; ALLARY et al., 1972, 1976; BOUABDELLI, 1989). Because of lack of detailed information regarding stratigraphy, facies, and tectonics, the original location of the Mrirt nappe sequence remains unknown. Moreover, the time of its emplacement cannot be defined with precision at the moment. WALLISER et al. (1999) suggested a time interval between the lower Visean and the Westphalian/Stephanian and interpreted the Mrirt unit as a gravitational nappe. Ordovician clastic rocks cover the most area of the unit and are locally overlain by scattered fragments of the Silurian to Visean sequence (BOUABDELLI, 1989). Devonian rocks occur at three localities (Gara de Mrirt, Anajdam, and Touchchent), where they display a similar lithological development.

9.2.1 Lithology and stratigraphy

Upper Devonian rocks were sampled from the Gara de Mrirt succession, which is exposed in numerous sections at the southern slope of the Gara de Mrirt, about 5 km southeast of Mrirt (Fig. 13). There are two allochthonous, imbricated thrust units involving Middle Devonian to Visean sediments. The Upper Devonian, which is most resistant to weathering within the sequence, builds two distinct morphological cliffs. The section Gara de Mrirt was described for the first time by TERMIER (1936), and subsequently investigated by several authors (HOLLARD et al., 1970; BOUABDELLI, 1989; LAZREQ, 1992, 1999; WALLISER et al., 1996; JOACHIMSKI et al., 2002). During the present study the samples were collected in the lower cliff (Fig. 23), very close to the section line of LAZREQ (1992, 1999). The sampled interval ranges from the Frasnian conodont Zone 10 to the Lower triangularis Zone of the Famennian (Fig. 24). The sequence is about 4 m thick and consists predominantly of gray micritic to bioclastic limestones, mudstone to wackestone in texture, which alternate with gray shales. Their macrofauna is represented by rather rare ammonoids that become more frequently in the upper part of the sequence. The Lower Kellwasser horizon is a 25 cm thick layer of black wackestone that comprises most of the conodont Zone 12 (*winchelli*), whereas the Upper Kellwasser horizon is developed as lenses and layers of black limestone, alternating with black shales. Conodonts sampled during the present study reveal that the deposition of black Upper Kellwasser sediments did not terminate at the Frasnian-Famennian boundary, as reported by LAZREQ (1992, 1999) and adopted by other authors, but it continued into the Famennian (Fig. 24). The uppermost black carbonate layer contains a

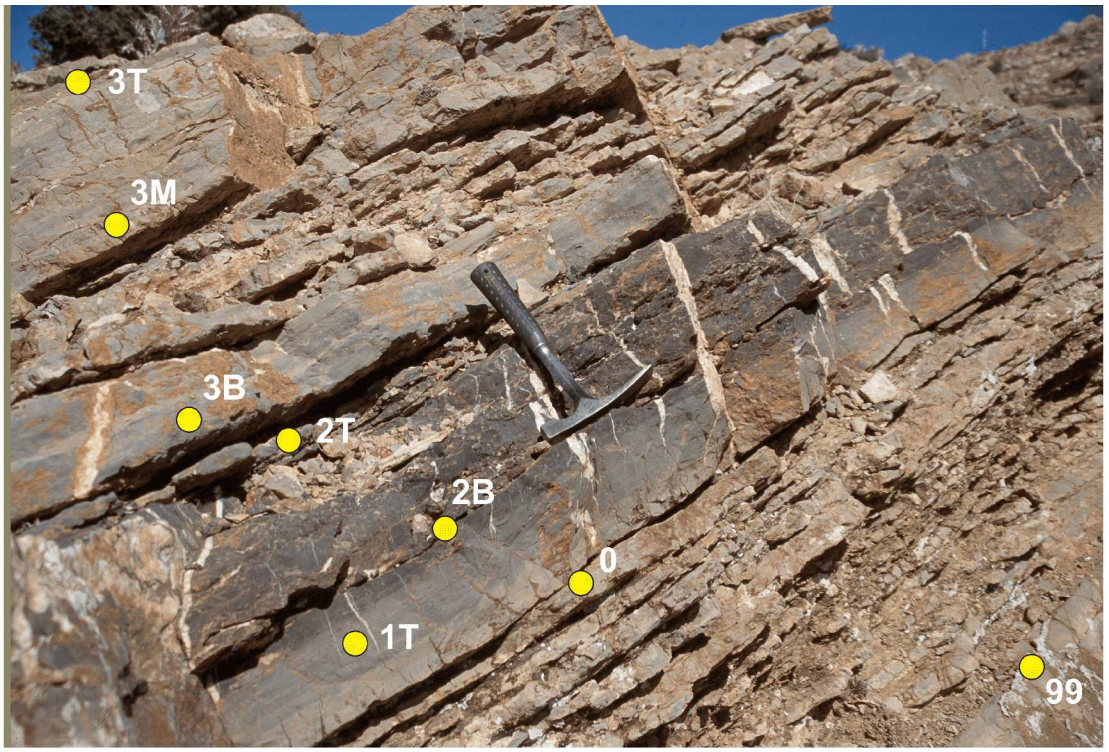

Fig. 23. Exposure of the upper Frasnian 1 km north-west of the village Bou Ounabdou, showing the position of conodont samples within the section at Gara de Mrirt (MR). The dark layer in the central part of the sequence is the Lower Kellwasser horizon.

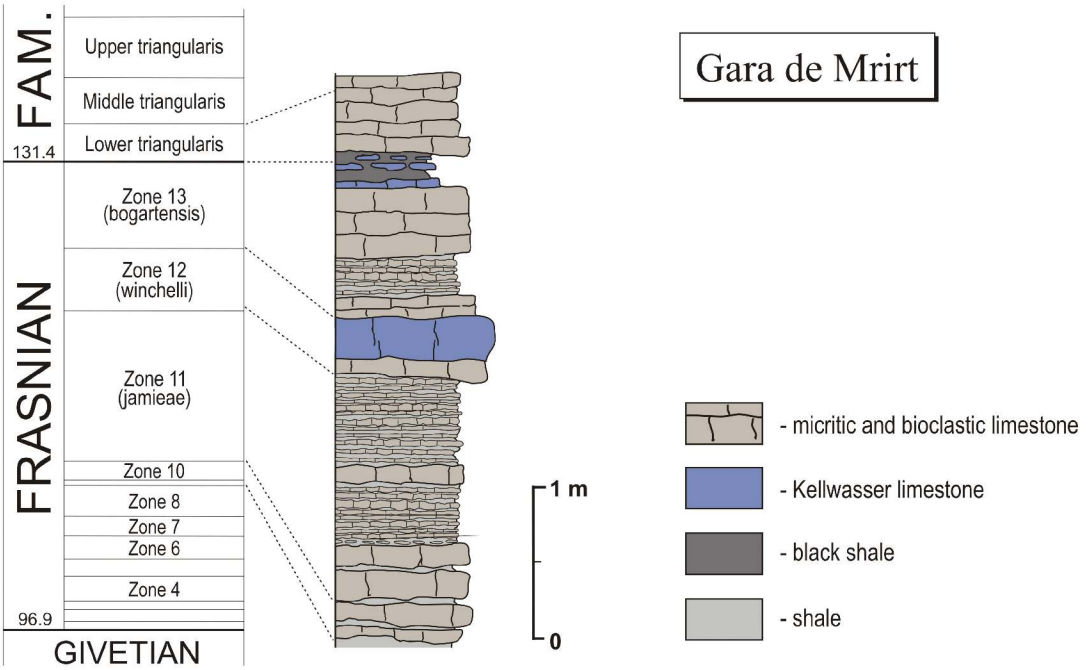

Fig. 24. Lithology and stratigraphy of the Frasnian and the lowest Fammenian at Gara de Mrirt. Note that the Frasnian-Famennian boundary lies within the Upper Kellwasser horizon. Conodont stratigraphy after Belka (unpublished data).

fauna characteristic for the Lower *triangularis* Zone. Both Kellwasser horizons yield a very similar fauna, dominated by *Buchiola* (bivalve) and styliolinids accompanied by less frequent orthoconic cephalopods and rare ammonoids.

9.3 Montagne Noire

The Montagne Noire belongs to the Variscan structures of the French Massif Central (Fig. 25). Along with the domains of Cevennes and Albigeois, it constitutes the southern, external margin of the Variscan Belt in France (e.g. MATTE, 1991; LEDRU et al., 1994). The Montagne Noire is subdivided into three ENE-WSW elongated tectono-metamorphic units: (1) the northern thrust zone represented by Cambrian to Silurian strata, overfolded towards SW and metamorphosed, (2) the central metamorphic core (Zone Axiale) composed of Proterozoic to Cambrian gneisses and schists, and (3) the southern zone composed of a pile of southward facing, recumbent fold nappes with very low-grade or even non-metamorphic Cambrian to Carboniferous rocks (FEIST et al., 1994 and references therein). In addition, there are several granitic intrusions of both pre-Variscan and Variscan age that were emplaced into the northern and central zones (Fig. 25). The southern nappe complex, which comprises the parautochthonous Faugères Nappe (Devonian and Carboniferous), the Mont Peyroux and Minervois nappes (Ordovician to Carboniferous), and the Pardailhan Nappe (Cambrian to Devonian), was formed as a result of complex, polyphased

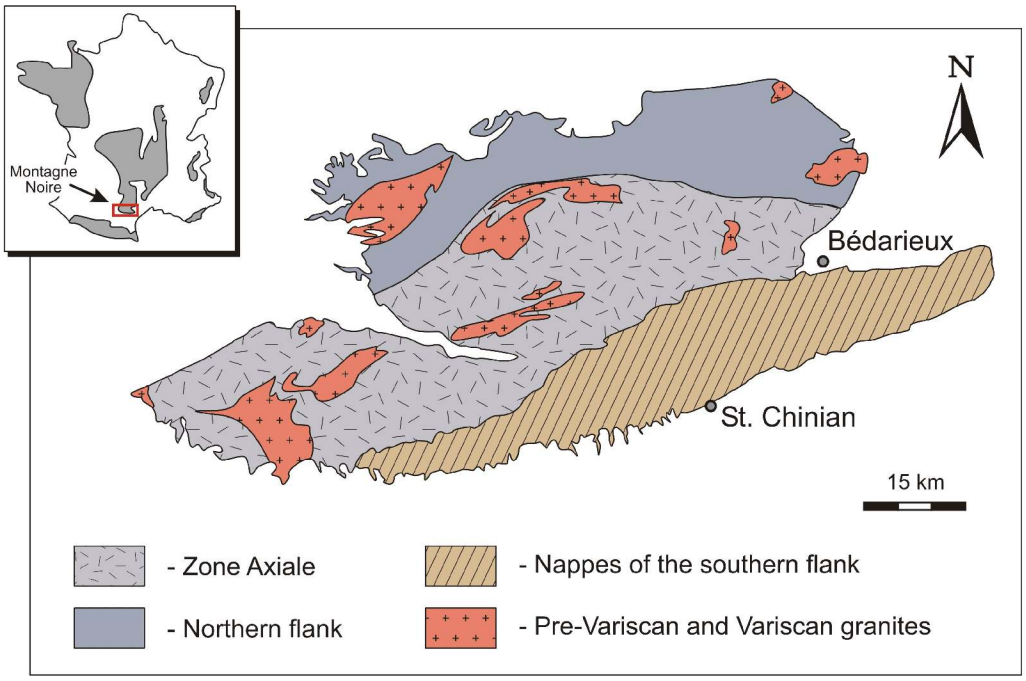

Fig. 25. Schematic geological map showing the tectonostratigraphic units of the Montagne Noire. Inset with Paleozoic massifs of France and location of the Montagne Noire (after Wiederer et al., 2002, simplified).

Variscan deformation (see for summary WIEDERER et al., 2002). The thick sequence of the Visean-Namurian flysch sediments with large olistoliths ("Éscailles de Cabrières"), occurring in the eastern part of the Mont Peyroux Nappe, points to an external position of the Montagne Noire within the orogen. Both the gravitational synorogenic transport of the detritus and the tectonic nappe movement exhibit the same direction towards the south (ENGEL et al., 1982).

Palaeomagnetic and stratigraphic data from slightly metamorphic or non-metamorphic rocks in the southern zone permit to sketch the paleogeographic evolution of the Montagne Noire during Paleozoic time. Early Paleozoic fauna and sedimentary evolution are characteristic for the NW Gondwana margin (FEIST et al., 1994). Recently, NYSÆTHER et al. (2002) showed that the Montagne Noire was still attached to the Gondwana margin during the Mid-Ordovician. They also suggest that Armorica (sensu MATTE, 2001) had rifted off the NW Gondwana by the Late Ordovician. The intervening ocean is supposed to be only a few hundred kilometres wide. Subduction beneath Armorica started probably in the Early Silurian and the subsequent collision with the northern Massif Central took place during the Emsian. In contrast to this scenario, TAIT et al. (2000) postulated a wide ocean (2000-4000 km) between Armorica (including the Montagne Noire) and Gondwana from Late Ordovician to Late Devonian times.

Devonian rocks occur exclusively in the southern Montagne Noire, within the Mont Peyroux and Minervois nappes (Fig. 26). The succession is nearly continuous and almost entirely composed of carbonates. Although there are some differences in facies and stratigraphy between the Devonian of the nappes and of the Cabrières area, a clear upward trend from shallow-water neritic carbonates and clastics to pelagic carbonates can generally be observed. In the last decades, much attention was drawn to fauna and stratigraphy of the Upper Devonian sequence. In consequence, a high-resolution biostratigraphical framework, based predominantly on conodonts,

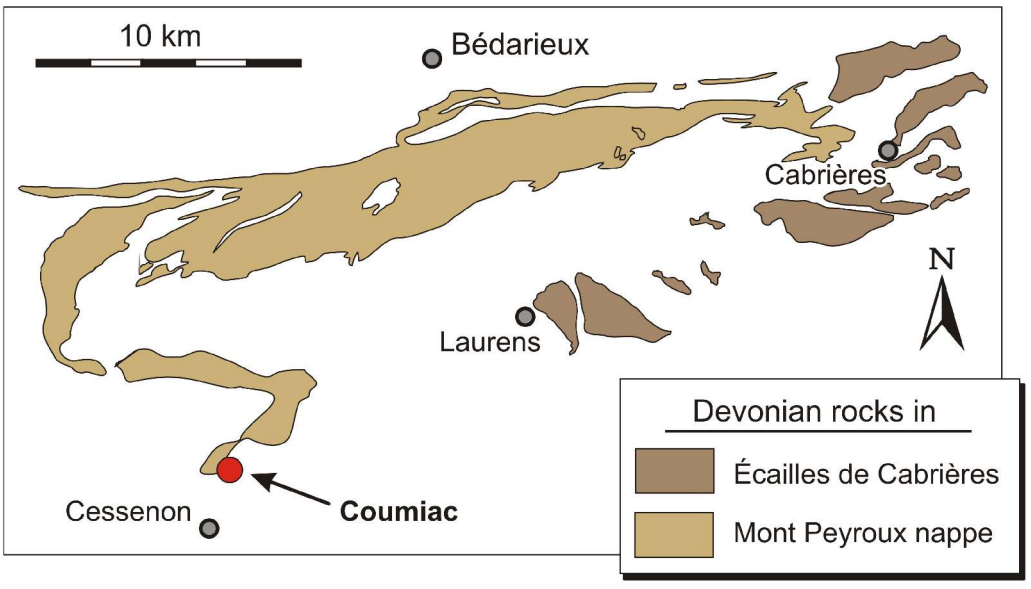

Fig. 26. Map showing outcrops of Devonian rocks in the southeastern part of the Montagne Noire and location of the Coumiac section (modified from House et al. 1985).

was established (for review, see FEIST, 2002). Contrary to that, detailed sedimentological work was rare (e.g. TUCKER, 1974). In the course of the present study, conodont samples were collected from the Upper Devonian sequence of Coumiac, where the Frasnian-Famennian stage boundary has been defined (KLAPPER et al., 1993).

9.3.1 Lithology and stratigraphy

The Upper Devonian sequence of Coumiac belongs to the Mont Peyroux Nappe (Fig. 26). It crops out in two small marble quarries situated north of the local road D 136 from Cessenon to Causses-et-Veyran, opposite the abandoned farm house "Coumiac" (Fig. 27). The Upper Coumiac Quarry (Loc. CO in Tab. 1), sampled during this study, is located about 400 m north of the road and 200 m west of the farm house "Les Granges". The section is composed of almost vertical dipping strata that comprise a continuous carbonate succession from the Zone 5 (Frasnian) up to the *marginifera* Zone (Famennian). The conodont record has been described in detail in numerous publications (FEIST, 2002; and references therein).

The sampled interval ranges from the Upper Frasnian (Zone 12) to the *rhomboidea* Zone of the Famennian (Fig. 27). This part of the sequence is exposed in the southeastern part of the quarry. In terms of lithostratigraphy, it comprises the upper part of the Coumiac Formation and the lower part of the Griotte Formation. The Frasnian consists of well-bedded, pink bioclastic mudstones and wackestones (Fig. 27). There are some iron crusts that mark episodes of very slow sedimentation (FLAJS in BECKER et al., 1989). Fossils are moderately frequent and represented by ammonoids, nautiloids, conodonts, trilobites, fish remains, ostracods, dacryoconarids, brachiopods, bivalves, gastropods and crinoid ossicles. The Frasnian succession is interrupted in its upper part by two dark grey to black limestone horizons (Fig. 27), which are regarded as equivalents of the Lower and Upper Kellwasser Limestone of the Rhenohercynian belt in Germany. In the Coumiac section, these horizons form the uppermost parts of the conodont zones 12 and 13, respectively. The Frasnian-Famennian boundary is drawn just above the Upper Kellwasser horizon. The Upper Kellwasser horizon is black and characterized by organic content up to 2.3 % (WENDT & BELKA, 1991), whereas the lower horizon is light grey and seems to yield a low organic content. Their macrofauna is composed of nektonic (ammonoids) and planktonic (pteriomorph bivalves, homoctenids) organisms; benthic forms are very rare. Conodonts are extremely abundant in both horizons, but there is a peculiar difference in the composition of the fauna between the upper and the lower horizon. Palmatolepids, which represent the dominant group of elements both in the Upper Frasnian and in the Famennian, are very frequent in the upper horizon but they are almost lacking in the lower one. The Famennian succession starts with

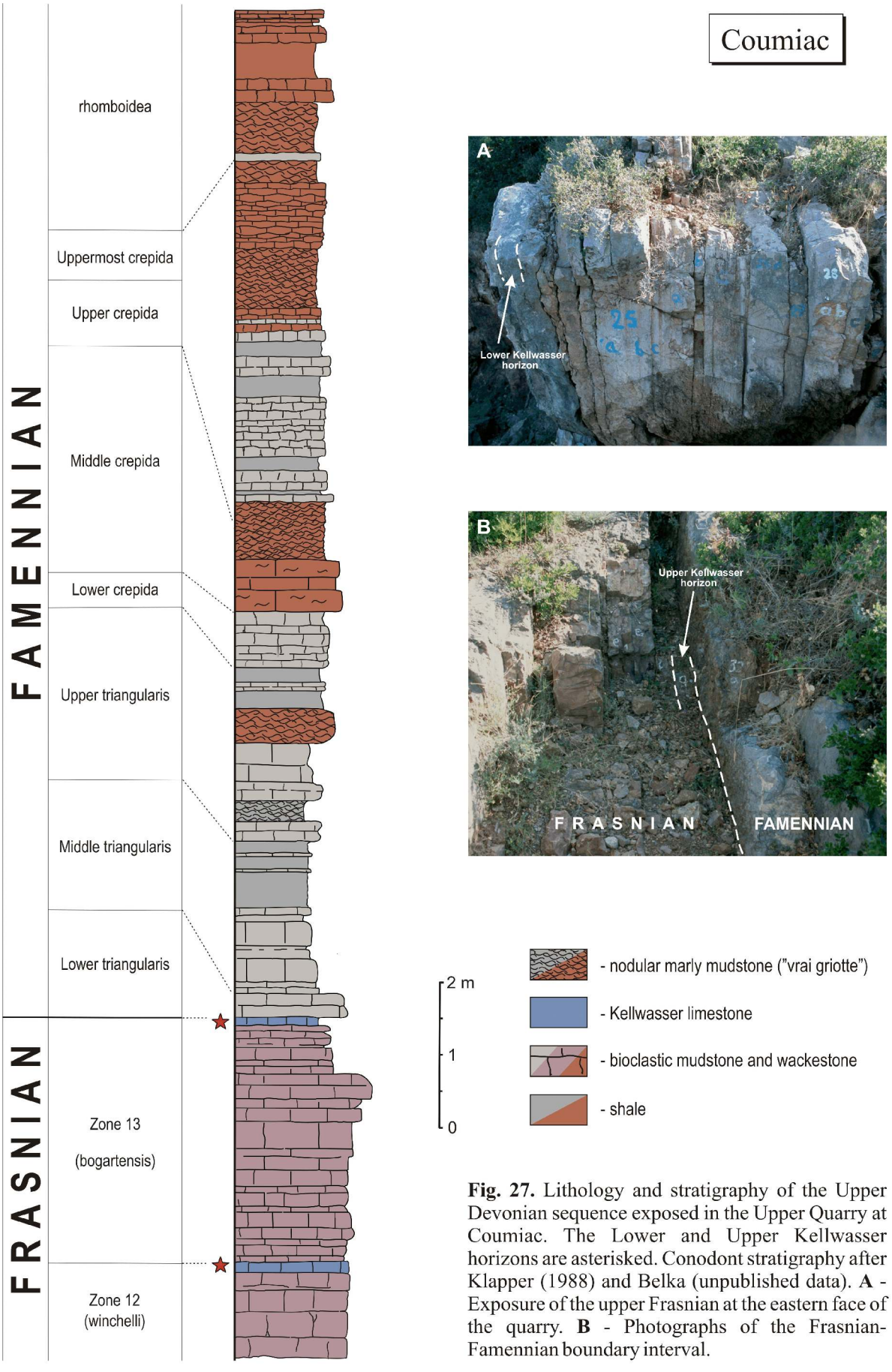

Fig. 27. Lithology and stratigraphy of the Upper Devonian sequence exposed in the Upper Quarry at Coumiac. The Lower and Upper Kellwasser horizons are asterisked. Conodont stratigraphy after Klapper (1988) and Belka (unpublished data). **A** - Exposure of the upper Frasnian at the eastern face of the quarry. **B** - Photographs of the Frasnian-Famennian boundary interval.

alternating grey and brick-red, partially nodular wackestones and mudstones, which are intercalated with shales. The macrofauna is rather rare in this part of the section. Overlying are brick-red nodular, marly mudstones (“vrai griotte”) interbedded with red shales. Small cheiloceratids are noted to occur very abundantly in the carbonate nodules.

Tucker (1974) noticed that the sequence does not contain any univocal sedimentary features and, in fact, only the fauna points to pelagic depositional conditions. According to FEIST (2002), the upper Frasnian carbonates were deposited on a carbonate ramp, whereas the lower Famennian is interpreted to represent a slope environment. During the present study, however, no sedimentary features that could testify a slope or a carbonate ramp were observed in the section.

10 Results

10.1 Nd systematics of conodonts

10.1.1 Nd concentration

Although there is already more than a dozen publications providing Nd data from conodonts, the systematics of Nd and other REEs in conodont elements is still poorly understood. This is mainly because samples with different types of conodont material were used in the previous studies, making a systematic comparison of data difficult. Measurements of the Nd and other REE contents in conodont elements were mostly performed on bulk samples, i.e. containing discrete elements of various species with a wide variety of shapes (e.g. WRIGHT et al., 1984; KETO & JACOBSEN, 1988; MARTIN & MACDOUGALL, 1995; HAUNOLD et al., 1999; FANTON et al., 2002). There are only few data for monospecific samples (e.g. WRIGHT et al., 1987; BERTRAM et al., 1992) and just first surveys of the REE distributions in individual conodont elements (GRANDJEAN & ALBARÉDE, 1989; GRANDJEAN-LÉCUYER et al., 1993; GIRARD & ALBARÈDE, 1996). Another difficulty in evaluation and comparison of published data results from different analytical procedures and measurement techniques applied in the studies. Nd concentrations of bulk conodont samples were determined by neutron activation analysis or by isotope dilution mass spectrometry (IDMS), whereas individual elements were analysed by secondary ion mass spectrometry (SIMS) or by inductively coupled plasma emission spectrometry (ICP-MS). GRANDJEAN & ALBARÉDE (1989) showed that REE distributions in fish teeth measured with an ion probe and IDMS were mutually consistent. However, the ICP-MS method seems to provide higher REE concentrations than those obtained by secondary ion mass spectrometry. GRANDJEAN-

LÉCUYER et al. (1993) used the SIMS method and obtained Nd concentrations in individual conodont elements from the Coumiac Quarry ranging between 11 and 69 ppm, whereas GIRARD & ALBARÈDE (1996) measured conodont elements, recovered from the same layers, by ICP-MS and received significantly higher values, mostly from 50 to 500 ppm. Some palmatolepid elements displayed Nd concentrations even higher than 1000 ppm (max. ~3200 ppm). Unfortunately, the authors did not give any explanation for this discrepancy. It is unlikely that chemical processing of samples or variations in Nd distribution related to histology of conodont elements are responsible for such systematic difference in the Nd contents; problems in the analytical technique are much more probable.

In summary, previous work has shown that conodonts display a wide range in Nd concentrations, from tens of to more than a thousand ppm. There is, however, a difference that conodont crowns have low Nd concentrations whereas basal bodies have very high contents (PIETZNER et al., 1968; HOLMDEN et al., 1996). A wide range of REE concentrations is also characteristic for recent fish debris and results from differential exposure times at the sediment-water interface (WRIGHT et al., 1987). Thus, REE concentrations in recent biogenic apatites provide a general gauge of sedimentation rates. Recently, HAUNOLD et al. (1999) postulated the same relation also for REEs in conodonts.

Productive conodont samples contain commonly numerous elements that belong to several different species. Because each conodont animal bore an apparatus composed of various elements different in morphology, it is quite common that several dozens of different discrete elements can be found within a single sample. Therefore, when "multielement" samples are used in geochemical and isotopic studies, it is important to know whether geochemical characteristics of a single element (or elements belonging to one species) are similar to geochemical signatures of other elements in the sample or not. In order to recognize the Nd elemental and isotopic systematics in conodont elements and to test the homogeneity of the Nd isotopic signatures of individual samples, more than a hundred samples were investigated during the present study. Measurements were performed separately on different conodont elements present in the same sample, or elements having identical morphology were picked up and analysed together.

The results confirm earlier observations that conodont fluorapatite contains significant amounts of Nd and that there is no correspondence between the Nd isotopic composition and the Nd concentration (Fig. 28). Conodont crowns are characterized by Nd concentrations ranging from 25 to 280 ppm, whereas complete elements with basal fillings display Nd concentrations higher than 200 ppm (up to 820 ppm). Basal fillings were not separately measured but it is evident from theses data that basal fillings, which have smaller volume than crowns, must exhibit Nd concentrations of up to > 1000 ppm. In the investigated material, conodonts with basal fillings show a narrower range of ε_{Nd} values than crowns do. This is because the former were available

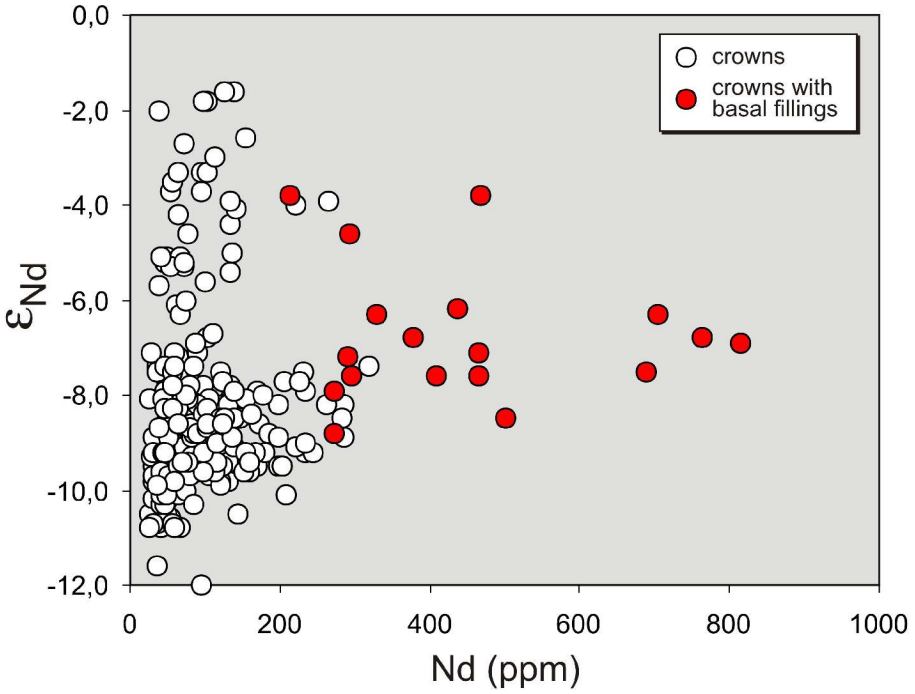

Fig. 28. The Nd concentration in Late Devonian conodonts compared to their Nd isotopic composition. Note the very high Nd content in all complete conodont elements (with basal fillings).

from the Sudetes and southern Poland only, where isotopic signatures of all conodonts fluctuate between -4 and -9.

The Nd concentration varies significantly within each conodont sample but different elements in the sample show identical Nd isotopic compositions (Figs. 29-30). The variation of ε_{Nd} values within individual samples is small, about ± 0.20 epsilon units on average. In fact, each individual conodont element present in the sample has a different Nd content, which is not related to taxonomy. Elements that formed the same apparatus and thus represent one species differ in their Nd concentrations. BELKA et al. (2000) showed that the Nd concentration in the conodont crowns depends on their morphology. The higher the surface/volume ratio of elements the higher is their Nd content. New data from more than hundred samples support these conclusions and, in addition, they also reveal some minor effect of rapid burial on the Nd content. Wide palmatolepids, for instance, display concentrations up to 275 ppm, whereas ancyrodellids, bispathodids, and narrow palmatolepids contain less than 150 ppm of Nd. The relation between the shape of conodont elements and their Nd content is depicted in Figure 31. It is, however, important to note that conodonts recovered from basinal sediments deposited at high sedimentation rates (e.g. from the section Lahmida) yield generally lower Nd concentrations than those recovered from limestones deposited on carbonate platforms. The fact that conodont elements with a given shape achieved a similar content of Nd proves the presence of a saturation limit for fluorapatite tissue exposed to seawater. This saturation level has apparently been attained

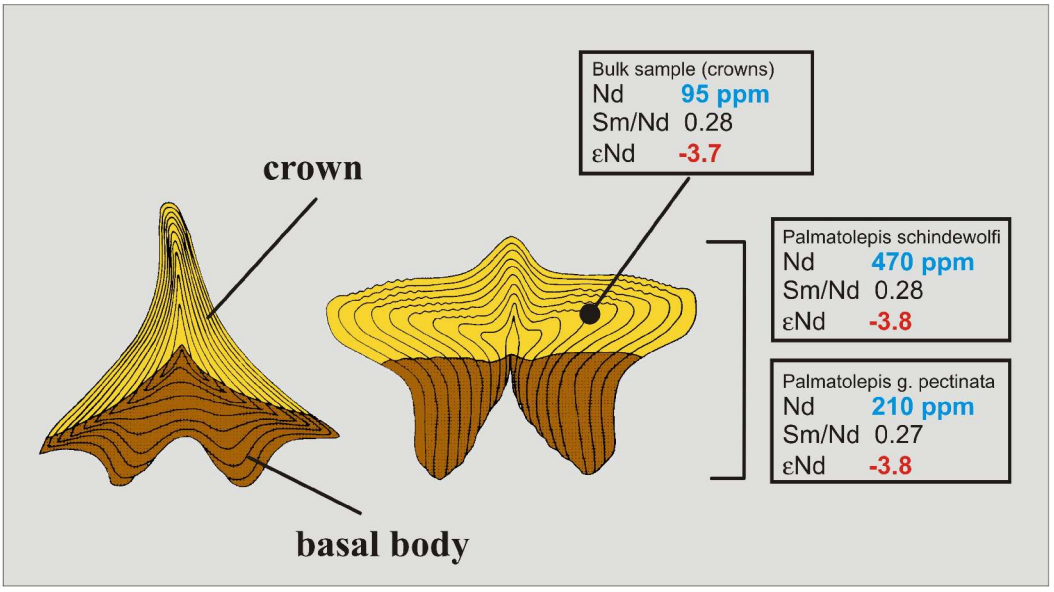

Fig. 29. Nd systematics of conodont elements from a single sample (Lower *marginifera* Zone, Famennian; Holy Cross Mountains). Note the uniform ε_{Nd} values and Sm/Nd ratios in the entire sample, but differring Nd contents (see text for explanation). Schematic structure of conodont elements modified from Sweet (1988).

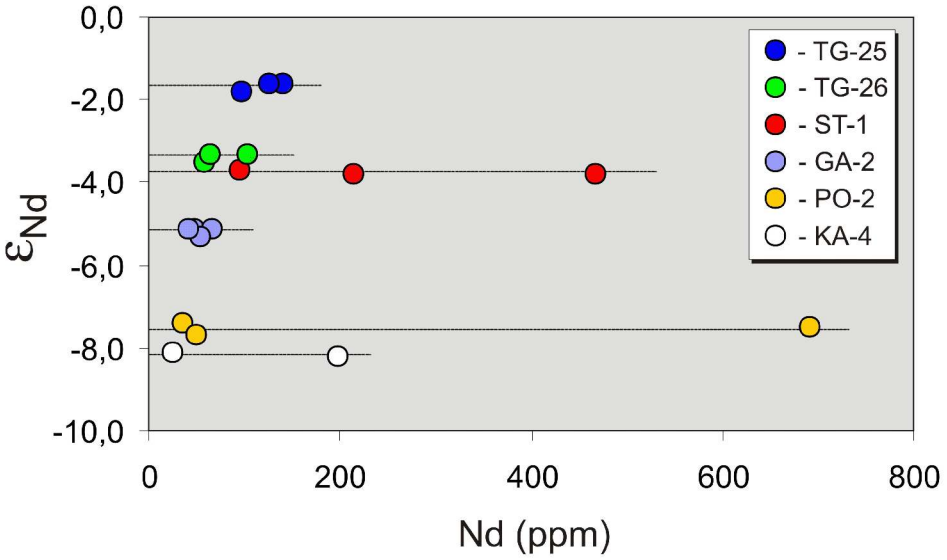

Fig. 30. Variation of Nd concentration in conodonts within individual samples. Note the wide range of Nd concentration within a single sample but uniform Nd isotopic composition of all elements. The horizontal lines indicate the mean ε_{Nd} value for each sample. For more information on samples see Tab. 6.

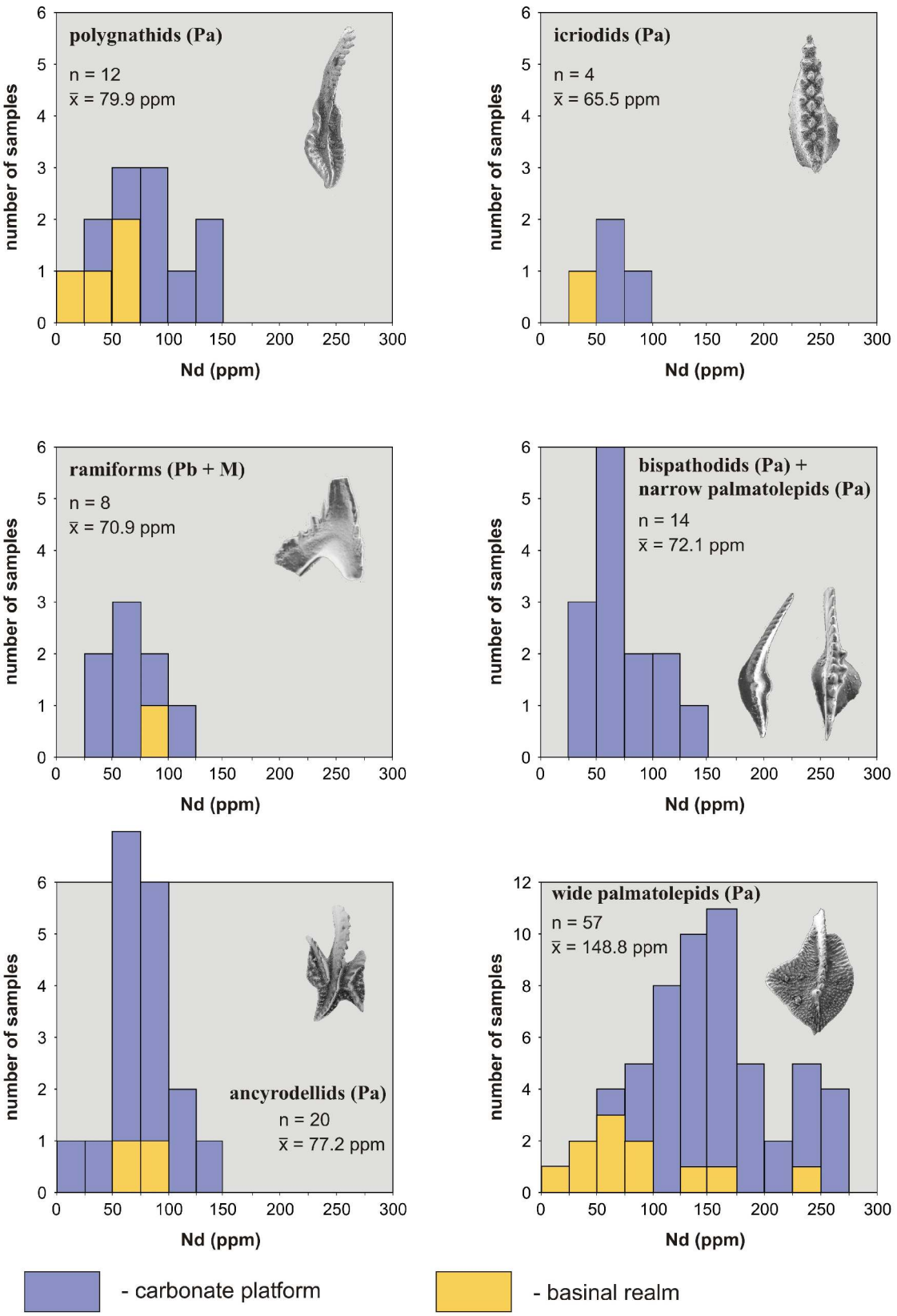

Fig. 31. Histograms of Nd concentration in Late Devonian conodonts. Pa elements of palmatolepids exhibit much higher concentrations than those of other genera and ramiforms. Note that conodonts collected from basinal deposits display generally very low Nd contents. For more information on samples see Tab. 2 and 6.

in most cases on the carbonate platform but less frequently in the basinal realm. This strongly indicates that conodont elements must have acquired their Nd prior to burial while they were still in contact with seawater and that an additional incorporation of Nd during burial was negligible. According to STAUDIGEL et al. (1985), the REE uptake during burial is hindered due to limited availability of REEs in the pore waters. On the other hand, the REE uptake during the postmortem exposure on the sediment surface must have occurred during very short geological time because otherwise the Nd content of conodonts would chiefly be related to sedimentation rates and not to their shapes.

It is concluded that the concentration of Nd varies widely within each multielement conodont sample; it is specific for any given element morphology. Thus, the Nd concentration of the multielement conodont samples reflects chiefly their histological and morphological composition. Therefore, the Nd content of multielement conodont samples cannot be used as an indicator of sedimentation rates as suggested by HAUNOLD et al. (1999).

10.1.2 Prediction of Nd concentration in conodonts

The fact that the Nd content in conodont elements depends on their morphology is very helpful for isotopic analysis. In the isotope dilution method the most accurate determination of element concentration is obtained if the measured isotopes in the sample-spike mixture have similar abundances (Dickin, 1995). This can be achieved when an appropriate amount of spike is added to the sample. If the Nd content of the sample is already roughly known, the optimum amount of spike can be calculated. This way the number of samples that are incorrectly spiked and therefore must be analysed a second time is extremely low.

An approximation of the Nd concentration in conodont samples is possible by a simple optical examination of conodont morphology under a microscope. Moreover, no detailed knowledge of the conodont taxonomy is necessary for such examination. During the present study, the morphological composition of conodont samples was systematically examined in the micropaleontological laboratory of the University of Halle. The predicted values were subsequently used in the isotopic laboratory at Giessen to calculate the optimum amount of spike. Figure 32 illustrates the accuracy of this method. In the majority of samples the difference between predicted and measured Nd concentrations was below 40 ppm. Only for a very few samples, in which probably some small fragments of basal bodies remained undetected, the measured Nd concentrations significantly exceeded the expected values. Experience also shows that the accuracy of the predicted values is higher for samples in which only conodont elements of identical morphology were selected for analysis.

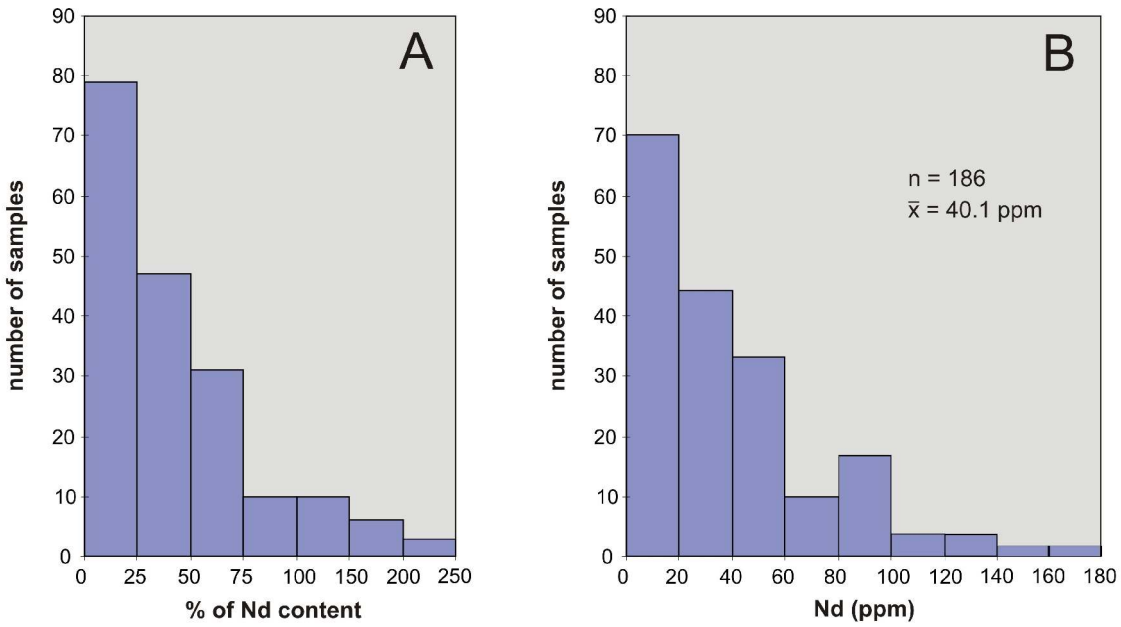

Fig. 32. Prediction of the Nd content in conodonts from morphology of conodont elements. Diagrams show deviation of predicted values from the measured Nd concentrations in percent (A) and in ppm (B).

10.1.3 REE patterns of conodonts

Several studies have already documented that REE patterns of conodonts do not resemble those of present-day seawater and modern biogenic phosphates (e.g. WRIGHT et al., 1984, 1987; GRANDJEAN-LÉCUYER et al., 1993; ARMSTRONG et al., 2001). Conodonts typically show a "bell-shaped" REE distribution with a strong HREE depletion, less depletion of LREE, and a maximum near Eu-Gd. Ce and Eu anomalies are absent. The "bell-shaped" REE pattern is characteristic for all biogenic phosphates older than the Cretaceous and was also observed in some Tertiary fish remains (WRIGHT et al., 1987; GRANDJEAN-LÉCUYER et al.,1993; GIRARD & ALBARÉDE, 1986). It seems, therefore, that REE distributions in pre-Cretaceous seawater, unlike in modern oceans, were not controlled by surface biological activity. Inorganic processes must rather have been responsible for the REE behaviour in ancient oceans. GRANDJEAN-LÉCUYER et al. (1993) proposed a selective uptake of LREE controlled by adsorption/desorption on inorganic particles as a possible mechanism. KIDDER & EDDY-DILEK (1994) argued for the primary nature of the "bell-shaped" REE distribution patterns in phosphatic nodules. Conversely, REYNARD et al. (1999) suggested that "bell-shaped" pattern can be explained by recrystalization in the presence of fresh or oceanic water during extensive diagenesis and therefore should not be used for reconstruction of the REE distribution in ancient seawater. Recently, ARMSTRONG et al. (2001) interpreted the "bell-shaped" patterns of conodonts as the result of adsorption during early

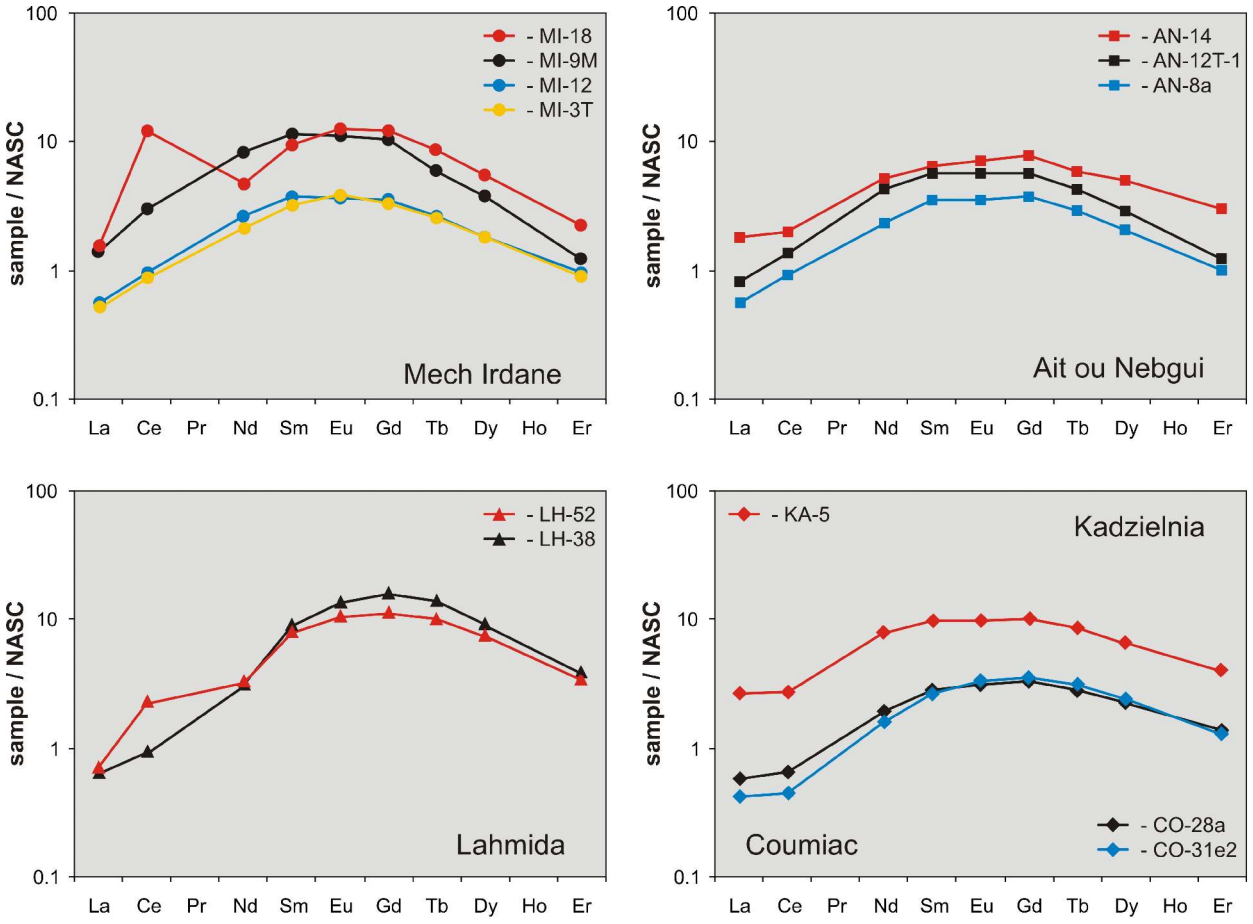

Fig. 33. REE abundances in the investigated Late Devonian conodonts, normalized to the North American shale composite (Gromet et al., 1984).

diagenesis, thus possibly reflecting original seawater chemistry. They also showed that REE abundances in conodonts decrease with increasing thermal alteration, whilst the"bell-shaped" patterns remain stable.

In the present study, the whole spectrum of REEs was investigated in eleven conodont samples (Tab. 7 and Fig. 33). Although the absolute REE concentrations in conodonts vary significantly, the shale-normalised patterns are relatively homogeneous, "bell-shaped" and very similar to those known from the literature. It is remarkable that REE distribution patterns of conodont samples taken from the same locality are more homogenous than those of samples from different localities. Moreover, conodonts from the Anti-Atlas display a slightly stronger enrichment in MREE than conodonts from the Montagne Noire and the Holy Cross Mountains. This can be related to local differences in original seawater chemistry. The new data, however, do not confirm the relation between the absolute REE abundance in conodonts and their thermal maturation, as suggested by ARMSTRONG et al. (2001).

10.2 Nd systematics in other biogenic apatites

In several investigated rock samples, conodont elements were accompanied by fish remains (shark teeth and fragments of placoderms), which can also be used as proxies for ancient seawater chemistry (for more details see chapter 4). Various types of phosphatic remains occurring in the same samples provide an excellent opportunity for a direct comparison of the Nd isotopic and elemental systematics in different biogenic apatites and allow to test the integrity of these proxies. It can be assumed that apatites recovered from the same sample were most probably exposed to the same bottom waters and experienced the same diagenetic alteration.

The analysed fish debris and shark teeth reveal Nd concentrations that are generally an order of magnitude higher than those of conodonts (Tab. 5). This is consistent with the results of previous studies (STAUDIGEL et al.1985; MARTIN & HALEY, 2000). No systematic relation can be recognized between Nd concentrations in different phosphates. There is, however, an obvious correlation between the Nd isotopic composition of conodonts and fish remains. The latter are generally less radiogenic than conodonts (Figs. 34-35), i.e. they exhibit lower ε_{Nd} values than those of coeval conodonts. In most cases, the deviation is lower than 1.0 epsilon unit. There are a few samples that do not fit this general trend. This is the case in the samples from the Anti-Atlas in which fish remains are more radiogenic than conodonts. Because Devonian rocks in the Anti-Atlas, display a higher thermal overprint (CAI = 4) than samples from the Montagne Noire (CAI = 2.5) and southern Poland (CAI = 1-2), it appears that thermal metamorphism influences the Sm-Nd isotopic system in shark teeth and placoderm tissue, in a similar way as it is in case of Sr already at very low thermal overprint. In the investigated material, all shark teeth and placoderm remains display $^{87}Sr/^{86}Sr$ ratios that are more radiogenic (Tab. 5) than those of coeval conodonts and of the Devonian seawater. The ε_{Nd} values obtained from the conodont material are considered to be more reliable because their fluorapatite exhibits excellent thermal stability and is less susceptible to diagenetic alteration than other biogenic apatites. Perturbations resulting from the thermal alteration can also be observed in the Sm/Nd ratios. In samples with CAI values lower than 3 different biogenic apatites show approximately identical Sm/Nd ratios within the same sample (Fig. 35). With increasing CAI, however, fish remains tend to exhibit Sm/Nd ratios slightly lower than those of conodonts.

The new data suggest that Devonian shark teeth and placoderm fragments preserve Nd signatures that in some cases approximate the ancient seawater. Contrary to previous suggestions (STAUDIGEL et al., 1985), the extremely high Nd content of these apatites does not make them impervious to diagenetic alteration. Because of apparent thermal effects on their Sm-Nd isotopic system, fossil fish remains are less suitable as tools for palaeoceanography than conodonts. Nevertheless, fossil fish remains can be useful as palaeoceanographic proxies in the Palaeozoic

shallow-water or lagoonal sediments, where conodonts are generally rare or absent.

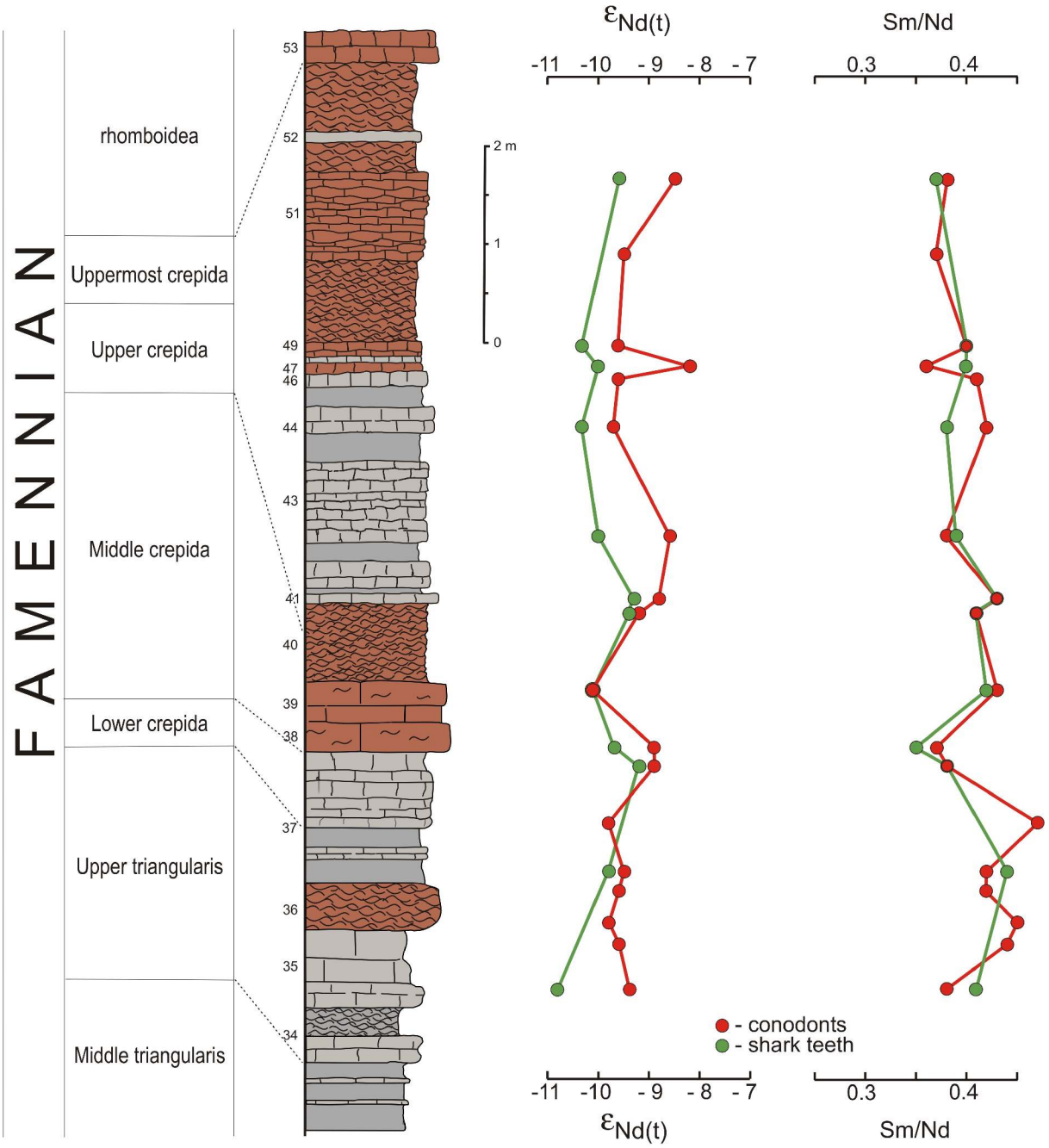

Fig. 34. Comparison of Nd isotopic compositions and Sm/Nd ratios in conodonts and shark teeth in the Famennian sequence of Coumiac. Note the consistently less radiogenic ε_{Nd} values of shark teeths compared to those of conodonts. Conodont stratigraphy after Belka (unpublished data).

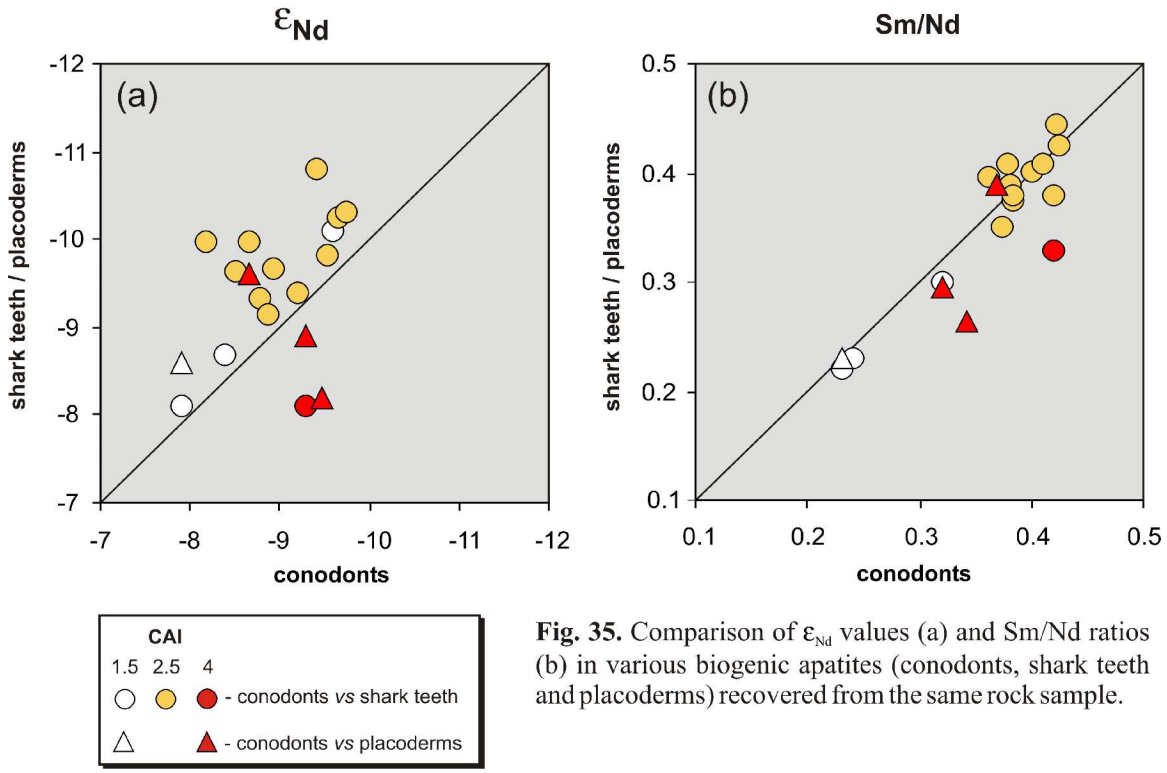

Fig. 35. Comparison of ε_{Nd} values (a) and Sm/Nd ratios (b) in various biogenic apatites (conodonts, shark teeth and placoderms) recovered from the same rock sample.

10.3 Eastern Anti-Atlas

Late Devonian conodonts of the eastern Anti-Atlas show very wide ranges in both ε_{Nd} values and Sm/Nd ratios. The ε_{Nd} value fluctuates between -2.7 and about -12, whereas Sm/Nd ratios range between 0.22 and about 0.85. These inferred seawater values, however, were locally more uniform and distinct (Fig. 36). The remarkable dispersion of data points within each studied location reflects local differences in seawater geochemistry and its temporal evolution at each site. These individual scenarios are presented in detail below.

10.3.1 Mech Irdane

In the central part of the pelagic Tafilalt Platform at Mech Irdane, conodonts exhibit low ε_{Nd} values that vary between - 8 and -10.6 (Fig. 37). Although this range is relatively narrow, a general trend towards more radiogenic signatures can be observed in the upper Frasnian/lower Famennian interval. This trend, however, is punctuated by sharp positive shifts in ε_{Nd} values that coincide with the occurrence of stratigraphic gaps recognized in the Kellwasser succession. Below each gap, the ε_{Nd} values decrease whereas conodonts collected from carbonates above the gaps yield signatures that are up to 1,5 epsilon units higher than those of the underlying samples. Because these gaps

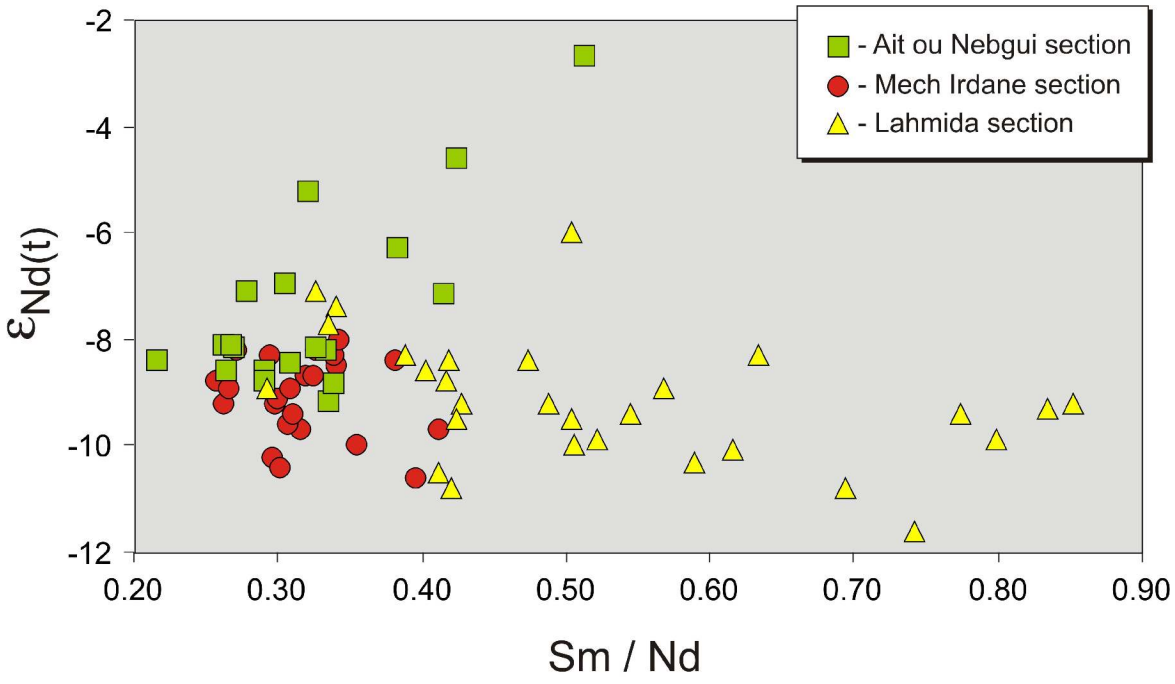

Fig. 36. Variation of ε_{Nd} values and Sm/Nd ratios in the Upper Devonian of the eastern Anti-Atlas. Diagram showing local differences in the isotopic composition of seawater across the shelf of the Anti-Atlas, from the Rheris Basin (Lahmida section) in the north to the central region of Tafilalt Platform (Mech Irdane section), and to the Mader Platform (Ait ou Nebgui section) in the southwest.

are products of subaerial exposure due to regression, the positive shifts in ε_{Nd} values are interpreted to have resulted from the regressive-transgressive sea-level pulses. The lower ε_{Nd} values below the gap reflect stronger Nd supply from continental sources during the regression phase. The more radiogenic signatures of conodonts from above the gap record the influence of open-marine waters during the subsequent transgression.

One of the most surprising results in the Mech Irdane section concerns the onset of the Kellwasser facies which is associated with a gradual decrease of ε_{Nd} values. This trend attains an ε_{Nd} value of -10.6 at the base of the first black layer. This is the lowest value in the whole sequence. It indicates that anaerobic (or dysaerobic) conditions at the sea bottom developed during a shallowing sedimentary regime. Thus, the Nd isotopic data markedly contrast with the common interpretation of the Kellwasser lithology as a transgressive unit (e.g. SCHINDLER, 1990; SANDBERG et al., 1992).

The Sm/Nd elemental ratios in conodonts range from 0.26 to 0.41 at Mech Irdane. The temporal pattern shows a clear, but reverse relation to the ε_{Nd} values (Fig. 37). A decrease in Sm/Nd coincides with an increase in ε_{Nd} and vice versa. The Sm/Nd curve is thus almost a mirror image of the trends to ε_{Nd} values of conodonts.

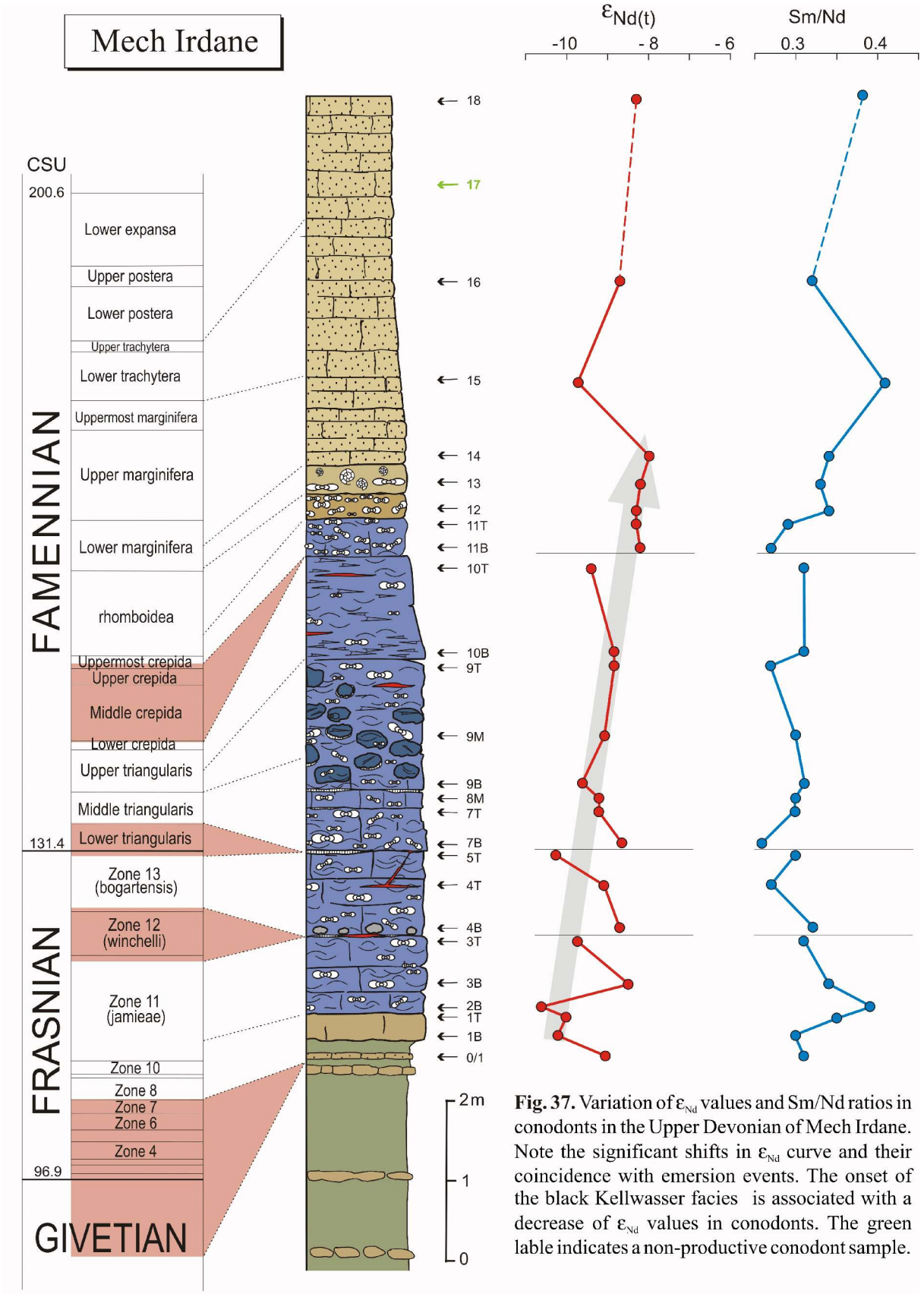

Fig. 37. Variation of ε_{Nd} values and Sm/Nd ratios in conodonts in the Upper Devonian of Mech Irdane. Note the significant shifts in ε_{Nd} curve and their coincidence with emersion events. The onset of the black Kellwasser facies is associated with a decrease of ε_{Nd} values in conodonts. The green lable indicates a non-productive conodont sample.

10.3.2 Ait ou Nebgui

In this strongly condensed sequence, conodonts reveal a wide range of ε_{Nd} values from -2.7 to -9.2 (Fig. 38). The most conspicuous feature in the Nd isotopic evolution is a prominent positive excursion in ε_{Nd} that attains a maximum of -2.7. This is the highest ε_{Nd} value recognized in the Upper Devonian of the Anti-Atlas area. The stratigraphic position of this peak within the conodont Zone 11 (*jamieae*) suggests a relation to the most pronounced Devonian transgression (cycle IId *sensu* JOHNSON et al., 1985), recognized worldwide on the basis of coastal onlap and biotic data. This diastrophic event is also known as the *semichatovae* transgression because the conodont species *Palmatolepis semichatovae* expanded rapidly at that time throughout

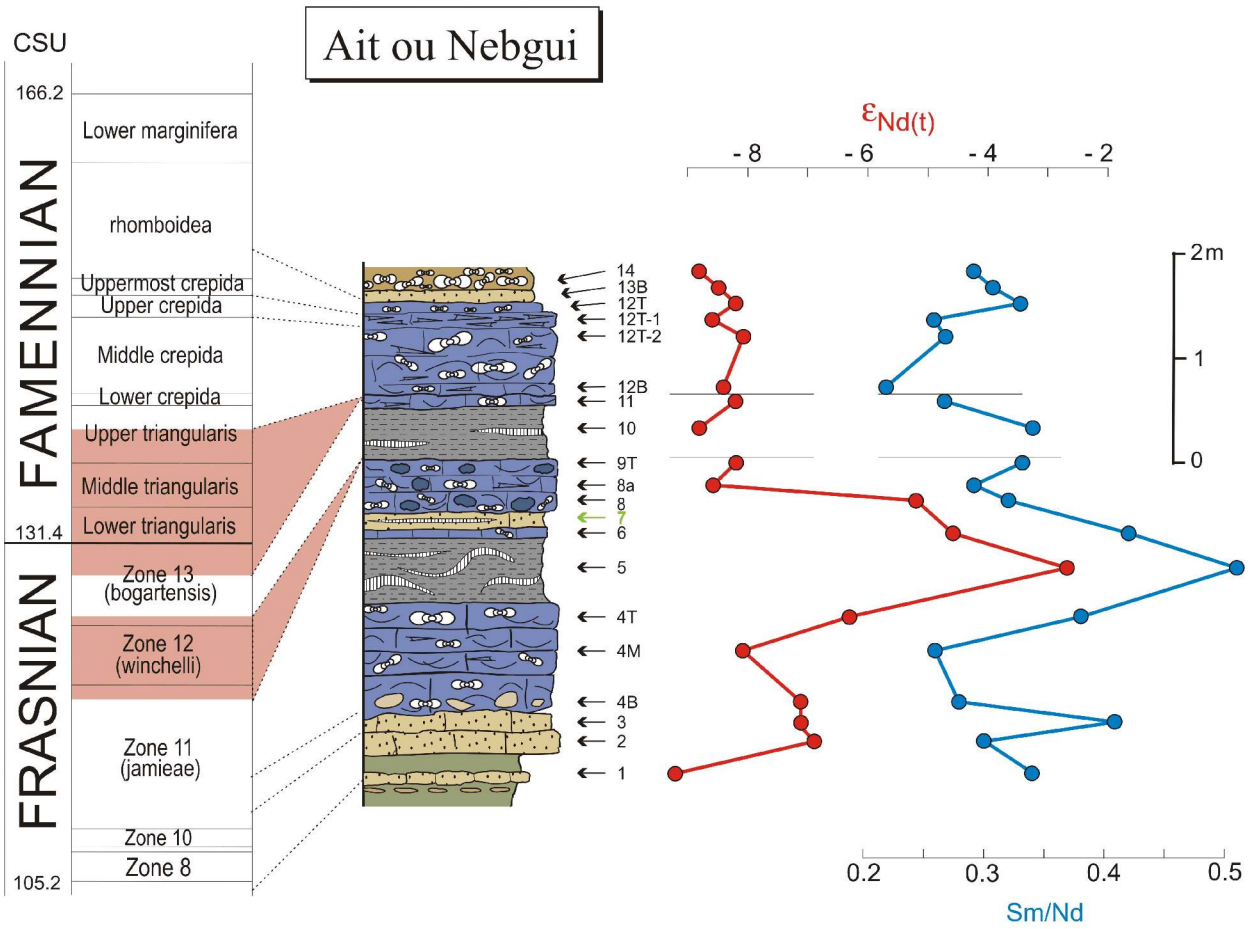

Fig. 38. Variation of ε_{Nd} values and Sm/Nd ratios in conodonts in the Upper Devonian of Ait ou Nebgui. Note the significant peak in ε_{Nd} in the Zone 11 related to the "*semichatovae*" transgression. The green lable indiates a non-productive conodont sample.

Euramerica (e.g. JOHNSON & SANDBERG, 1988; SANDBERG et al. 1992). The observed peak in the ε_{Nd} curve is an excellent example to demonstrate that conodonts preserve the original isotope signal of seawater, independently of the lithology of their host rocks and different diagenetic conditions. Moreover, this peak well illustrates that the lithological response to sea-level change may be less sensitive than the Nd isotopic composition of seawater. The positive excursion in ε_{Nd} starts long before the onset of shale deposition (Fig. 38). In fact, neither the onset nor the termination of the *semichatovae* transgression are expressed by changes in the lithological column.

At the base of the Kellwasser facies, conodonts exhibit an ε_{Nd} value of -7.1, identical to that of conodonts in the underlying oxidized carbonates. Both data points, however, fall within a trend of decreasing ε_{Nd} values. This trend reflects a regression phase, recognized already at Mech Irdane, which caused the development of oxygen-depleted water on the shelf during the Zone 11. In contrast to the trends at Mech Irdane, the Sm/Nd ratios show here a strong positive correlation with ε_{Nd} values. This may indicate that the strongly radiogenic water which entered the Mader Platform during the *semichatovae* transgression, was presumably characterized by REE fractionation different from that of the shelf seawater.

10.3.3 Lahmida

Because the Upper Devonian sequence at Lahmida is very thick and no stratigraphic gaps were detected, the record of temporal changes in the Nd isotopic composition of seawater is probably more complete than in the sections of Mech Irdane and Ait ou Nebgui. Unfortunately, because of the large number of non-productive samples, the Nd isotopic data are only fragmentary available in this basinal sequence (Figs. 39-40). The ε_{Nd} curve is characterized by a strong fluctuation in the upper Frasnian, from -6 to -11.6, and by a more uniform pattern in the Famennian, with ε_{Nd} values from -7.7 to -10.3. A most prominent positive peak within the Zone 11 is certainly related to the *semichatovae* transgression. It is important to note that the increase of ε_{Nd} values from about -9 to -6 coincides with the deposition of light, oxidized carbonates and green shales. This indicates that the *semichatovae* transgression introduced well-oxygenated seawater into the basin and caused enhanced ventilation at the seafloor. This, in turn, prevented deposition of black, organic-rich sediments. The Nd isotopic record within the Zone 13 with shifts in ε_{Nd} up to 4.5 suggests the presence of high-frequency sea-level fluctuation at the end of the Frasnian (Fig. 39). Surprisingly, only one of these events, which was of regressive nature, improved ventilation at the sea bottom and led to the formation of light carbonates. The Famennian Nd isotopic curve is well constrained only in the *rhomboidea* and the Lower

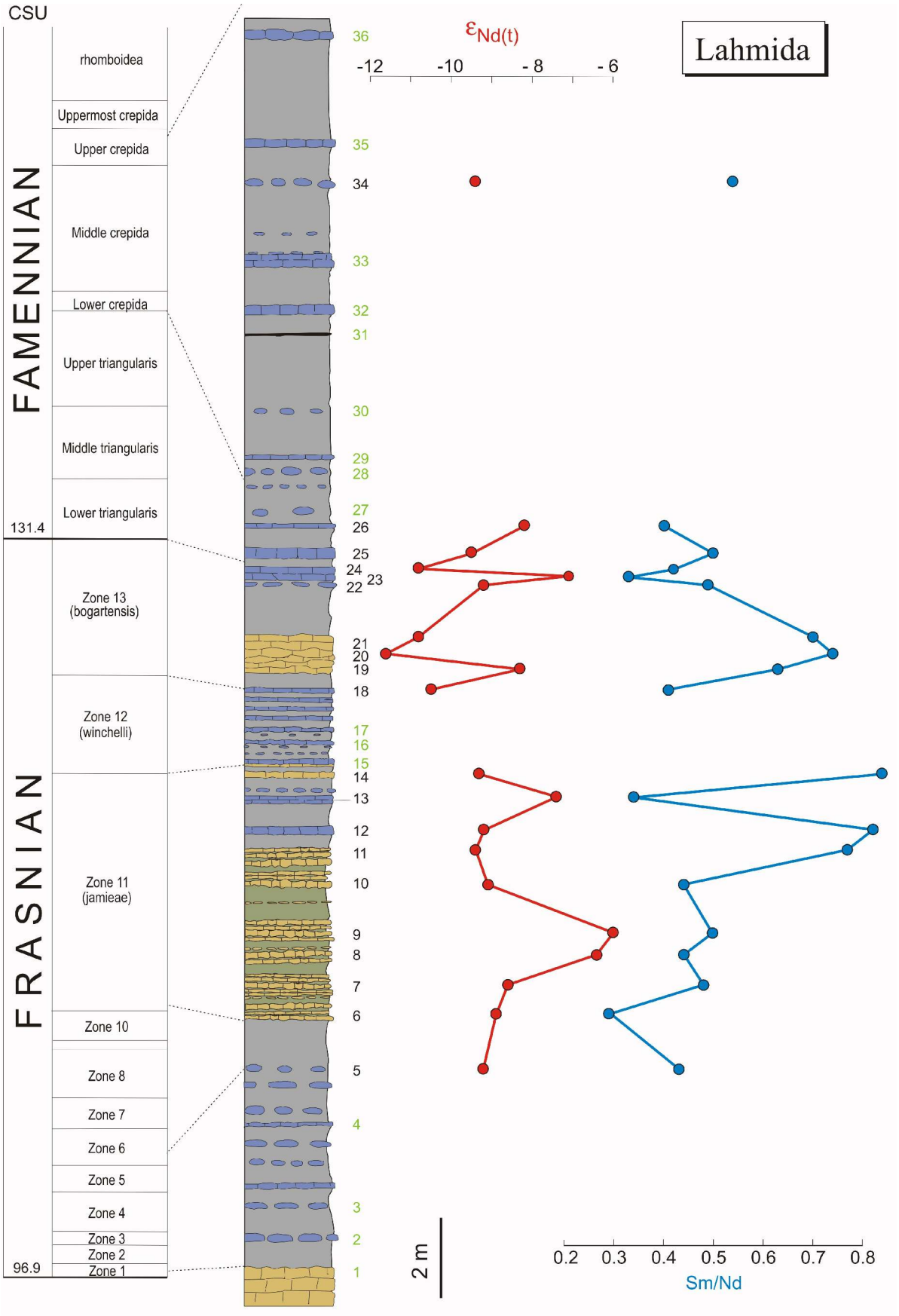

Fig. 39. Variation of ε_{Nd} values and Sm/Nd ratios in conodonts in the Frasnian and the lower Famennian of Lahmida. Non-productive conodont samples are indicated in green.

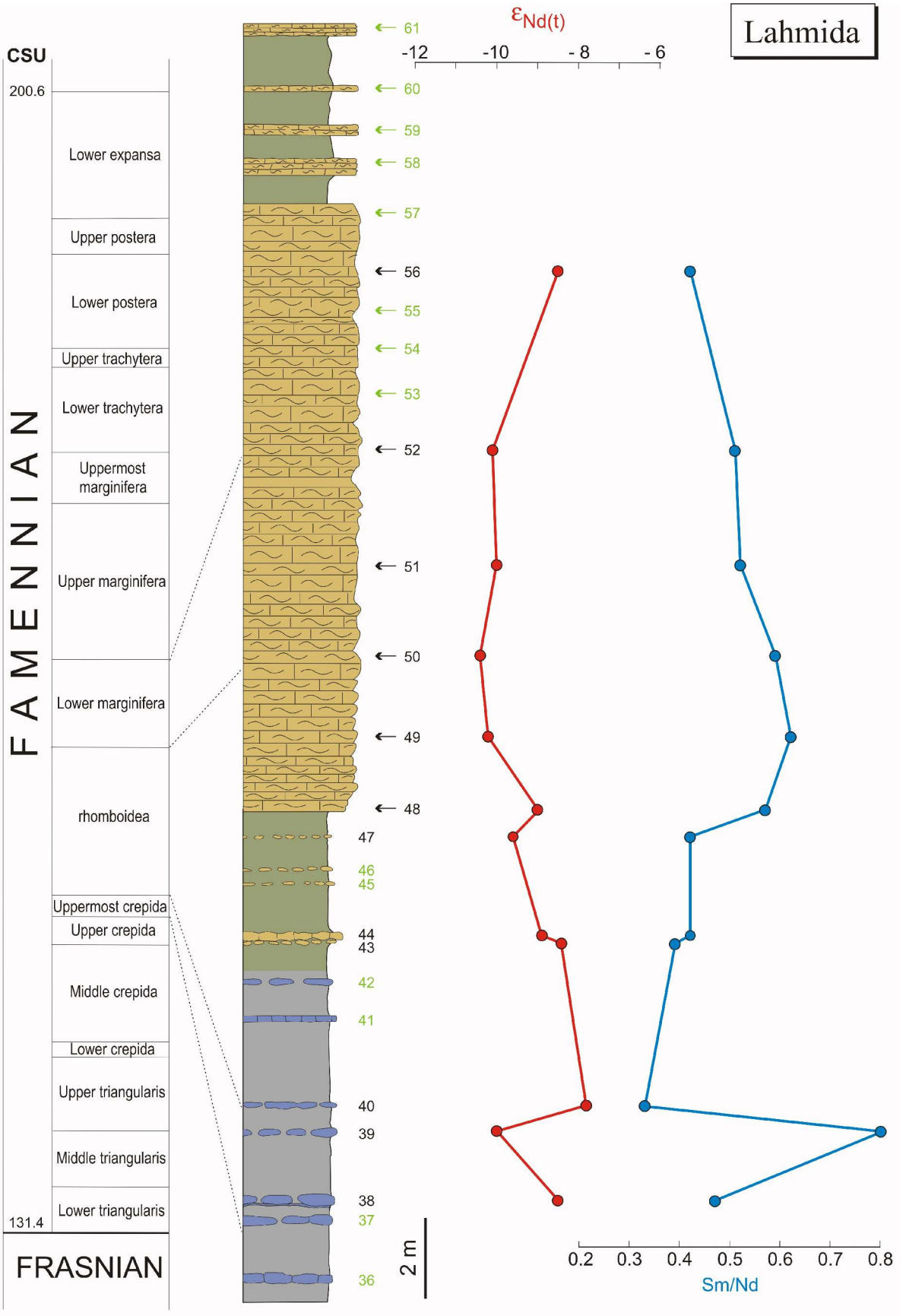

Fig. 40. Variation of ε_{Nd} values and Sm/Nd ratios in conodonts in the middle Famennian of Lahmida. Non-productive conodont samples are indicated in green.

marginifera zones (Fig. 40). In the Uppermost *crepida* Zone, two isolated samples document a decrease in ε_{Nd} from -8.4 to -9.9. It is likely that a regression event is responsible for this shift in ε_{Nd} because it coincides stratigraphically with an erosional gap at Mech Irdane. The *rhomboidea* Zone starts with a relatively high ε_{Nd} value of 7.7 that is followed by a long-termed gradual decrease to -10.3. Unfortunately, there are no data from the top of the Kellwasser facies. On the basis of trends recognized at Mech Irdane and Ait ou Nebgui, it can be speculated that the termination of organic-rich deposition on the Moroccan shelf during the Famennian was not associated with any significant eustatic event.

The REE data from the Lahmida sequence differ remarkably from those of the other studied sections and isolated samples. The Sm/Nd ratios vary between 0.29 and 0.80. Several values are significantly higher than 0.45, which is the known upper limit for the present-day seawater. This problem will be discussed in more detail in chapters 10.6 and 10.7. The Sm/Nd ratios and the ε_{Nd} values generally show reverse trends, similar to those observed in the sequence at Mech Irdane. Surprisingly, the ε_{Nd} excursion of the *semichatovae* transgression is not associated with any significant increase in Sm/Nd.

10.3.4 Circulation pattern

In order to trace lateral variations in the Nd isotopic composition of seawater on the Moroccan shelf numerous samples from two stratigraphic levels, the base and the top of the Kellwasser facies, have been evaluated. In addition, samples from the base of the *marginifera* Zone were also collected in the initial phase of this study but the preliminary results revealed trends in ε_{Nd} values that were almost identical to those at the top of the Kellwasser facies. This is why the evaluation of Nd isotopic data for the *marginifera* Zone has been terminated and the data are not presented in this treatise.

At the base of the Kellwasser facies, in the conodont Zone 11 (*jamieae*), conodonts yield a wide range of ε_{Nd} values, from -6.1 to -11.1 (Fig. 41). The most radiogenic signatures occur on the Mader Platform and seem to document the influence of oceanic waters. Relatively high ε_{Nd} values (-7.5, -8.1) are also recorded in the northeasternmost part of the studied area, whereas values lower than -10 are characteristic for the central and southern part of the Tafilalt Platform. The latter values correspond well with the distribution of clastic material on the shelf (Fig. 41). The lateral variations in ε_{Nd} values permit reconstruction of the seawater circulation but the interpretations of trends require a careful analysis. This is because the ε_{Nd} values can decrease or increase with the flow direction of seawater. An increase can be observed when radiogenic oceanic waters enter the shelf area. Due to mixing with shelf seawater, its impact is getting gradually

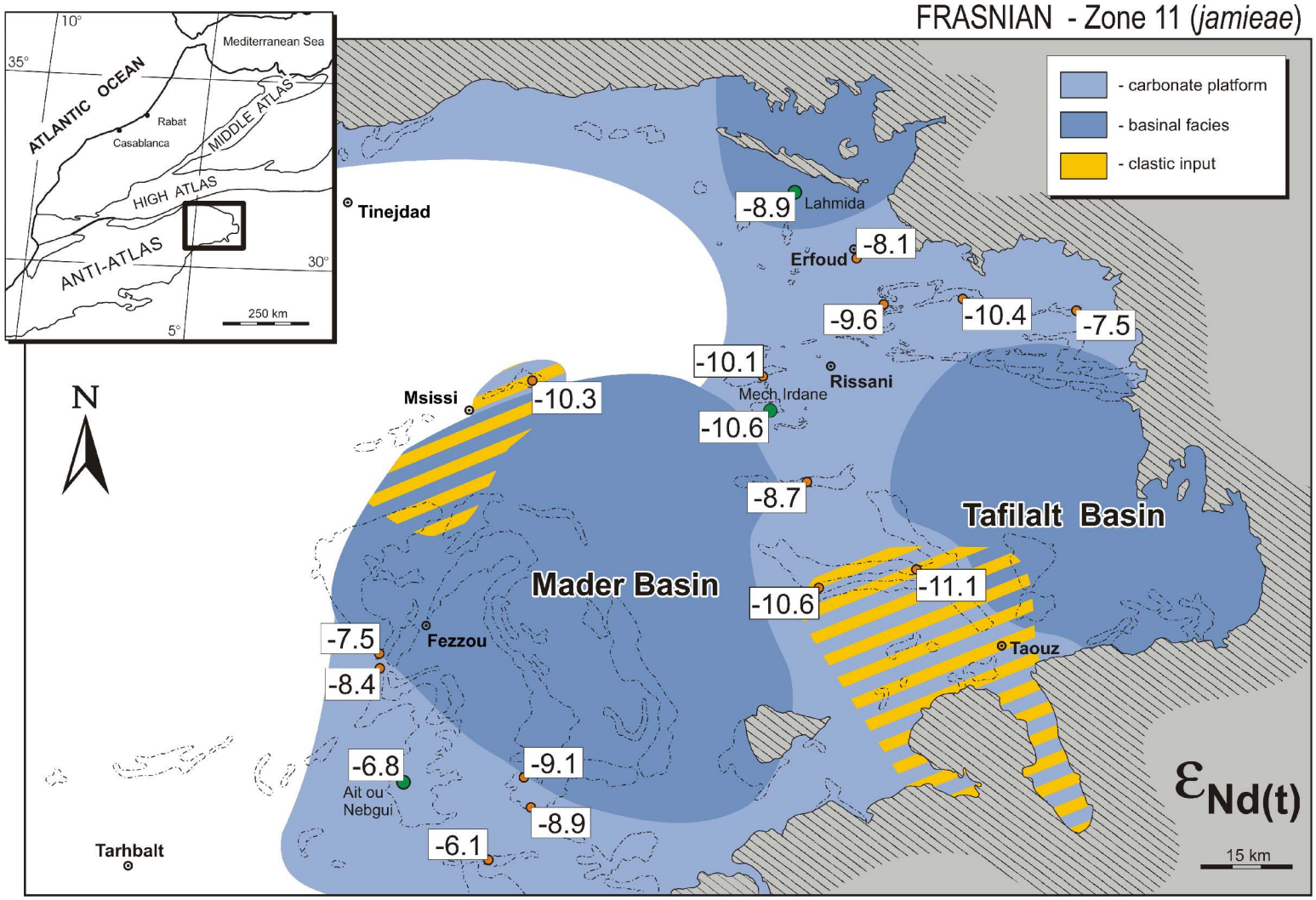

Fig. 41. Lateral variation of ε_{Nd} values across the eastern Anti-Atlas during the Frasnian (*jamieae* Zone). All data points are from the base of the Kellwasser facies. The high ε_{Nd} values on the Mader Platform suggest a southwestward connection to the Rheic Ocean.

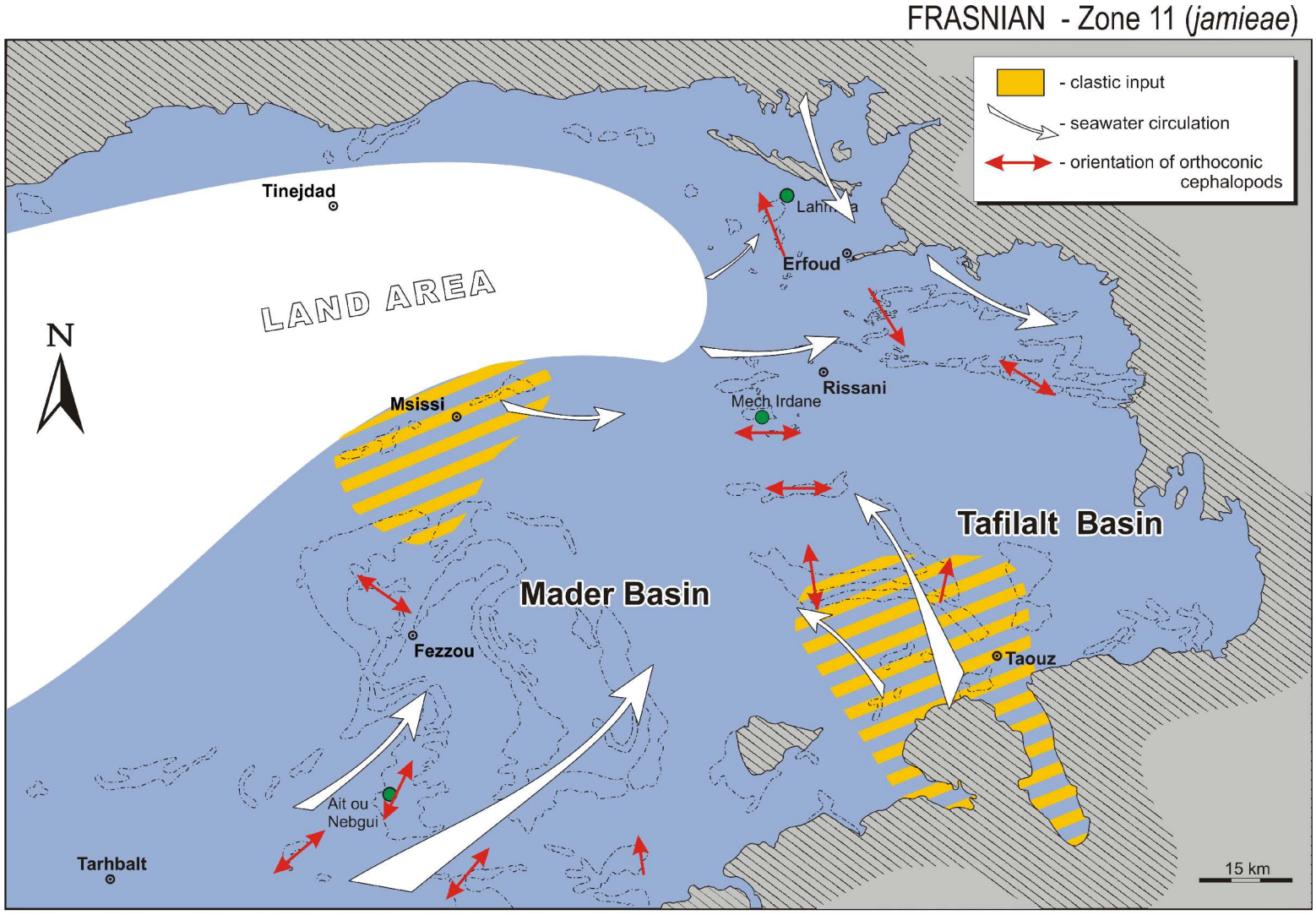

Fig. 42. Seawater circulation in the eastern Anti-Atlas during the onset of the Kellwasser facies (*jamieae* Zone) inferred from Nd isotopic variations in conodonts. Note the good agreement with the orientation of orthoconic cephalopods (data from Wendt, 1995).

weaker. The ε_{Nd} values can increase in the outer zone of deltas, for instance, where the influence of continental Nd decreases outwards. From the trends in the ε_{Nd} values recognized for the onset of the Kellwasser facies, a general seawater flow from the southwest towards the east can be inferred (Fig. 42). The circulation pattern was complex in detail and resulted from the local freshwater input. Riverine waters characterized by low, continental ε_{Nd} values were supplied from the south, presumably from the West African Craton, and from the west, i.e. the exposed Precambrian basement of Jebel Ougnate (Fig. 42). They mixed with the seawater and were further dispersed by northward and eastward currents, respectively. From the presence of Nd isotopic records of the *semichatovae* transgression at Lahmida and Ait ou Nebgui (see chapter 10.3) and the distribution of the highest ε_{Nd} values, it seems that the shelf area communicated with the Rheic Ocean to the southwest and with the Variscan Sea to the north. The shallow-water Mader Platform, however, constituted an effective bathymetric barrier that hindered an unconstrained inflow of oceanic water into the Mader Basin. The lateral trend in ε_{Nd} values on the Mader Platform could have been produced by currents that flowed from the southwest to the northeast, or vice versa. The first scenario is favoured because a rapid decrease of ε_{Nd} values, from about -6 to -9, is observed across the northeastern margin of the Mader Platform and it delineates the zone where oceanic water from the Rheic Ocean was mixed with less radiogenic seawater of the Mader Basin. An opposite flow direction over the extremely shallow-water Mader Platform would create such mixing zone across the southwestern margin of the platform. This is evidently not the case.

An advantage of the Devonian in the Anti-Atlas is that the reconstructed seawater circulation patterns can be tested by comparison with current-related sedimentary features. In the past, Wendt and co-workers (e.g. WENDT & BELKA, 1991; WENDT, 1995) provided a huge set of data on orientation of orthoconic cephalopods. Although these measurements were performed within a broader stratigraphic interval, the isotopically based circulation pattern for the base of the Kellwasser facies is in very good agreement with biostratonomical data for the upper Frasnian (Fig. 42).

The top of the Kellwasser facies (*rhomboidea* Zone) is characterized by a relatively small variation in the Nd isotopic composition of seawater. The ε_{Nd} values range from -7.7 to -10.3 (Fig. 43). This small variation results presumably from the highstand regime that promoted also an expansion of basinal facies during the *rhomboidea* Zone. It can be speculated that the highstand facilitated the seawater circulation which resulted in enhanced mixing of water masses and, hence, a more homogenous Nd isotopic composition. This uniform pattern of ε_{Nd} values, however, makes a reconstruction of seawater circulation very difficult and, thus, the inferred flow directions are relatively poorly established. Therefore, the model of seawater circulation for the top of the Kellwasser facies has been developed only by combination of Nd isotopic and biostratonomical data (Fig. 44). The latter, however, were only available for the cephalopod limestones overlying

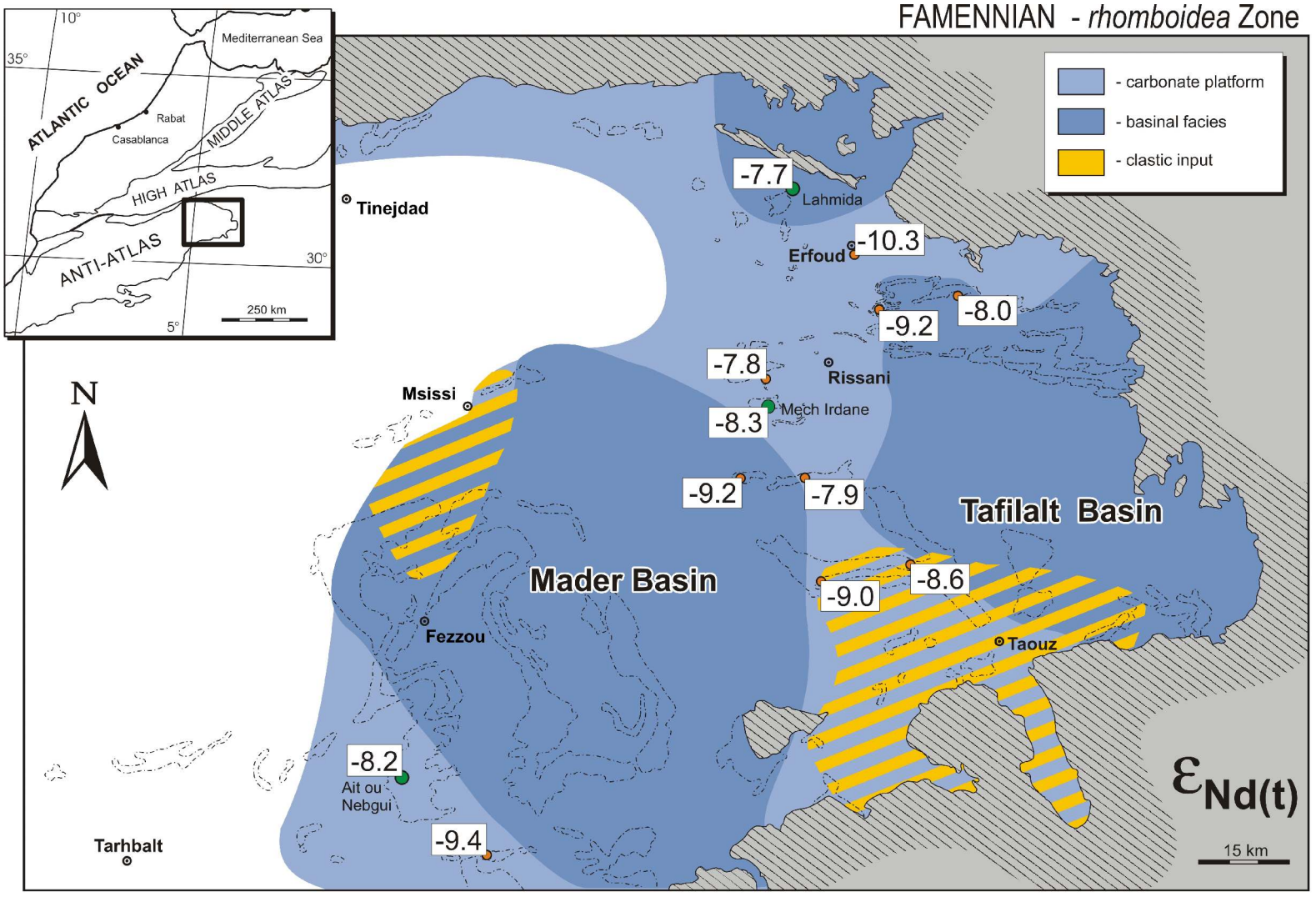

Fig. 43. Lateral variation of ε_{Nd} values across the eastern Anti-Atlas during the Famennian (lower part of the *rhomboidea* Zone). Data points are from the top of the Kellwasser facies.

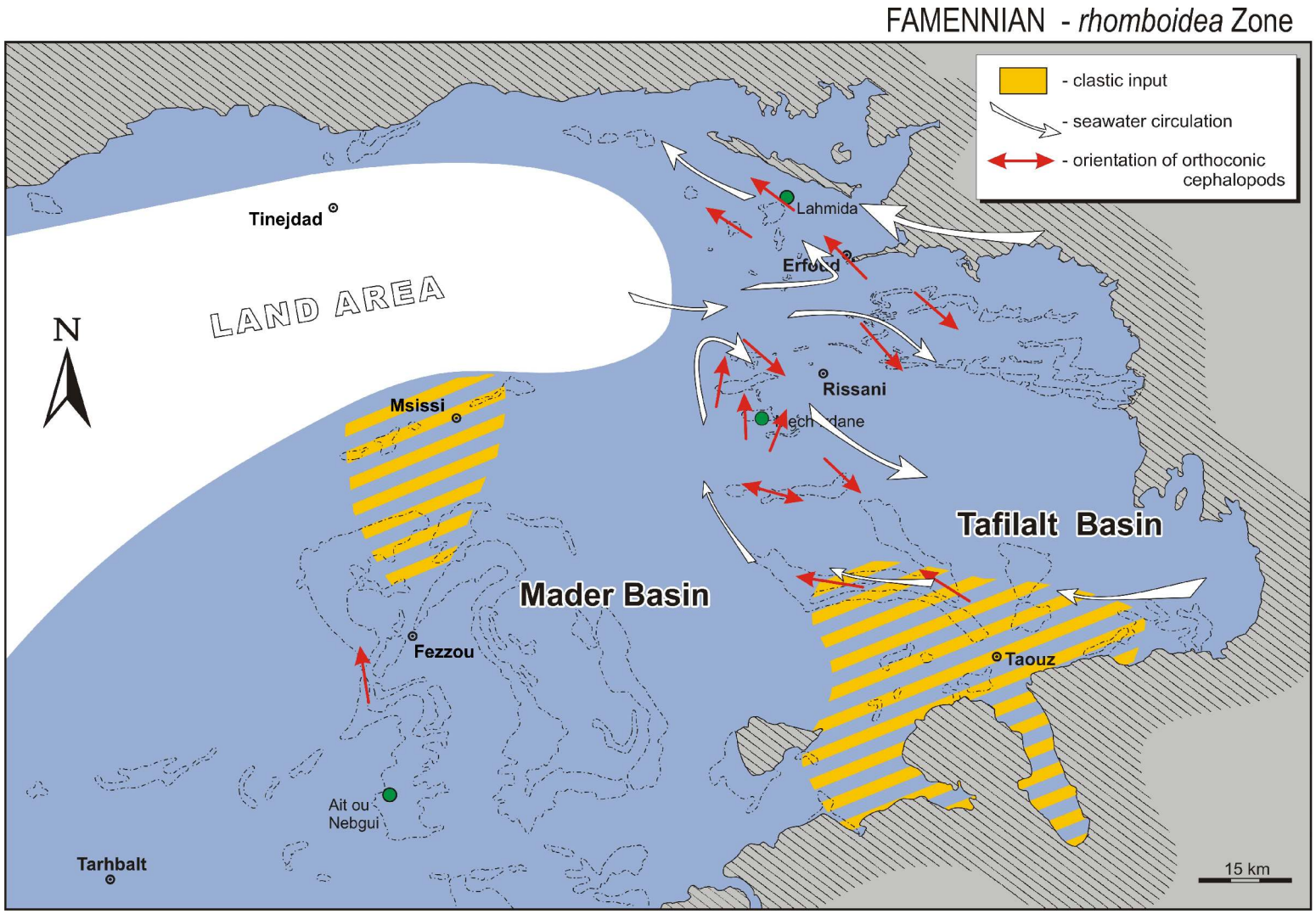

Fig. 44. Seawater circulation in the eastern Anti-Atlas during the termination of the Kellwasser facies (*rhomboidea* Zone) inferred from the Nd isotopic variations in conodonts and orientation of orthoconic cephalopods. However, data on shell accumulations (from Wendt, 1995) are from the lower part of the *marginifera* Zone. This is because orthoconic cephalopods are very rare in sediments of the *rhomboidea* Zone.

the Kellwasser sediments (WENDT, 1995).

The southern part of the Tafilalt Platform shows ε_{Nd} values (Fig. 43) that are about two units higher than those measured at the base of the Kellwasser facies in this area (see Fig. 41). This may have resulted from a decline in the input of continental Nd from the West African Craton due to the highstand. The increase of water depth caused a shift of the depositional patten towards the south and, therefore, the impact of clastic material on the area south of Rissani was insignificant. Moreover, the collateral progradation of prodelta sediments towards the east and the west in the area of Taouz (Fig. 43) strongly suggests the presence of a shoreline current. This is also supported by the arrangement of orthoconic shells in the Amessoui Synline, northwest of Taouz, that indicates a westward flow (WENDT, 1995 and Fig. 44). A relatively low ε_{Nd} value of -9.2 determined for the northeastern margin of the Mader Basin seems to have been affected by Nd input from the southeast (Fig. 43). This appears to be plausible when assuming that the generally westward flow north of Taouz turned to the north (Fig. 44). In addition, such flow direction could explain the orientation of orthoconic cephalopods west of Mech Irdane. A complex circulation pattern inferred from shell orientation and Nd isotopic data in the central Tafilalt Platform can be explained by a countercurrent that originated from the northwest of Rissani. This would also explain the relatively non-radiogenic isotope signatures observed in the northeastern part of the Tafilalt Platform (ε_{Nd} values of -10.3 and -9.2) which may have resulted from an eastward transport of more continental Nd from the emerged land area of the Jebel Ougnate. The northern Tafilalt Platform was certainly controlled by a dominant current with a northwest direction. This is well constrained by orientation of cephalopods. Because only two Nd isotope data points are available from the Mader Platform, no attempt has been made to reconstruct the seawater circulation in this part of the Moroccan shelf during the time of the *rhomboidea* Zone.

10.4 Moroccan Meseta, Gara de Mrirt

In the section of Gara de Mrirt, the ε_{Nd} values of conodonts vary within a wide range from -2.6 to -9.4 (Fig. 45). The most conspicuous feature in the Nd isotopic curve of this section is a positive excursion in the Zone 11 (*jamieae*), related to the *semichatovae* transgression. During this event, the ε_{Nd} values attain a level similar to that of the coeval excursion observed in the Ait ou Nebgui section. This excursion is contrasted by uniformly low ε_{Nd} values in the overlying upper Frasnian/lower Famennian interval. They fluctuate within a narrow range from –8.5 to –9.4. There are two small, negative peaks in ε_{Nd}, only about 1 epsilon unit, at the base of both the Lower and the Upper Kellwasser units. This suggests that the onset of these organic-rich facies was initiated

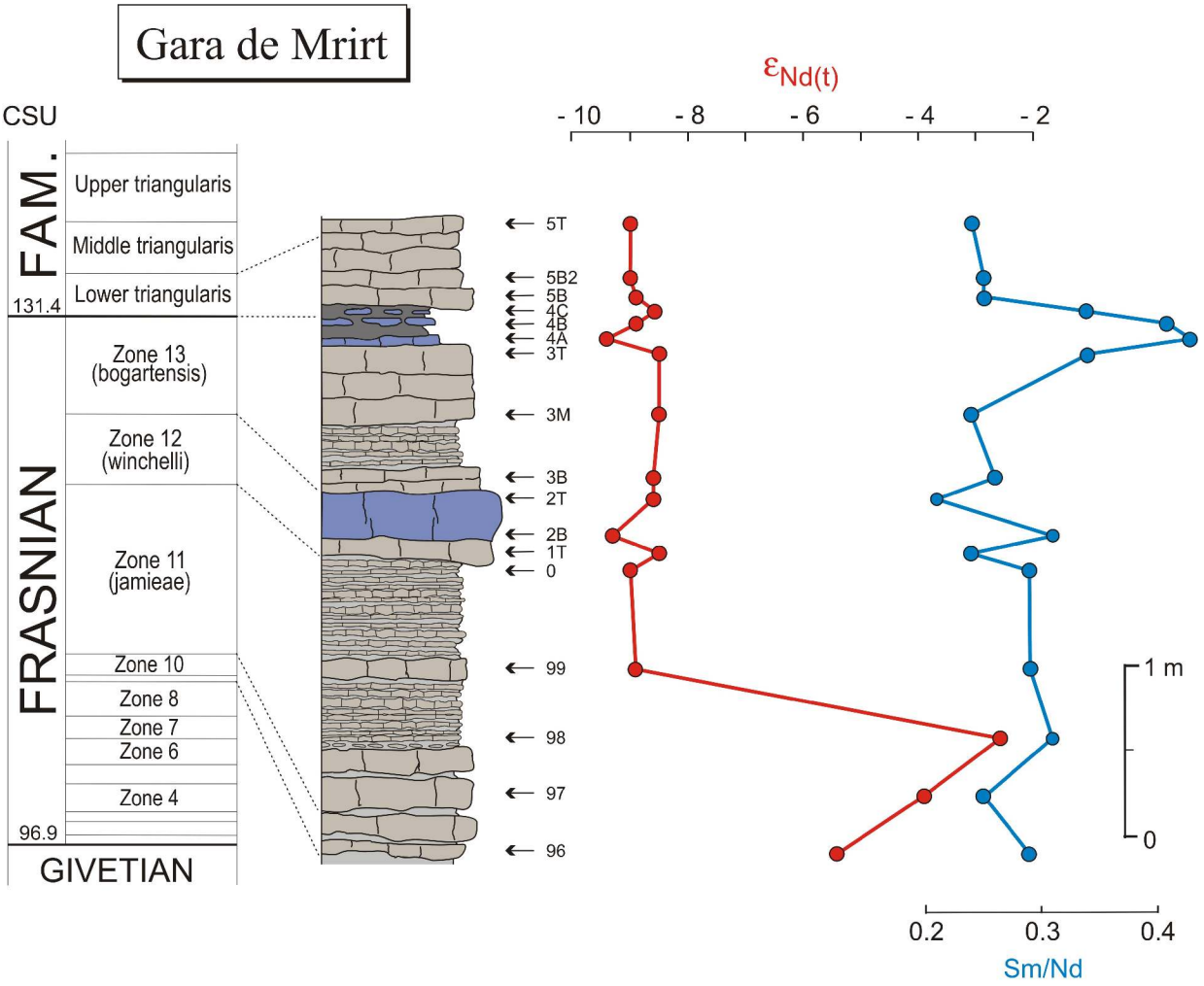

Fig. 45. Variation of ε_{Nd} values and Sm/Nd ratios in conodonts in the Upper Devonian of Gara de Mrirt. Note the significant excursion in ε_{Nd} within the Zone 11, related to the "*semichatovae*" transgression.

by short-term regressive events.

With the exception of a peak in the Upper Kellwasser unit, the Sm/Nd ratios in the Gara de Mrirt section are very uniform, between 0.21 and 0.30 (Fig. 45). Most of them overlap with Sm/Nd ratios typical for modern epeiric seawater (for details see chapter 10.6) and the lowest ratios, below 0.22, correspond to ratios of modern oceanic water. These are the lowest Sm/Nd ratios recognized in the western part of the Variscan realm. At Gara de Mrirt, the Sm/Nd ratios and the ε_{Nd} values of seawater display a close relation. Negative excursions associated with the onset of both Kellwasser units correlate with positive peaks of the Sm/Nd curve. It is, however, remarkable that the peak of the *semichatova*e transgression is not accompanied by any significant change in the Sm/Nd ratios, which remain more or less stable during this event.

10.5 Montagne Noire, Coumiac

At Coumiac, conodonts display generally low ε_{Nd} values that range from -7.4 to -10.1 (Fig. 46). The Frasnian samples yield generally more radiogenic signatures than the Famennian ones. Similarly higher are also amplitudes of fluctuations in ε_{Nd} values in the Frasnian compared to those in the Famennian. Two distinct negative peaks in ε_{Nd} occurring within the Frasnian segment of the section coincide with the deposition of Kellwasser horizons. The lower peak, with a drop in ε_{Nd} from -8.0 to -9.7, starts at the base of the Lower Kellwasser unit and continues into the lowermost part of the Zone 13 (*bogartensis*). This negative trend provides evidence that oxygen deficiency at the sea bottom, which created the Kellwasser lithology, developed within a regressive phase. Upwards the section, the ε_{Nd} values increase gradually and achieve a level of about -7.5 in the upper part of the Zone 13. This curve interval is interpreted to reflect a highstand in sea level that was terminated by a rapid regression expressed as a decrease in ε_{Nd} values from -7.4 to -9.1. This negative shift begins just below the base of the Upper Kellwasser horizon, similarly to the negative excursion at the base of the Lower Kellwasser unit (Fig. 46).

The Famennian starts with a small positive peak followed by a negative trend in ε_{Nd} values from -8.2 to -9.9 during the Middle *triangularis* zone. Throughout the rest of the Famennian, ε_{Nd} values show rather small fluctuations around a value of -9.0. There are only two slightly higher deviations from this uniform trend, a negative peak during the Middle *crepida* Zone and a positive one within the Upper *crepida* Zone. Both, however, are not well constrained because each of them is documented by only one data point. The generally low ε_{Nd} values in the Famennian seem to reflect supply of Nd from old Precambrian crustal sources. This implies that rocks yielding Precambrian model ages were exposed in the proximity of the Montagne Noire. However, the location of the source area cannot be precisely identified. Two areas are proposed as possible targets, the northern part of the Massif Central and the Pyrenees. Fragments of Precambrian crust are known to occur in both these regions. Moreover, clastic facies is widespread in the Devonian of the West Pyrenees (WIRTH, 1967; KRYLATOV & STOPPEL, 1971; CYGAN, 1995) and indicates an exposed crystalline basement. Further studies and data from other locations outside of the Montagne Noire are necessary to reconstruct the derivation of the non-radiogenic, continental Nd recognized at Coumiac.

Late Devonian conodonts at Coumiac are characterized by Sm/Nd ratios ranging from 0.28 to 0.47. The Sm/Nd curve shows excursions that correlate well with peaks in the ε_{Nd} curve. These fluctuations, however, are perfectly inverse. In addition, they do not show any clear correlation with the Sr isotopic compositions of conodonts. $^{87}Sr/^{86}Sr$ ratios of conodonts fluctuate between 0.70808 and 0.70826 (Fig. 46) and are consistent with the Sr isotopic evolution of seawater during the Late Devonian (BURKE et al., 1982; VEIZER et al., 1997, 1999). Moreover, a more or less

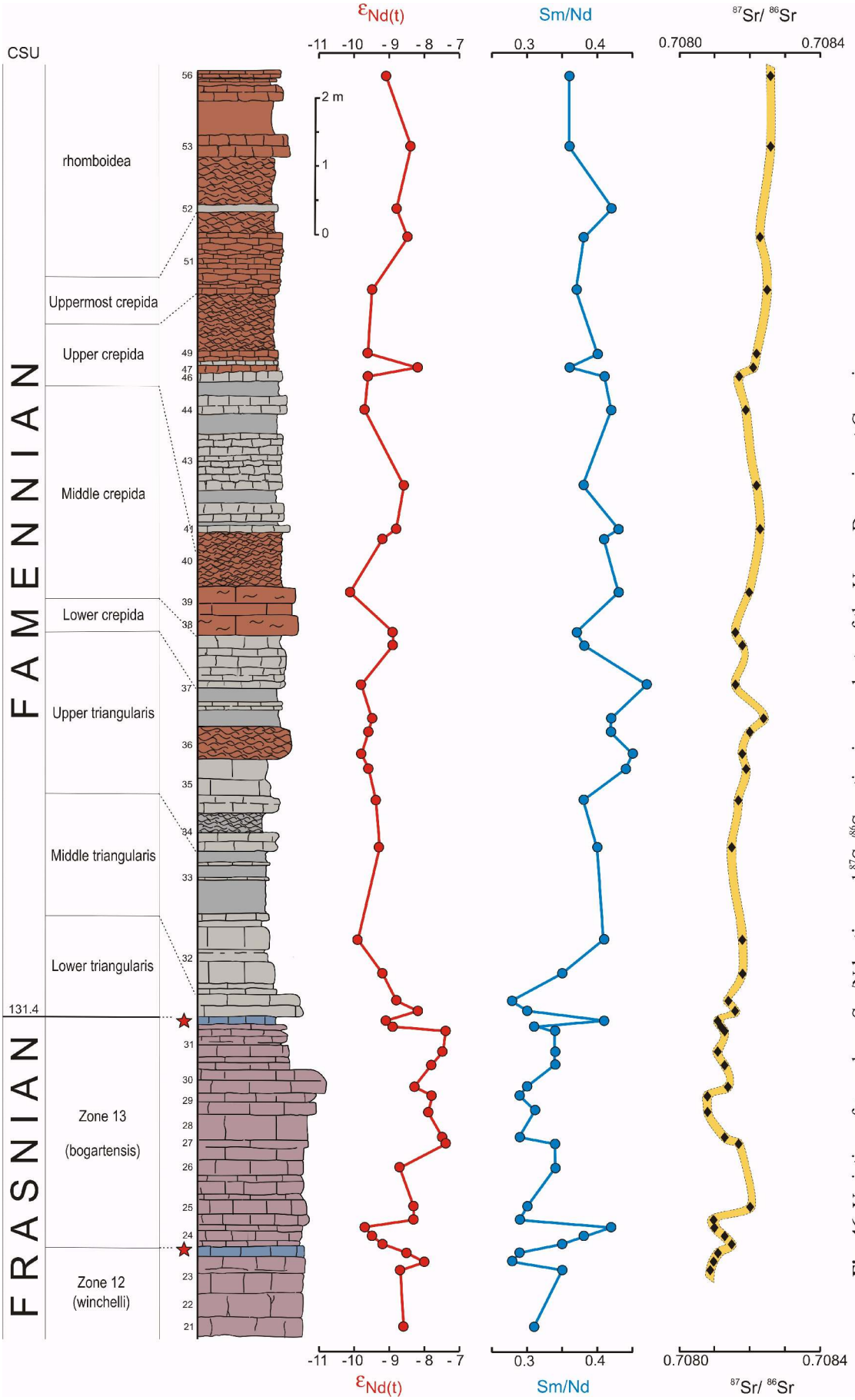

Fig. 46. Variation of ε_{Nd} values, Sm/Nd ratios and $^{87}Sr/^{86}Sr$ ratios in conodonts of the Upper Devonian at Coumiac.

gradual trend to more radiogenic $^{87}Sr/^{86}Sr$ values is observed throughout the Upper Devonian. The most frequent oscillations in the Sr isotopic curve occur in the upper Frasnian. However, this can be an effect of low accumulation rate or/and short hiatuses below the level of biostratigraphical resolution. Nevertheless, the oscillatory nature of the Sr isotopic evolution during the Frasnian was also documented by VEIZER et al. (1997) for the Aachen region. Their Sr isotopic curve resembles in several details the Sr curve established for the Coumiac section. Some discrepancies arise probably from insufficient biostratigraphic control of the Aachen succession and, thus, inaccurate stratigraphic correlation of both curves.

10.6 Nd isotopic signatures of seawater in the Variscan realm

Conodonts recovered from various locations across the Variscan realm reveal distinct Nd isotopic and Sm/Nd elemental characteristics that reflect local and regional differences in seawater geochemistry during the Late Devonian (Fig. 47). Most remarkable is the difference between the geochemical signatures of seawater in southern Poland and that of the Anti-Atlas area. According to BELKA et al. (2000), the Baltic shelf of Euramerica (southern Poland) is characterized by ε_{Nd} values from about -2 to -9 and a relatively narrow range of Sm/Nd ratios from 0.16 to 0.29. The Sm/Nd ratios fall within an interval of Sm/Nd ratios considered as characteristic for modern oceanic water. Several studies reported Sm/Nd ratios for major oceans that vary between about 0.16 and 0.23 (PIEPGRAS & WASSERBURG, 1980; BERTRAM & ELDERFIELD, 1993; SHOLKOVITZ et al., 1994; ALIBO & NOZAKI, 1999). The low Sm/Nd ratios observed in southern Poland (Holy Cross Mountains, Cracow-Silesia area) reflect a marginal, open marine position of the studied regions on the Baltic shelf. According to NARKIEWICZ (1988), the nearest land area, the Belorussian Land, was at least 300 km away from the studied regions. Hence, the seawater chemistry on the shelf margin was influenced rather by oceanic waters than by riverine supply of REE from continental sources.

In contrast to the Baltic shelf, the conodonts from the eastern Anti-Atlas, located on the northern Gondwana shelf, display a much broader range of Sm/Nd ratios from 0.21 to 0.85. Moreover, the average Nd isotopic signatures are less radiogenic than in southern Poland. The majority of data points yield ε_{Nd} values ranging from about -7 to -12. Only a few samples display higher ε_{Nd} values up to -2.6. The dominantly low ε_{Nd} signatures suggest supply of Nd from old Precambrian crust, most probably from the West Sahara Craton. It is likely that the surprisingly high Sm/Nd ratios may result from the very proximal position of the Anti-Atlas area on the inner shelf of Gondwana. The values are remarkably higher than those reported from modern epeiric seas (Fig. 47), but REE data from modern marine environments are predominantly from sites

located in open oceanic spaces, and not from coastal zones. AMAKAWA et al. (2000) provided the hitherto only extensive documentation of the Nd seawater geochemistry in epeiric seas. They showed that the Sm/Nd ratios in seas between SE Asia and Australia may be as high as 0.44.The majority of values obtained from the Anti-Atlas samples is compatible with signatures of seawater in the SE Asiatic region, but there is also a large number of samples that significantly exceed the value of 0.44 (Fig. 47). Considering a relatively small distance that separated the investigated Anti-Atlas locations from the coast during the Devonian (WENDT, 1991), the unusual high Sm/Nd ratios may have resulted from fractionation processes that are known from modern estuarine settings. Reports on REE behaviour in rivers, estuarine transects, and coastal seawater, document a large-scale removal of REEs from solution during the mixing of riverine water with seawater (e.g. MARTIN et al., 1976; HOYLE et al., 1984; GOLDSTEIN & JACOBSEN, 1988c; SHOLKOVITZ &

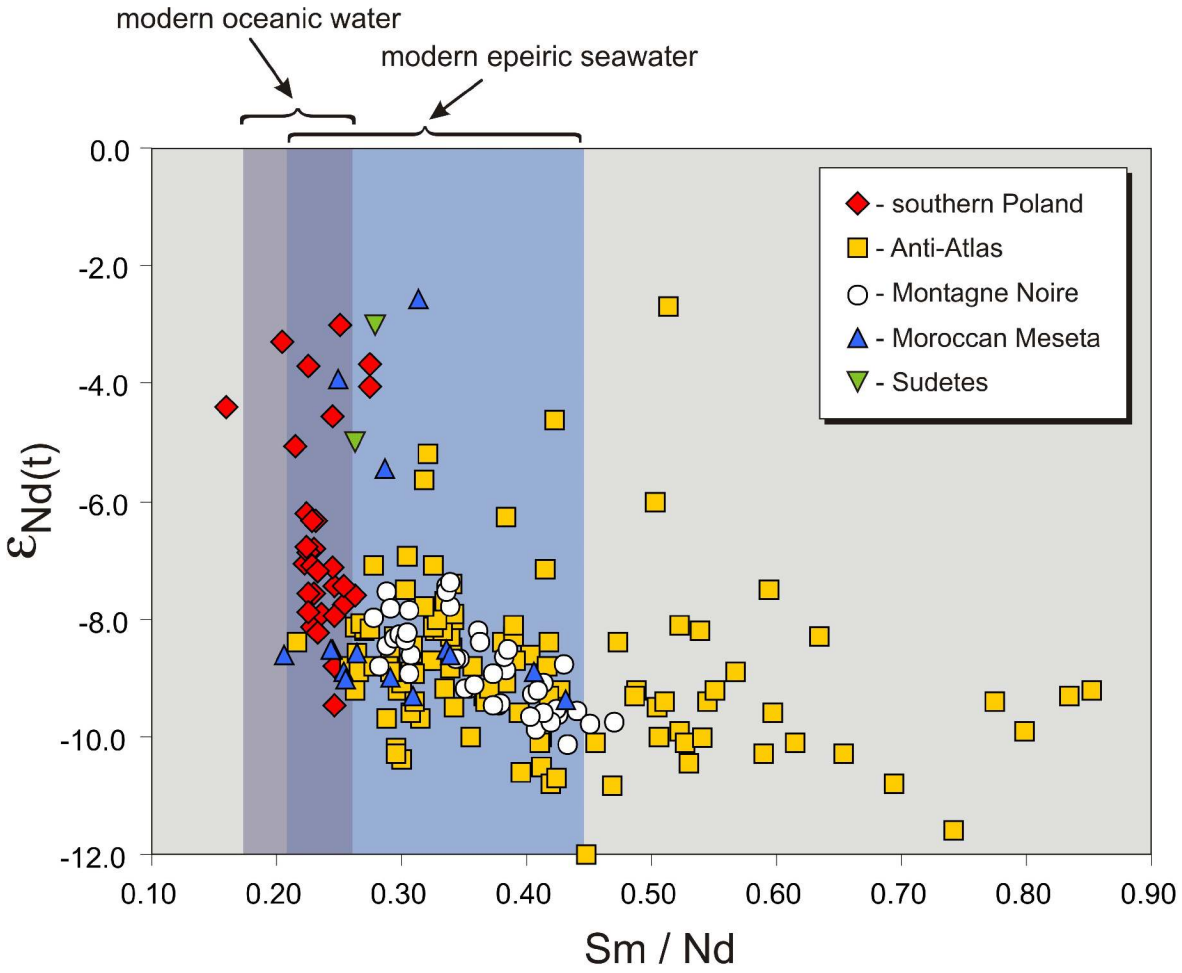

Fig. 47. Variation of ε_{Nd} values and Sm/Nd ratios in conodonts showing different water masses within the western part of the Variscan Sea and on the Baltic shelf of Euramerica (southern Poland). The range of Sm/Nd ratios in modern epeiric seas is based on data from seas between Asia and Australia (Amakawa et al., 2000) and that of modern oceans taken from several literature sources (see text for more references).

ELDERFIELD, 1988; ELDERFIELD et al., 1990; SHOLKOVITZ & SZYMCZAK, 2000). In many estuaries, the removal is accompanied by fractionation of REE, which is usually explained by preferential removal of colloidally associated light REEs (MARTIN et al., 1976; GOLDSTEIN & JACOBSEN, 1988c; ELDERFIELD et al., 1990; SHOLKOVITZ, 1992; SHOLKOVITZ & SZYMCZAK, 2000). Several other factors have also been suggested as being responsible for the REE fractionation in rivers and estuaries, e.g. planktonic absorption and coprecipitation with natural hydrous ferric oxides (MARTIN et al., 1976), the patterns of local sedimentary rock types (KEASLER & LOVELAND, 1982), stabilization and coagulation by organic colloids (HOYLE et al., 1984; SHOLKOVITZ & ELDERFIELD, 1988), and the pH level (KEASLER & LOVELAND, 1982; GOLDSTEIN & JACOBSEN, 1988 b, c). However, there is no agreement as to which processes play the dominant role.

The geochemical characteristics of conodonts from the Montagne Noire and the Moroccan Meseta are consistent with the seawater geochemistry of recent epeiric seas (Fig. 47). In the former area, however, no high radiogenic ε_{Nd} values have been recorded and consequently the range of Nd signatures is narrower than in other studied regions. The high radiogenic values (-2 to -5) seem to represent a distinct aquafacies (an another reservoir of seawater) compared to that characterized by ε_{Nd} values between -6 and -12. The duality of seawater masses in the Variscan realm, expressed by distinct Nd isotopic signatures, is most evident in southern Poland but it can also be observed in the Anti-Atlas and the Moroccan Meseta. It attests a decoupling in the geochemical evolution between shelf waters, being dominated by Nd supply from continental sources, and oceanic waters characterized by much more radiogenic signatures. The latter enter only episodically the shelf and coastal regions during sea-level rises. Overall, fluctuations in sea level modified the participation of both aquafacies on the shelves and generated temporal and spatial variations in the Nd isotopic signal. Both aquafacies differed not only in their Nd isotopic signatures but also in their C isotopic evolution. Compilation of ε_{Nd} and $\delta^{13}C$ values from the Devonian of the Gara de Mrirt (Fig. 48) reveals that the oceanic aquafacies was characterized by high ε_{Nd} values and strongly negative $\delta^{13}C$ signatures, whereas the shelf aquafacies displayed lower ε_{Nd} values and less negative to positive $\delta^{13}C$ values. Therefore, care must be taken when interpreting trends in C isotopic composition, because exchange and/or mixing of seawater can produce certain excursions in the C isotope record.

Geochemical decoupling between various water masses in marine environments is known both from the past and the present time. HOLMDEN et al. (1998) provided Nd and C isotopic evidence for geochemical decoupling between the epicontinental Mohawkian Sea in the Midcontinent region of North America and the bordering Iapetus Ocean during the Ordovician. Although the C isotopic composition of modern surface seawater is very uniform (CHARLES & FAIRBANKS, 1992) and shows variations smaller than 1.5‰, differences as high as 4‰ can occur

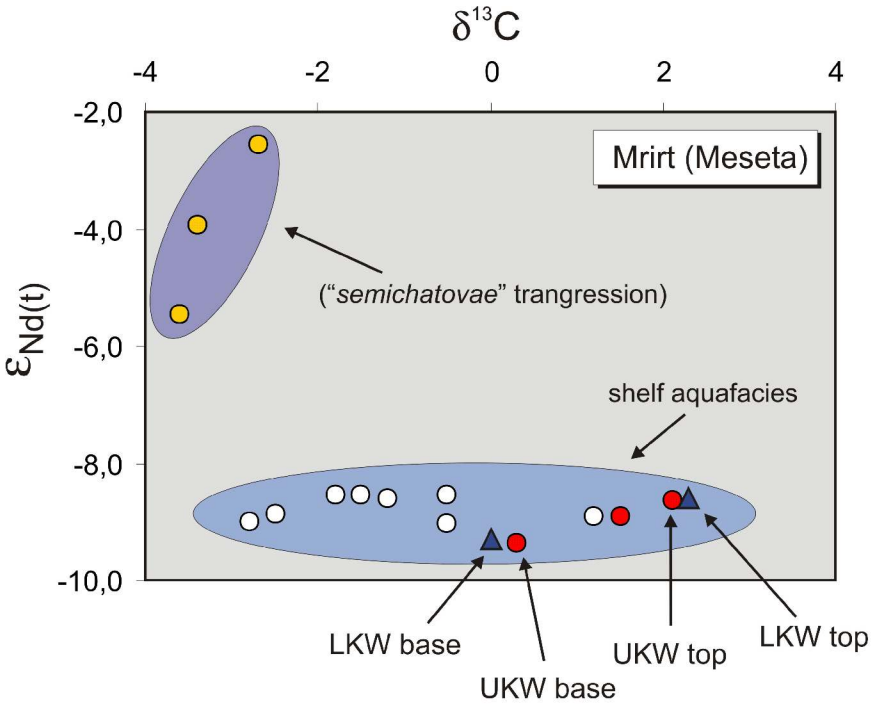

Fig. 48. Diagram showing contrasting geochemical characteristics for the Variscan oceanic aquafacies (semichatovae transgression) and shelf aquafacies recorded in the Upper Devonian sequence of Mrirt. The ε_{Nd} values of conodonts are plotted against $\delta^{13}C$ values of carbonate host rocks. The carbon data are taken from Joachimski et al. (2002).

in certain oceanographic situations, such as on the Bahamas carbonate platforms (e.g. LLOYD, 1964; PATTERSON & WALTER, 1994).

Considering the ε_{Nd} values in seawater of the Variscan realm it can be concluded that the Variscan oceanic aquafacies (both within the Rheic Ocean and the Variscan Sea) resembled the seawater in the modern Pacific Ocean (average ε_{Nd} = -3.5) rather than those of the Atlantic or Indian oceans, with average ε_{Nd} values of -12.1 and -8.3, respectively. Because records of the oceanic aquafacies in southern Poland as well as in the Anti-Atlas and Meseta originated from an ingression of oceanic waters onto the shelve areas and were, at least partially, modified by mixing with the shelf aquafacies, it is very likely that pristine Variscan oceanic water may have displayed even more radiogenic Nd isotopic signatures than the ε_{Nd} value of -2.6 determined at Gara de Mrirt. BELKA et al.(2000) reported ε_{Nd} values as high as -1.6 from the margin of the Euramerica shelf (Tournaisian of southern Poland).

It is important to stress that a two-component mixture model cannot be applied for estimation of the isotopic and chemical composition of the end members (here pristine oceanic and shelf aquafacies) and their participation in the isotopic and elemental characteristics of the seawater. This is because the Nd concentrations in conodonts do not reflect those of the seawater but are related to the morphology of conodont elements and, to some extend, to the sedimentation rates (see chapter 10.1.1).

10.7 Sm/Nd fractionation

As already mentioned in the previous chapter, the level of Sm/Nd ratios in seawater can be, to some extend, attributed to the position of a given location relative to the coast. The temporal fluctuations in Sm/Nd ratios, however, are more complex and thus difficult to explain. In most cases, there is a clear relation between Sm/Nd ratios and ε_{Nd} values. Positive excursions in the former coincide with negative peaks in the latter, and vice versa. Such relation, however, seems to be valid only for seawater of the shelf aquafacies. During the *semichatovae* transgression, when the Variscan oceanic waters entered shelf areas, the relation between Sm/Nd ratios and Nd isotopic signatures is not unequivocal. In the Ait ou Nebgui section, a strong positive excursion in ε_{Nd} is associated with a prominent increase of the Sm/Nd ratio. In two other locations, where the oceanic aquafacies has been identified (Lahmida and Gara de Mrirt), the positive excursion in ε_{Nd} is contrasted by almost constant Sm/Nd ratios. Although no explanation can yet be proposed for the REE behaviour during the *semichatovae* transgression, it appears that the Variscan oceanic waters differed from the shelf aquafacies not only in thir Nd and C isotopic compositions, but also in REE fractionation.

FANTON et al.(2002) found evidence in the Ordovician of North America that variations in Sm/Nd ratios can correlate with changes in water depth. They suggested that an increase in Sm/Nd usually coincides with increasing ε_{Nd} and water depth and vice versa. However, their conclusion is based on correlations that are not precise and unequivocal. In some cases, a contrasting development of Sm/Nd and ε_{Nd} is evident. Therefore, the general usefulness of the Sm/Nd ratio of carbonate rocks as a tool for reconstruction of palaeo-water depth appears to be questionable.

10.8 Sea-level fluctuations

The correlation of temporal variations in ε_{Nd} values of conodonts with regression/transgression events in the Upper Devonian of the Tafilalt Platform provides crucial evidence for the sensibility of the Nd isotopic composition of seawater in response to fluctuations in the sea level (Fig. 49). Although variations in ε_{Nd} values may also result from changes in seawater circulation, the eustasy appears to be the most effective factor that governed temporal changes in the Nd isotopic composition of seawater. Because regressions accelerate erosional processes and thus provoke an enhanced supply of nonradiogenic Nd to the ocean, they cause a decline in ε_{Nd}. Consequently, transgressions are responsible for positive shifts in ε_{Nd} values of seawater. Thus, the ε_{Nd} curves seem to be very useful for deciphering sea-level fluctuations. Effects of other factors on temporal

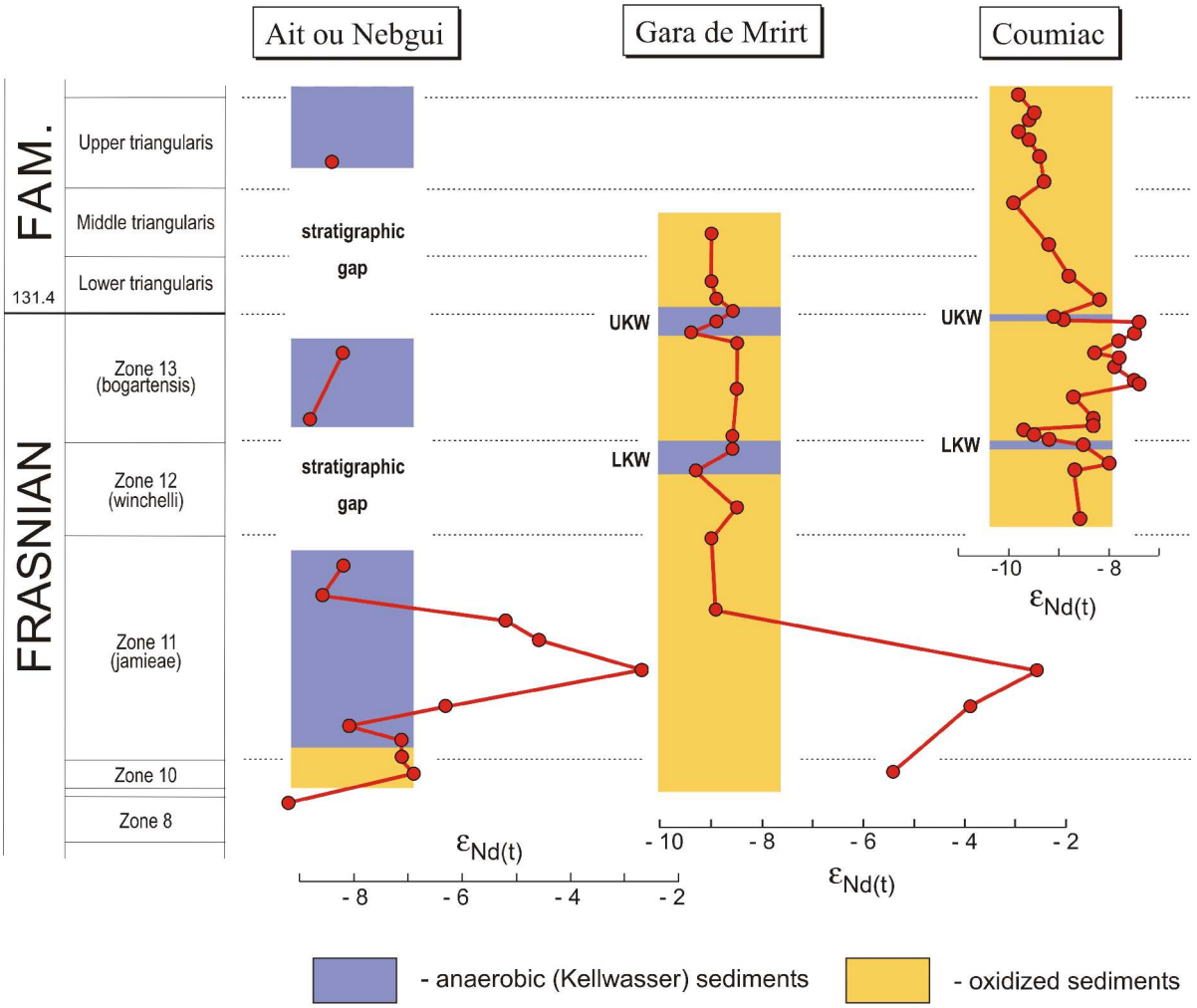

Fig. 49. Temporal variations of ε_{Nd} values in conodonts of the Frasnian/Famennian transition of the Anti-Atlas (Ait ou Nebgui section), Moroccan Meseta (Gara de Mrirt section) and the Montagne Noire (Coumiac section). Note the strong diachronous development of the organic-rich Kellwasser facies and coincidence of regressive trends (Coumiac, Mrirt) with stratigraphic gaps in the succession of the eastern Anti-Atlas. UKW = Upper Kellwasser unit, LKW = Lower Kellwasser unit.

changes in ε_{Nd} values can be minimized or even excluded by analysis of trends in different sections located at various palaeoceanographic positions.

On the basis of the ε_{Nd} curves obtained during this study, an attempt has been made to reconstruct the sea-level fluctuations during the Late Devonian. The amplitudes of sea-level changes are proportional to peak dimensions in the ε_{Nd} curves and the magnitude of erosional events. The relative changes in sea level inferred from the Nd isotopic data are presented in Figure 50 and compared with the conventional Late Devonian eustatic sea-level curve derived from facies data. The latter was constructed by JOHNSON et al. (1985) and modified by JOHNSON & SANDBERG (1988) and SANDBERG et al. (1992). In the present study, an additional modification of this curve has been performed by plotting against the quantitative biostratigraphic framework for the

Frasnian (KLAPPER, 1997) and the Famennian (BELKA, unpublished). The new, isotopically-based eustatic curve shows five main fluctuations labelled with numbers from I to V (Fig. 50):

I. This most prominent transgressive phase took place during the Zone 11 (*jamieae*). It is well constrained by a strong positive excursion in $\varepsilon_{Nd,}$ which can be recognized in all of investigated sections in the eastern Anti-Atlas (Figs. 37-39) and in the Moroccan Meseta (Fig. 45). It correlates perfectly with the most pronounced Devonian transgression (cycle IId *sensu* JOHNSON et al., 1985) recognized worldwide on the basis of facies onlap and expansion of the conodont species *Palmatolepis semichatovae* (e.g. JOHNSON & SANDBERG, 1988; SANDBERG et al. 1992). The isotopic data reveal, however, a significantly shorter duration of this transgression than previously postulated on the basis of facies data.

II. The regression within the uppermost part of the Zone 12 is indicated by a decrease in ε_{Nd} noticed in the Coumiac and Mrirt sections (Fig. 45-46). It is also supported by the presence of a stratigraphic gap comprising the entire Zone 12 in the eastern Anti-Atlas (Figs. 37-38). The lower Kellwasser unit in the Moroccan Meseta and the Montagne Noire developed during this regression. It is important to note that SANDBERG et al. (1992) postulated that the regression occurred immediately after the deposition of the Lower Kellwasser unit.

III. This long-term highstand phase within the Zone 13 is well documented in the Coumiac section (Fig. 46). It was interrupted by several, most probably subordinate fluctuations. Another evidence for the sea-level rise in the Zone 13 is the positive shift in ε_{Nd} recognized in the Mech Irdane section (Fig. 37). SANDBERG et al. (1992) suggested that this transgressive phase terminated during deposition of the Upper Kellwasser unit. The Nd isotopic data do not confirm this hypothesis; they document an earlier termination of this phase.

IV. This regression in the uppermost part of the Zone 13 is documented by a negative excursion in the ε_{Nd} curves of Coumiac (Fig. 46), Mrirt (Fig. 45) and Lahmida (Fig. 39). In the Mech Irdane and Ait ou Nebgui sections (Figs. 37-38), it is responsible for shallowing resulting in a stratigraphic gap that comprises the Frasnian/Famennian boundary level. Like during regression II, organic-rich sediments (the Upper Kellwasser unit) was deposited during this event. As indicated by data from Coumiac and Mrirt sections, the regression commenced before the onset of the Kellwasser facies and terminated already before its end. The upper part of the Upper Kellwasser unit was deposited already during the subsequent transgressive trend. SANDBERG et al. (1992) proposed that, with the exception of its basal layer, the Upper

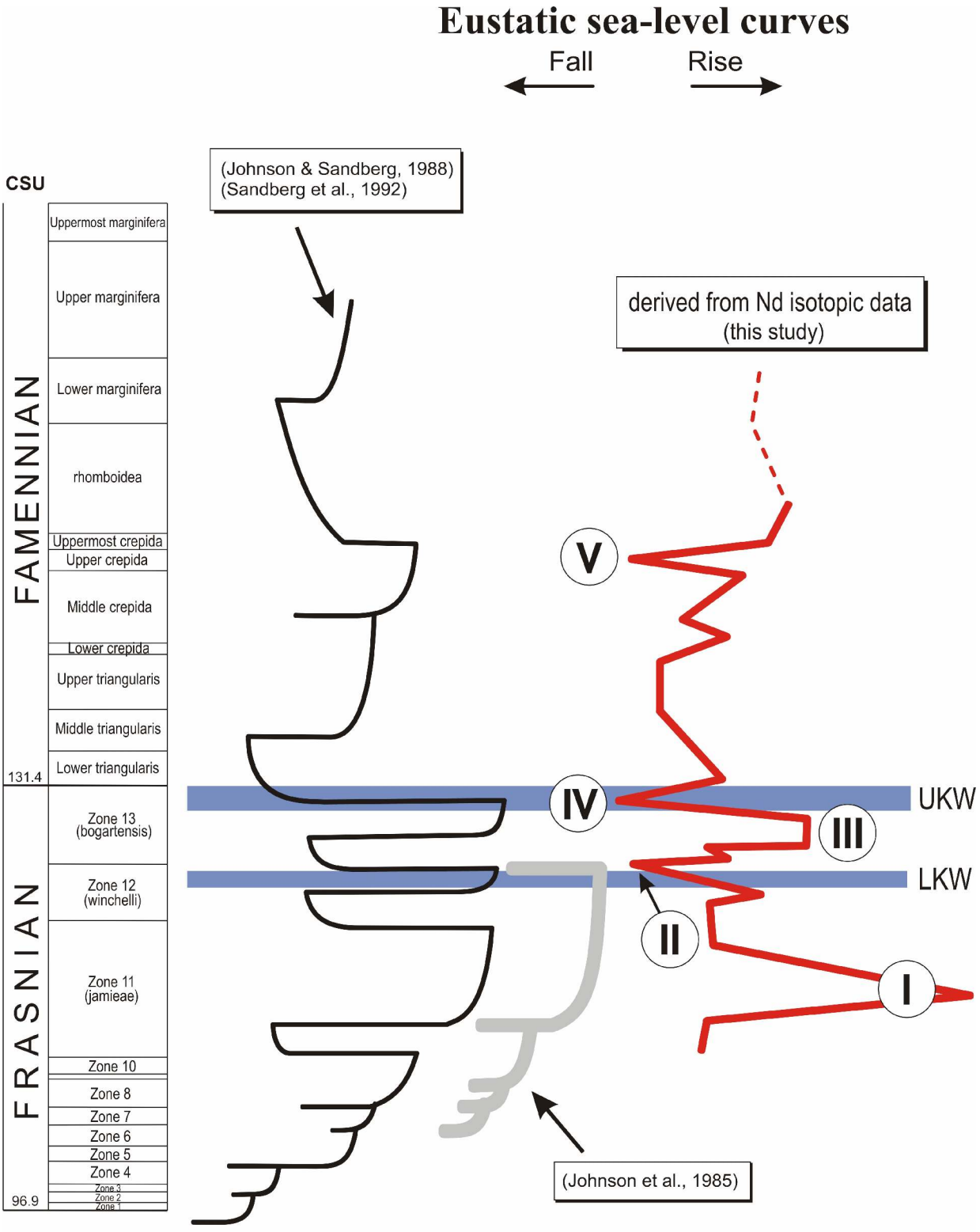

Fig. 50. Comparison of the Late Devonian eustatic sea-level curve inferred from temporal trends in ε_{Nd} values (red) with that derived from facies data (black and grey). Labels I to V indicate prominent sea-level changes. The Nd isotopic data document that the deposition of both Kellwasser units took place during regressive phases. The curves are plotted against the quantitative biostratigraphic framework of the Frasnian (Klapper, 1997) and the Famennian (Belka, unpublished).

Kellwasser unit developed entirely during a regressive regime.

V. The regression within the Upper *crepida* zone is based on the stratigraphic gap recognized in the Mech Irdane section (Fig. 37). Negative peaks in ε_{Nd} curves occur in the Coumiac and Lahmida sections (Figs. 37, 40) but they are weak and insufficiently constrained by biostratigraphy. JOHNSON & SANDBERG (1988) recognized a strong regressive event at more or less the same stratigraphic level. A precise correlation with regression V is difficult because they used an old zonal scheme with tripartite subdivision of the *crepida* zone.

11 Conclusions

The large number of conodont samples investigated during the present study allowed new insights into the Nd isotopic and elemental systematics of conodonts. The data suggest that conodonts provide a reliable record of the Nd isotopic signatures of ancient seawater. Hence, this study puts constraints on the role of the Nd isotopic composition of conodonts as a tool for palaeoceanography and sea-level research of the Paleozoic seas. It is concluded that:

1. Conodont fluorapatite contains large amounts of Nd. Although significant variation in Nd concentrations occurs between different conodont elements within a single conodont sample, each element in the sample yields identical Nd isotopic composition.

2. There is no correlation between Nd isotopic signatures of conodont samples, their Nd content and the level of thermal alteration. Thus, it seems that Nd concentrations of conodonts were not modified by secondary (diagenetic) processes. All this confirms earlier suggestions that ε_{Nd} values of conodonts represent a signature of a single reservoir, namely that of ancient seawater.

3. Nd concentrations in conodont crowns (from 25 to 280 ppm) depend on their morphology; the higher the surface /volume ratio of conodont elements the higher is their Nd content. Conodonts with a similar shape achieved mostly a similar level of Nd concentration. This proves the presence of a saturation limit for fluorapatite tissue exposed to seawater. Because this saturation level was often attained for conodonts deposited on the carbonate platforms and less frequently in the basinal realm, with a higher sedimentation rate, it is very likely that conodonts have acquired their Nd prior to burial while still in contact with seawater.

4. The relation between the morphology of conodonts and their Nd contents allows an easy

approximation of the Nd concentration in conodont samples. This is very useful for isotopic analysis, because samples can be spiked appropriately.

5. Shark teeth and fragments of placoderms are more susceptible to diagenetic alteration than conodonts. If unaltered, shark teeth and placoderm tissue exhibit slightly less radiogenic ε_{Nd} values than coeval conodonts. Their Sm/Nd isotopic system can already be disturbed by a moderate thermal overprint. Nevertheless, fossil fish remains can be useful as palaeoceanographic proxies in the Palaeozoic shallow-water or lagoonal sediments where conodonts are generally rare or absent.

6. Temporal trends in Nd isotopic composition of conodonts reflect sea-level fluctuations. The ε_{Nd} values decreased during regression phases when enhanced erosion accelerated supply of low radiogenic Nd from old continental sources. A rise in sea level generated a positive shift in ε_{Nd} values due to input of more radiogenic oceanic water into the seawater reservoir of the shelf areas. The range and rate of changes in ε_{Nd} values depended on the dynamics of eustatic sea-level fluctuations and also on the palaeoceanographic position of the studied sections. The method has a great potential for sea-level research and palaeoceanography because sea-level changes can be recognized independently from facies, biota and lithology. Sea-level fluctuations can even be recognized in successions yielding a uniform, monotonous lithological development, which are useless for sequence stratigraphy and conventional facies analysis.

7. On the basis of temporal fluctuations in the Nd isotopic composition of conodonts from the western part of the Variscan realm (Anti-Atlas, Moroccan Meseta, Montagne Noire) an eustatic sea-level curve for the late Frasnian and early Famennian was constructed. It reveals five prominent eustatic events. These are:

I - "*semichtovae*" transgression during the Zone 11
II - regression at the end of the Zone 12
III - highstand phase in the Zone 13
IV - regression at the end of the Zone 13
V - regression during the Upper *crepida* Zone

8. Nd isotopic data do not confirm the hitherto commonly postulated transgressive character of the Kellwasser lithology. In the western part of the Variscan realm, the onset and duration of the organic-rich Kellwasser facies is strongly diachronous. In the eastern Anti-Atlas, its development began during the regressive phase in the lower part of the Zone 11. Similarly,

the Upper and Lower Kellwasser Limestones in the Coumiac and Mrirt sections were deposited during the regressions II and IV, respectively. These two eustatic events are responsible for the extensive erosion and the origin of stratigraphic gaps on the carbonate platforms of the Anti-Atlas.

9. On the basis of the lateral variations in ε_{Nd} of conodonts an attempt was made to reconstruct the seawater circulation on the Anti-Atlas shelf. Data from two horizons, the base and the top of the Kellwasser facies, were selected for this purpose. During the onset of the Kellwasser facies (Zone 11) a general seawater flow from the southwest towards the east was recognized. The circulation pattern was complex due to local riverine input from the West African Craton in the south and from the exposed Precambrian basement in the west. During the end of the Kellwasser facies (*rhomboidea* Zone) seawater circulation was dominated by a general westward flow and a much weaker countercurrent in the central Tafilalt. The isotopically based circulation patterns are in very good agreement with orientation of orthoconic cephalopods, which is interpreted to be created by currents. The episodic entrance of oceanic waters on the shelf during the Frasnian (Zone 11) documents the connection of the Anti-Atlas shelf area with the Rheic Ocean to the southwest and with the Variscan Sea to the north.

10. Regionally different Nd isotopic and Sm/Nd elemental characteristics of conodonts in the Variscan realm indicate the presence of two different water masses. The oceanic aquafacies was characterized by high radiogenic ε_{Nd} values (from -2 to -5), similar to those of the modern Pacific Ocean. The shelf aquafacies yielded low ε_{Nd} values (from -6 to -12), reflecting Nd supply from Precambrian continental sources, and a wide range of Sm/Nd ratios, comparable with those of the modern epeiric seas. Both aquafacies differed not only in their Nd isotopic signatures but also showed different C isotopic evolution. The geochemical decoupling between different aquafacies in the Variscan realm testifies a restricted water exchange between shelves and the ocean. The oceanic waters entered the shelf areas only episodically during transgressions. Fluctuations of the sea level modified the participation of both aquafacies on the shelves and produced temporal and spatial variations in the Nd isotopic signal.

References

ALBARÈDE, F. & GOLDSTEIN, S.L. (1992) World map of Nd isotopes in sea-floor ferromanganese deposits. *Geology*, **20**, 761-763.

ALDRIDGE, R.J., BRIGGS, D.E.G., SMITH, M.P., CLARKSON, E.N.K. & CLARK, N.D.L. (1993) The anatomy of conodonts. *Philosophical Transactions of the Royal Society of London, Series B*, **340**, 405-421.

ALIBO, D.S. & NOZAKI, Y. (1999) Rare earth elements in seawater: Particle association, shale-normalized and Ce oxidation. *Geochimica et Cosmochimica Acta*, **63**, 363-372.

ALLARY, A., ANDRIEUX, J, LAVENU, A. & RIBEYROLLES, M.(1972) Les nappes hercyniennes de la Meseta orientale (Maroc central). *Comptes Rendus, Académie des Sciences de Paris*, **274 D**, 2284-2287.

ALLARY, A., LAVENU, A. & RIBEYROLLES, M. (1976) Etude tectonique et microtectonique d´un segment de la chaîne hercynienne dans la partie sud-orientale du Maroc central. *Notes et Mémoires, Service Géologique du Maroc*, **261**, 1-169.

AMAKAWA, H., ALIBO, D.S & NOZAKI, Y. (2000) Nd isotopic composition and REE pattern in the surface waters of the eastern Indian Ocean and its adjacent seas. *Geochimica et Cosmochimica Acta*, **64**, 1715-1727.

ARMSTRONG, H.A., PEARSON, D.G. & GRISELIN, M. (2001) Thermal effects on rare earth element and strontium isotope chemistry in single conodont elements. *Geochimica et Cosmochimica Acta*, **65**, 435-441.

BECKER, R.T., FLAJS, G., HUOSE, M.R. & KLAPPER, G. (1989) Frasnian-Famennian extinction events in the Devonian at Coumiac, southern France. *Comptes Rendus, Académie des Sciences de Paris*, sér. II, **309**, 259-266.

BELKA, Z. (1991) Conodont colour alteration patterns in Devonian rocks of the eastern Anti-Atlas, Morocco. *Journal of African Earth Sciences*, **12**, 417-428.

BELKA, Z. (1993) Thermal and burial history of the Cracow-Silesia region (southern Poland) assessed by conodont CAI analysis. *Tectonophysics*, **227**, 161-190.

BELKA, Z. (1998) Taxonomy, phylogeny and biogeography of the late Famennian conodont genus *Mashkovia*. *Journal of Micropalaeontology*, **17**, 119-124.

BELKA, Z. & WENDT, J. (1992) Conodont biofacies patterns in the Kellwasser facies (upper Frasnian/lower Famennian) of the eastern Anti-Atlas, Morocco. *Palaeogeography, Palaeoclimatology, Palaeoecology*, **91**, 143-173.

BELKA, Z., KAZMIERCZAK, M. & KAUFMANN, B. (1997) Tectonic control on the sedimentation, volcanic activity and the growth of mud mounds in the Palaeozoic of the eastern Anti-

Atlas, Morocco. In: First International Conference on North Gondwanan Mid-Palaeozoic Biodynamics (IGCP Project 421), Vienna 17-21 September, *Meeting Program and Abstracts*, **9**.

BELKA, Z., KLUG, C., KAUFMANN, B., KORN, D., DÖRING, S., FEIST, R. & WENDT, J. (1999) Devonian conodont and ammonoid succession of the eastern Tafilalt (Ouidane Chebbi section), Anti-Atlas, Morocco. *Acta Geologica Polonica*, **49**, 1-23.

BELKA, Z., HEGNER, E. & DOPIERALSKA, J. (2000) Sea-level fluctuations and palaeo-oceanography of the Variscan Sea inferred from Nd isotopic composition of conodonts. EPA Workshop *„Biomarkers and Stable Isotopes in Palaeontology“*, 17-18. Frankfurt.

BELKA, Z., DOPIERALSKA, J. & SKOMPSKI, S.(2002) Conodont stratigraphy of the Late Devonian Kellwasser facies in the eastern Anti-Atlas, Morocco. *Strata*, **12**, 20.

BERKOWSKI, B. (2002) Famennian Rugosa and Heterocorallia from southern Poland. *Palaeontologia Polonica*, **61**, 1-87.

BERNAT, M. (1975) Les isotopes de l´uranium et du thorium et les terres rares dans l´environment marin: Cahiers ORSTOM Séries. *Geology*, **7**, 65-83.

BERTRAM, C.J., ELDERFIELD, H., ALDRIDGE, R.J. & CONWAY MORRIS, S. (1992) $^{87}Sr/^{86}Sr$, $^{143}Nd/^{144}Nd$ and REEs in Silurian phosphatic fossils. *Earth and Planetary Science Letters*, **113**, 239-249.

BERTRAM, C.J. & ELDERFIELD, H. (1993) The geochemical balance of the rare earth elements and neodymium isotopes in the oceans. *Geochimica et Cosmochimica Acta*, **57**,1957-1986.

BOUABDELLI, M. (1989) Tectonique et sédimentation dans un bassin orogénique: Le sillon viséen d´Azrou-Khénifra (Est du massif hercynien central du Maroc). PhD thesis, University of Strasbourg, 1-256.

BRACHERT, T.C., BUGGISCH, W., FLÜGEL, E., HÜSSNER, H.M., JOACHIMSKI, M.M., TOURNEUR, F., & WALLISER, O.H. (1992) Controls of mud mound formation: the Early Devonian Kess-Kess carbonates of the Hamar Laghdad, Antiatlas, Morocco. *Geologische Rundschau*, **81**, 15-44.

BRAUNS, M. & HAACK, U. (2001) Osmium isotopes and the Upper Devonian “Kellwasser” event. *Terra Nostra*, **2001/4**, 3-6.

BRUHN, F., KORTE, Ch., MEIJER, J., STEPHAN, A. & VEIZER, J. (1997) Trace element concentrations in conodonts measured by the Bohum proton microprobe. *Nuclear Instruments and Methods in Physical Research B*, **130**, 636-640.

BULTYNCK, P. (1985) Lower Devonian (Emsian) - Middle Devonian (Eifelian and lowermost Givetian) conodont successions from the Ma'der and the Tafilalt, southern Morocco. *Courier Forschungsinstitut Senckenberg*, **75**, 261-286.

BULTYNCK, P. & HOLLARD, H. (1980) Distribution comparée de Conodontes et Goniatites dévoniens des plaines du Dra, du Ma'der et du Tafilalt (Maroc). *Aardkundige Mededelingen*, **1**, 7-75.

BUGGISCH, W. & CLAUSEN, C.D. (1972) Conodonten- und Goniatiten-Faunen aus dem oberen Frasnium und unteren Famennium Marokkos (Tafilalt, Antiatlas). *Neues Jarbuch für Geologie und Paläontologie, Abhandlungen*, **141**, 137-167.

BURKE, W.H., DENISON, R.E., HETHERINGTON, E.A., KOEPNICK, R.B., NELSON, H.F. & OTTO, J.B. (1982) Variation of $^{87}Sr/^{86}Sr$ throughout Phanerozoic time. *Geology*, **10**, 516-519.

Charles, Ch.D. & Fairbanks, R.G. (1992) Evidence from Southern Ocean sediments for the effect of North Atlantic deep-water flux on climate. *Nature*, **355**, 416-419.

CHARPENTIER, R.R. (1984) Conodonts through time and space: Studies in conodont provincialism. *Geological Society of America, Memoir*, **196**, 11-32.

CHEN, Z., LI, Z.X., POWELL, C. M. & BALME, B.E. (1993) Palaeomagnetism of the Brewer Conglomerate in central Australia, and fast movement of Gondwanaland during the Late Devonian. *Geophysical Journal International*, **115**, 564-574.

CYGAN, C. (1995) Les biofaciès à Conodontes dans le Dévonien des Pyrénees: leur évolution dans l'espace et le temps. *Travaux du Laboratorie de Géologie Structurale et Tectonophysique, Université Paul-Sabatier*, 1-639.

DALZIEL, I.W.D., DALLA SALDA, L.H. & GAHAGAN, L.M. (1994) Paleozoic Laurentia-Gondwana interaction and the origin of the Appalachian-Andean mountain system. *Geological Society of America, Bulletin*, **106**, 243-252.

DASH, D.J. & BISCAYE, P.E. (1971) Isotopic composition of Cretaceous-to-Recent pelagic foraminifera. *Earth and Planetary Science Letters*, **11**, 201-204.

DENISON, R.E., KOEPNICK, R.B., BURKE, W.H., HETHERINGTON, E.A. & FLETCHER, A. (1994) Construction of the Mississippian, Pennsylvanian and Permian seawater $^{87}Sr/^{86}Sr$ curve. *Chemical Geology*, **112**, 145-167.

DEPAOLO, D.J. (1988) Neodymium Isotope Geochemistry, 1-187. Springer Verlag, Berlin.

DEPAOLO, D.J. & WASSERBURG, G.J. (1977) The sources of island arcs as indicated by nd and Sr isotopic studies. *Geophysical Research Letters*, **4**, 465-468.

DESTOMBES, J., HOLLARD, H. & WILLEFERT, S. (1985) Lower Palaeozoic rocks of Morocco. In: HOLLAND, C. H. (ed.), Lower Palaeozoic Rocks of North-Western and West-Central Africa. Chichester, John Wiley and Sons, 91-336.

DICKIN, A.P. (1995) Radiogenic Isotope Geology, 1-490. Cambridge University Press,

Cambridge.

DIENER, A., EBNETH, S., VEIZER, J. & BUHL, D. (1996) Strontium isotope stratigraphy of the Middle Devonian: Brachiopods and conodonts. *Geochimica et Cosmochimica Acta*, **60**, 639-652.

DONOGHUE, P.C.J., FOREY, P.L. & ALDRIDGE, R.J. (2000) Conodont affinity and chordate phylogeny. *Biological Review*, **75**, 191-251.

EBNETH, S., DIENER, A., BUHL, D. & VEIZER, J. (1997) Strontium isotope systematics of conodonts: Middle Devonian, Eifel Mountains, Germany. *Palaeogeography, Palaeoclimatology, Palaeoecology*, **132**, 79-96.

ELDERFIELD, H., HAWKESWORTH, C.J., GRAVES, M.J. & CALVERT, S.E. (1981) Rare earth element geochemistry of oceanic ferromanganese nodules and associated sediments. *Geochimica et Cosmochimica Acta*, **45**, 513-528.

ELDERFIELD, H. (1986) Strontium isotope stratigraphy. *Palaeogeography, Palaeoclimatology, Palaeoecology*, **57**, 71-90.

ELDERFIELD, H. & GIESKES, J.M. (1982) Sr isotopes in interstitial waters of marine sediments from Deep Sea Drilling Project Cores. *Nature*, **300**, 493-497.

ELDERFIELD, H. & GRAVES, M.J. (1982) The rare earth elements in seawater. *Nature*, **296**, 214-219.

ELDERFIELD, H. & PAGETT, R. (1986) REE in ichthyoliths: variations with redox conditions and depositional environment. *The Science of the Total Environment*, **49**, 175-197.

ELDERFIELD, H., UPSTILL-GODDARD, R. & SHOLKOVITZ, E.R. (1990) The rare earth elements in rivers, estuaries, and coastal seas and their significance to the composition of ocean waters. *Geochimica et Cosmochimica Acta*, **54**, 971-991.

ENGEL, W., FEIST, R. & FRANKE, W. (1982) Le Carbonifère anté-stéphanien de la Montagne Noire: rapports entre mise en place des nappes et sédimentation. *Bull. Bureau Recherches Géol. et Miniéres*, 2e série, section I, **4**, 341-389.

EPSTEIN, A.G., EPSTEIN, J.B. & HARRIS, L.D. (1977) Conodont color alteration - an index to organic metamorphism. *U.S. Geological Survey, Professional Papers*, **995**, 1-27.

FANTON, K.C., HOLMDEN, C., NOWLAN, G.S. & HAIDL, F.M. (2002) 143Nd/144Nd and Sm/Nd stratigraphy of Upper Ordovician epeiric sea carbonates. *Geochimica et Cosmochimica Acta*, **66**, 241-255.

FARMER, G.L. & DEPAOLO, D.J. (1984) Origin of Mesozoic and Tertiary granite in the western US and implications for pre-Mesozoic crustal structure. II. Nd and Sr isotopic studies of unmineralized and Cu- and Mo-mineralized granite in the Precambrian craton. *Journal of*

Geophysical Research, **89**, 10141-10160.

FEIST, R. (1990) The Frasnian - Famennian boundary and adjacent strata of the eastern Montagne Noire, France. Guidebook of the Field Meeting, Subcommission on Devonian Stratigraphy, 69 p.

FEIST, R. (2002) The Palaeozoic of the Montagne Noire, southern France. Guidebook of the Field Excursion, ECOS VIII and IGCP 421. 82 p.

FEIST, R., ECHTLER, H., GALTIER, J. & MOUTHIER, B. (1994) The Massif Central - Biostratigraphy and dynamic of the nonmetamorphic sedimentary record. In: KEPPIE, J. D. (ed.) Pre-Mesozoic geology in France and related areas, 289-304.

FELISTYN, S., STURESSON, U., POPOV, L. & HOLMER, L. (1998) Nd isotopic composition and rare earth element distribution in early Paleozoic biogenic apatite from Baltoscandia: A signature of Iapetus ocean water. *Geology*, **26**, 1083-1086.

FRANKE, W. (2000) The mid-European segment of the Variscides: tectonostratigraphic units, terrane boundaries and plate tectonic evolution. In: FRANKE, W., HAAK, V., ONCKEN, O. & TANNER, D. (eds), Orogenic Processes: Quantification and Modelling in the Variscan Belt. *Geological Society, London, Special Publications*, **179**, 21-34.

GIRARD, C. & ALBARÉDE, F. (1996) Trace elements in conodont phosphates from the Frasnian/Famennian boundary. *Palaeogeography, Palaeoclimatology, Palaeoecology*, **126**, 195-209.

GOLDSTEIN, S.J. & JACOBSEN, S.B. (1987) Nd and Sr isotope systematics of river water dissolved material: Implications for the sources of Nd and Sr in seawater. *Chemical Geology*, **66**, 245-272.

GOLDSTEIN, S.J. & JACOBSEN, S.B. (1988a) Nd and Sr isotope systematics of river water suspended material: Implications for crustal evolution. *Earth and Planetary Science Letters*, **87**, 249-265.

GOLDSTEIN, S.J. & JACOBSEN, S.B. (1988b) Rare earth elements in river waters. *Earth and Planetary Science Letters*, **89**, 35-47.

GOLDSTEIN, S.J. & JACOBSEN, S.B. (1988c) Rare earth elements in the Great Whale estuary, N.W. Quebec. *Earth and Planetary Science Letters*, **88**, 241-252.

GOLDSTEIN, S.J. & O´NIONS, R.K. (1981) Nd and Sr isotopic relationships in pelagic clays and ferromanganese deposits. *Nature*, **291**, 324-327.

GRANDJEAN, P., CAPPETTA, H., MICHARD, A. & ALBARÉDE, F. (1987) The assessment of REE patterns and $^{143}Nd/^{144}Nd$ ratios in fish remains. *Earth and Planetary Science Letters*, **84**, 181-196.

GRANDJEAN, P., CAPPETTA, H. & ALBARÉDE, F. (1988) The REE and eNd of 40-70 Ma old fish debris from the West-African Platform. *Geophysical Research Letters*, **15**, 389-392.

GRANDJEAN, P. & ALBARÉDE, F. (1989) Ion probe measurements of rare earth elements in biogenic phosphates. *Geochimica et Cosmochimica Acta*, **53**, 3179-3183.

GRANDJEAN-LÉCUYER, P., FEIST, R. & ALBARÉDE, F. (1993) Rare earth elements in old biogenic apatites. *Geochimica et Cosmochimica Acta*, **57**, 2507-2514.

HAMILTON, P.J., O´NIONS, R.K., BRIDGWATER, D. & NUTMAN, A. (1983) Sm-Nd studies of Archean metasediments and metavolcanics from West Greenland and their implications for the Earth´s early history. *Earth and Planetary Science Letters*, **62**, 263-272.

HAUNOLD, Y., DOBROZEMSKY, G., KRYSTYN, L., KIESL, W.& BICHLER, M. (1999) REE distribution in Triassic conodonts. *Bollettino della Società Paleontologica Italiana*, **37**, 515-525.

HECKEL, P.H. & WITZKE, B.J. (1979) Devonian world paleogeography determined from distribution of carbonates and related lithic paleoclimatic indicators. In: HOUSE, M.R., SCRUTTON, C.T. and BASSETT, M.G. (eds), The Devonian System. *Palaeontological Association, London, Special Papers in Palaeontology*, **23**, 99-123.

HESS, J., BENDER, M.L. & SCHILLING, J.G. (1986) Seawater $^{87}Sr/^{86}Sr$ evolution from Cretaceous to Present - Applications to Paleoceanography. *Science*, **231**, 979-984.

HOLLARD, H. (1967) Le Dévonien du Maroc et du Sahara nord-occidental. In: OSWALD, D.H. (ed.), International Symposium on the Devonian System, Calgary. *Alberta Society of Petroleum Geologists*, 203-244.

HOLLARD, H. (1974) Recherches sur la stratigraphie des formations du Dévonien moyen, de l´Emsien supérieur au Frasnien, dans le Sud du Tafilalt et dans le Ma´der (Anti-Atlas oriental). *Notes et Mémoires, Service Géologique du Maroc*, **264**, 7-68.

HOLLARD, H. (1981) Tabeleaux de corrélations du Silurien et du Dévonien de l´Anti-Atlas. *Notes et Mémoires, Service Géologique du Maroc*, **308**, 23.

HOLMDEN, C., CREASER, R.A., MUEHLENBACHS, K., BERGSTRÖM, S.M. & LESLIE, S.A. (1996) Isotopic and elemental systematics of Sr and Nd in 454 Ma biogenic apatites: Implications for paleoseawater studies. *Earth and Planetary Science Letters*, **142**, 425-437.

HOLMDEN, C., CREASER, R.A., MUEHLENBACHS, K., LESLIE, S.A. & BERGSTRÖM, S.M. (1998) Isotopic evidence for geochemical decoupling between ancient epeiric sea and bordering oceans: Implications for secular curves. *Geology*, **26**, 567-570.

HOUSE, M.R., KIRCHGASSER, W.T., PRICE, J.D. & WADE, G. (1985) Goniatites from Frasnian (Upper Devonian) and adjacent strata of the Montagne Noire. *Hercynica*, **1**, 1-19.

HOYLE, J., ELDERFIELD, H., GLEDHILL, A. & GREAVES, M. (1984) The behaviour of the rare earth elements during mixing of river and sea waters. *Geochimica et Cosmochimica Acta*, **48**, 143-149.

HUVELIN, P. (1970) Mouvements hercyniens précoces dans la région de Mrirt (Maroc). *Comptes Rendus, Académie des Sciences de Paris*, **271 D**, 953-955.

HUVELIN, P. (1973) Déformations hercyniennes précoces dans la région compise entre Azrou, Aguelmous et Khénifra (massif hercynien central). *Notes et Mémoires, Service Géologique du Maroc*, **254**, 93-107.

JAMES, D.E. (1982) A combined O, SR, Nd, and Pb isotopic and trace element study of crustal contamination in central Andean lavas, I. Local geochemical variations. *Earth and Planetary Science Letters*, **57**, 47-62.

JEANDEL, C. (1993) Concentration and isotopic composition of Nd in the South Atlantic Ocean. *Earth and Planetary Science Letters*, **117**, 581-591.

JEANDEL, C., BISHOP, J.K. & ZINDLER, A. (1995) Exchange of neodymium and its isotopes between seawater and small and large particles in the Sargasso Sea. *Geochimica et Cosmochimica Acta*, **59**, 535-547.

JENKYNS, H.C., JONES, Ch.E., GRÖCKE, D.R., HASSELBO, S.P. & PARKINSON, D.N. (2002) Chemostratigraphy of the Jurassic System: applications, limitations and implications for palaeoceanography. *Journal of the Geological Society*, London, **159**, 351-378.

JOACHIMSKI, M.M. & BUGGISCH, W. (2002) Conodont apatite $\delta^{18}O$ signatures indicate climatic cooling as a trigger of the Late Devonian mass extinction. *Geology*, **30**, 711-714.

JOACHIMSKI, M.M., PANCOST, R.D., FREEMEN, K.H., OSTERTAG-HENNING, C. & BUGGISCH, W. (2002) Carbon isotope geochemistry of the Frasnian-Famennian transition. *Palaeogeography, Palaeoclimatology, Palaeoecology*, **181**, 91-109.

JOHNSON, J.G., KLAPPER, G. & SANDBERG, C.A. (1985) Devonian eustatic fluctuations in Euramerica. *Geological Society of America, Bulletin*, **96**, 567-587.

JOHNSON, J.G. & SANDBERG, C.A. (1988) Devonian eustatic events in the Western United States and their biostratigraphic responses. In: MCMILLAN, N. J., EMBRY, A. F. & GLASS, D. J.(eds), Devonian of the World, vol. III: Paleontology, paleoecology and biostratigraphy. *Canadian Society of Petroleum Geologist, Memoir*, **14**, 171-178.

JONES, C.E., HALLIDAY, A.N., REA, D.K. & OWEN, R.M. (1994) Neodymium isotopic variations in North Pacific modern silicate sediment and the insignificance of detrital REE contributions to seawater. *Earth and Planetary Science Letters*, **127**, 55-66.

JOSEPH, J. & TSIEN, H.H. (1977) Les Pyrénées dans la paléogéographie dévonienne. Nouveaux jalons fournis parles Tétracoralliares. *Mémoires du Bureau de Recherches Géologiques*

et Minieres, **89**, 112-115.

KASTING, J.R. (1989) Long-term stability of the Earth´s climate. *Palaeogeography, Palaeoclimatology, Palaeoecology*, **75**, 83-95.

KAUFMANN, B. (1998) Facies, stratigraphy and diagenesis of Middle Devonian reef- and mud-mounds in the Mader (eastern Anti-Atlas, Morocco). *Acta Geologica Polonica*, **48**, 43-106.

KAY, R.W., RUBENSTONE, J.L. & KAY, S.M. (1986) Aleutian terranes from Nd isotopes. *Nature*, **322**, 605-609.

KEASLER, K.M. & LOVELAND, W.D. (1982) Rare earth elemental concentrations in some Pacific Northwest rivers. *Earth and Planetary Science Letters*, **61**, 68-72.

KETO, L.S. & JACOBSEN, S.B. (1987) Nd and Sr isotopic variations of Early Paleozoic oceans. *Earth and Planetary Science Letters*, **84**, 27-41.

KETO, L.S. & JACOBSEN, S.B. (1988) Nd isotopic variations of Phanerozoic paleoceans. *Earth and Planetary Science Letters*, **90**, 395-410.

KIDDER, D.L & EDDY-DILEK, C.A. (1994) Rare-earth element variation in phosphate nodules from midcontinent Pensylvanian cyclothems. *Journal of Sedimentary Research*, **A64**, 584-592.

KLAPPER, G., FEIST, R., BECKER, R.T. & HOUSE, M. (1993). Definition of the Frasnian/Famennian Stage boundary. *Episodes*, **16 (4)**, 433-441.

KLAPPER, G. (1997) Graphic correlation of Frasnian (Upper Devonian) sequences in Montagne Noire, France, and western Canada. In: Klapper, G., Murphy, M.A. & Talent, J.A. (eds), Paleozoic Sequence Stratigraphy, Biostratigraphy, and Biogeography: Studies in Honor of J. Granville ("Jess") Johnson. *Geological Society of America, Special Paper,* **321,** 113-129.

KOVACH, J. & ZARTMAN, R.W. (1981) U-Th-Pb dating of conodonts. *Geological Society of America, Abstracts with Programs*, **13**, 285.

KRYLATOV, S. & STOPPEL, D. 1(971) Attribution au Frasnien de la série de Sia (Zone primaire axiale). Ses rapports avec celle des Agudes-Cap de Pales. Conséquences paléogéographiques. *Zeitschrift der Deutschen Geologischen Gesellschaft*, **122**, 213-230.

KUMP, L.R. (1989) Chemical stability of the atmosphere and ocean. *Palaeogeography, Palaeoclimatology, Palaeoecology*, **75**, 123-136.

LAZREQ, N. (1992) The Upper Devonian of Mrirt (Morocco). *Courier Forschungsinstitut Senckenberg*, **154**, 107-123.

LAZREQ, N. (1999) Biostratigraphie des conodontes du Givetien au Famennien du Maroc central -

biofaciés et événement Kellwasser. *Courier Forschungsinstitut Senckenberg*, **214**, 1-111.

LEDRU, P., AUTRAN, A. & SANTALLIER, D. (1994) Lithostratigraphy of Variscan terranes in the French Massif Central: A basis for palaeogeographical reconstruction. In: KEPPIE, J. D. (ed.) Pre-Mesozoic geology in France and related areas. Springer, Heidelberg, 276-288.

LEWANDOWSKI, M. (2002) Assembly of Pangea: combined paleomagnetic and paleoclimatic approach. *Advances in Geophysics*, (in press).

LLOYD, M.R. (1964) Variations in the oxygen and carbon isotope ratios of Florida Bay mollusks and the environmental significance. *Journal of Geology*, **72**, 84-111.

LUZ, B., KOLODNY, Y. & KOVACH, J. (1984) Oxygen isotope variations in phosphate biogenic apatites, III. Conodonts. *Earth and Planetary Science Letters*, **69**, 255-262.

MACKENZIE, F.T. & AGEGIAN, C. (1989) Biomineralization and tentative links to plate tactonics. In: CRICK, R.E. (ed.), Origin and Modern Aspects of Biomineralization in Plants and Animals. *Plenum Press*, 11-28.

MARTIN, J. M., HOGDAHL, O. & PHILIPPOT, J. C. (1976) Rare earth element supply to the ocean. *Journal of Geophysical Research*, **81**, 3119-3124.

MARTIN, E. E. & HALEY, B. A. (2000) Fossil fish teeth as proxies for seawater Sr and Nd isotopes. *Geochimica et Cosmochimica Acta*, **64**, 835-847.

MARTIN, E.E. & MACDOUGALL, J.D. (1995) Sr and Nd isotopes at the Permian/Triassic boundary: A record of climate change. *Chemical Geology*, **125**, 73-99.

MASSA, D. (1965) Observations sur les séries siluro-dévoniennes des confins algéro-marocaines du Sud (1954-1955). - *Notes et Mémoires, Compagnie Française des Pétroles*, **8**, 1-187

MATTE, Ph. (1991) Accretionary history and crustal evolution of the Variscan belt in Western Europe. *Tectonophysics*, **196**, 309-337.

MATTE, Ph. (2001) The Variscan collage and orogeny (480-290 Ma) and the tectonic definition of the Armorica microplate: a review. *Terra Nova*, **13**, 122-128.

MCKERROW, W. S., MAC NIOCAILL, C., AHLBERG, P. E., CLAYTON, G., CLEAL, C. J. & EAGAR, R. M. C. (2000) The late Palaeozoic relations between Gondwana and Laurussia. In: FRANKE, W., HAAK, V., ONCKEN, O. & TANNER, D. (eds), Orogenic Processes: Quantification and Modelling in the Variscan Belt. *Geological Society, London, Special Publications*, **179**, 9-20.

MORAD, S. & FELISTYN, S. (2001) Identification of primary Ce-anomaly signatures in fossil biogenic apatite: implication for the Cambrian oceanic anoxia and phosphogenesis. *Sedimentary Geology*, **143**, 259-264.

MORSE, J.W. & MACKENZIE, F.T. (1990) Geochemistry of Sedimentary Carbonates. *Developements in Sedimentology*, **48**, 1-707.

NARKIEWICZ, M. (1988) Turning points in sedimentary development in the Late Devonian in southern Poland. In: MCMILLAN, N. J., EMBRY, A. F. & GLASS, D. J.(eds), Devonian of the World, vol. II: Sedimentation. *Canadian Society of Petroleum Geologist, Memoir*, **14**, 619-635.

NEUGEBAUER, J. (1988) The Variscan plate tectonic evolution: an improved Iapetus model. *Schweizerische Mineralogisch-Petrographische Mitteilungen*, **68**, 313-333.

NYSÆTHER, E., TORSVIK, T. H., FEIST, R., WALDERHAUG, H. J., EIDE, E. A. (2002) Ordovician palaeogeography with new palaeomagnetic data from the Montagne Noire (Southern France). *Earth and Planetary Science Letters*, **203**, 329-341.

OCZLON, M. S. (1990) Ocean currents and unconformities: The North Gondwana Middle Devonian. *Geology*, **18**, 509-512.

PALMER, M. R. & EDMOND, J. M. (1989) The strontium isotopic budget of the modern ocean. *Earth and Planetary Science Letters*, **92**, 11-26.

PATTERSON, W.P. & WALTER, L.M. (1994) Depletion of ^{13}C in seawater ΣCO_2 on modern carbonate platforms: Significance for the carbon isotopic record of carbonates. *Geology*, **22**, 885-888.

PEDDER, A. E. H. (1999) Paleogeographic Implications of a Devonian (Givetian, Lower *Varcus* Subzone) Rugose Coral Fauna from the Ma´der Basin (Morocco)). *Abhandlungen der geologischen Bundesanstalt*, **54**, 385-434.

PETERMAN, Z. E., HEDGE, C. E. & TOURTELOT, H. A. (1970) Isotopic composition of strontium in sea water throughout Phanerozoic time. *Geochimica et Cosmochimica Acta*, **34**, 105-120.

PIEPGRAS, D. J., WASSERBURG, G. J. & DASH, E. J. (1979) The isotopic composition of Nd in different ocean masses. *Earth and Planetary Science Letters*, **45**,223-236.

PIEPGRAS, D. J. & WASSERBURG, G. J. (1980) Neodymium isotopic variations in seawater. *Earth and Planetary Science Letters*, **50**,128-138.

PIEPGRAS, D. J. & WASSERBURG, G. J. (1985) Strontium and neodymium isotopes in hot springs on the East Pacific Rise and Guaymas Basin. *Earth and Planetary Science Letters*, **72**, 341-356.

PIEPGRAS, D. J. & WASSERBURG, G. J. (1987) Rare earth element transport in the western North Atlantic inferred from Nd isotopic observations. *Geochimica et Cosmochimica Acta*, **51**, 1257-1271.

PIETZNER, H., VAHL, J., WERNER, H. & ZIEGLER, W. (1968) Zur chemischen Zusammensetzung und Mikromorphologie der Conodonten. *Palaeontographica, A,* **128**, 115-152.

PIN Ch., BRIOT D., BASSIN Ch. & POITRASSON, F. (1994) Concomitant separation of strontium and samarium-neodymium for isotopic analysis in silicate samples, based on specific extraction chromatography. *Analytica Chimica Acta,* **298**, 209-222.

PIQUE, A. & MICHARD, A. (1989) Moroccan Hercynides: a synopsis. The Paleozoic sedimentary and tectonic evolution at the northern margin of the West Africa. American *Journal of Science,* **289**, 286-330.

REYNARD, B., LÉCUYER, Ch. & GRANDJEAN, P. (1998) Crystal-chemical controls on rare-earth element concentrations in fossil apatites and implications from paleoenvironmental reconstructions. *Chemical Geology,* **155**, 233-241.

RICHTER, F. M., ROWLEY, D. B. & DE PAOLO, D. J. (1992) Sr isotope evolution of seawater: the role of tectonics. *Earth and Planetary Science Letters,* **109**, 11-23.

SANDBERG, P.A. (1983) An oscillating trend in Phanerozoic non-skeletal carbonate mineralogy. *Nature,* **305**, 19-22.

SANDBERG, C.A., ZIEGLER, W. DREESEN, R. & BUTLER, J.L. (1992) Conodont Biochronology, Biofacies, Taxonomy, and Event Stratigraphy around Middle Frasnian Lion Mudmound (F2h), Frasnes, Belgium. *Courier Forschungsinstitut Senckenberg*, **150**, 1-87.

SCHMITZ, B., ÅBERG, G., WERDELIN, L., FOREY, P. & BENEDIX-ALMGREEN, S.E. (1991) $^{87}Sr/^{86}Sr$, Na, F, Sr and La in skeletal fish debris as a measure of the paleosalinity of fossil-fish habitats. *Geological Society of America, Bulletin,* **103**, 786-794.

SCOTESE, C. R. & MCKERROW, W. S. (1990) Revised World maps and introduction. In: MCKERROW, W. S. & SCOTESE, C. R. (eds), Palaeozoic Palaeogeography and Biogeography, *Geological Society, London, Memoir,* **12**, 1-21.

SHAW, H. F. & WASSERBURG, G. J. (1985) Sm-Nd in marine carbonates and phosphates: Implications for Nd isotopes in seawater and crustal ages. *Geochimica et Cosmochimica Acta*, **49**, 503-518.

SCHINDLER, E. (1990) Die Kellwasser-Krise (hohe Frasne-Stufe, Ober-Devon). *Göttinger Arbeiten zur Geologie und Paläontologie,* **46**, 1-115.

SHOLKOVITZ, E. R. (1992) The geochemistry of rare earth elements in the Amazon River estuary. *Geochimica et Cosmochimica Acta,* **57**, 2181-2190.

SHOLKOVITZ, E. R. & ELDERFIELD, H. (1988) The cycling of dissolved rare earth elements in Chesapeake Bay. *Global Biogeochemical Cycles,* **2**, 157-176.

SHOLKOVITZ, E. R., LANDING, W.M. & LEWIS, B.L. (1994) Ocean particle chemistry: The

fractionation of rare earth elements between suspended particles and seawater. *Geochimica et Cosmochimica Acta*, **58**, 1567-1579.

SHOLKOVITZ, E. R. & SZYMCZAK, R. (2000) The estuarine chemistry or rare earth elements: comparison of the Amazon, Fly, Sepik and the Gulf of Papua systems. *Earth and Planetary Science Letters*, **179**, 299-309.

STAMPFLI, G. M. (1996) The intra-alpine terrain: a paleotethyan remnant in the Alpine Variscides. *Eclogae Geologicae Helvetiae*, **89**, 13-42.

STAMPFLI, G. M. & BOREL, G. D. (2002) A plate tectonic model for the Paleozoic and Mesozoic constrained by dynamic plate boundaries and restored synthetic oceanic isochrones. *Earth and Planetary Science Letters*, **196**, 17-33.

STAUDIGEL, H., DOYLE, P. & ZINDLER, A. (1985) Sr and Nd isotope systematics in fish teeth. *Earth and Planetary Science Letters*, **76**, 45-56.

STETS, J. & WURSTER, P. (1988) Atlas and Atlantic - structural relations. In: Jacobshagen, V. H. (ed.), The Atlas system of Morocco, studies on its geodynamic evolution. *Lecture Notes in Earth Sciences*, **15**, 219-244.

STILLE, P. (1992) Nd-Sr isotope evidence for dramatic changes of paleocurrents in the Atlantic Ocean during the past 80 m.y. *Geochimica at Cosmochimica Acta*, **20**, 387-390.

STILLE, P., STEINMANN, M. & RIGGS, S. R. (1996) Nd isotope evidence for the evolution of the paleocurrents in the Atlantic and Tethys Oceans during the past 180 Ma. *Earth and Planetary Science Letters*, **144**, 9-19.

SWEET, W. C. (1988) The Conodonta. Morphology, Taxonomy, Paleoecology, and Evolutionary History of a Long-Extinct Animal Phylum. *Oxford Monographs on Geology and Geophysics*, **10**, 1-212.

SWEET, W. C. & BERGSTRÖM, S. M. (1974) Provincialism exhibited by Ordovician conodont faunas. *The Society of Economic Paleontologists and Mineralogists, Special Publications*, **21**, 189-202.

TACHIKAWA, K., JEANDEL, C. & ROY-BARMAN, M. (1999) A new approach to the Nd residence time in the ocean: the role of atmospheric inputs. *Earth and Planetary Science Letters*, **170**, 433-446.

TAIT, J. A., BACHTADSE, V., FRANKE, W. & SOFFEL, H. C. (1997) Geodynamic evolution of the European Variscan fold belt: paleomagnetic and geological constraints. *Geologische Rundschau*, **86**, 585-598.

TAIT, J., SCHÄTZ, M., BACHTADSE, V. & SOFFEL, H. (2000) Palaeomagnetism and Palaeozoic palaeogeography of Gondwana and European terranes. In: FRANKE, W., HAAK, V., ONCKEN, O. & TANNER, D. (eds), Orogenic Processes: Quantification and Modelling in

the Variscan Belt. *Geological Society, London, Special Publications*, **179**, 21-34.

TERMIER, H. (1936) Etude géologique sur le Maroc central et le Moyen Atlas septentrional. *Notes et Mémoires, Service Géologique du Maroc*, **33**, 1-1566.

TORSVIK, T. H. & SOMETHURST, M. A. (1989-1997) GMAP32 - Geographic Mapping and Reconstruction System (software package). *Geological Survey of Norway*.

TORSVIK, T. H., SMETHURST, M. A., MEERT, J. G. (1996) Continental break-up and collision in the Neoproterozoic and Palaeozoic: a tale of Baltica and Laurentia. *Earth-Science Reviews*, **40**, 229-258.

TOYODA, K. & TOKONAMI, M. (1990) Diffusion of rare earth elements in fish teeth from deep sea sediments. *Nature*, **345**, 607-609.

TROTTER, J. A., KORSCH, M. J., NICOLL, R. S. & WHITFORD, D. J. (1999) Sr isotopic variation in single conodont elements: implications for defining the Sr seawater curve. *Bollettino della Società Paleontologica Italiana*, **37**, 507-514.

TUCKER, M. E. (1974) Sedimentology of Palaeozoic pelagic limestones: the Devonian Griotte (Southern France) and Cephalopodenkalk (Germany). In: HSÜ, K. J. & JENKYNS, H. C. (eds), Pelagic Sediments: on Land and under the Sea. *Special Publications of the International Association of Sedimentologists*, **1**, 71-92.

VANCE, D. & BURTON, K. (1999) Neodymium isotopes in planktonic foraminifera: a record of the response of continental weathering and ocean circulation rates to climate change. *Earth and Planetary Science Letters*, **173**, 365-379.

VEIZER, J. (1985) Carbonates and ancient oceans: Isotopic and chemical record on time scales of 10^7 - 10^9 years. In: SUNDQUIST, E.T. & BROECKER, W.S. (eds), The Carbon Cycle and Atmospheric $CO_{2;}$ Natural Variations, Archean to Present. *Geophysical Monographs*, 595-601.

VEIZER, J. (1989) Strontium isotopes in seawater trough time. Annual Review of *Earth and Planetary Science Letters*, **17**, 141-167.

VEIZER, J. & COMPSTON, W. (1974) $^{87}Sr/^{86}Sr$ composition of seawater during the Phanerozoic. *Geochimica et Cosmochimica Acta*, **38**, 1461-1484.

VEIZER, J. & COMPSTON, W. (1976) $^{87}Sr/^{86}Sr$ in Precambrian carbonates as an index of crustal evolution. *Geochimica et Cosmochimica Acta*, **40**, 905-914.

VEIZER, J., BUHL, D., DIENER, A., EBNETH, S., PODLAHA, O. G., BRUCKSCHEN, P., JASPER, T., KORTE, Ch., SCHAAF, M., ALA, D. & AZMY, K. (1997) Strontium isotope stratigraphy: potential resolution and event correlation. *Palaeogeography, Palaeoclimatology, Palaeoecology*, **132**, 65-77.

VEIZER, J., ALA, D., AZMY, K., BRUCKSCHEN, P., BUHL, D., BRUHN, F., CARDEN, G. A. F., DIENER, A., EBNETH, S., GODDERIS, Y., JASPER, T., KORTE, Ch., PAWELLEK, F., PODLAHA, O. G. & STRAUSS, H. (1999) $^{87}Sr/^{86}Sr$, $\delta^{13}C$ and $\delta^{18}O$ evolution of Phanerozoic seawater. *Chemical Geology*, **161**, 59-88.

WENDT, J. (1985) Disintegration of the continental margin of northwestern Gondwana, Late Devonian of the eastern Anti-Atlas (Morocco). *Geology*, **13**, 815-818.

WENDT, J. (1988) Facies pattern and paleogeography of the Middle and Late Devonian in the eastern Anti-Atlas (Morocco). In: MCMILLAN, N. J., EMBRY, A. F. & GLASS, D. J.(eds), Devonian of the World, vol. I: Regional Syntheses. *Canadian Society of Petroleum Geologist, Memoir*, **14**, 467-480.

WENDT, J. (1991) Depositional and Structural Evolution of the Middle and Late Devonian on the Northwestern Margin of the Sahara Craton (Morocco, Alkgieria, Libya). In: SALEM, M. J., SBETA, A. M. & BAKBAK, M. R. (eds), *The Geology of Libya*, **6**, 2195-2210.

WENDT, J. (1993) Steep-sided carbonate mud mounds in the Middle Devonian of the eastern Anti-Atlas, Morocco. *Geological Magazine*, **130**, 69-83.

WENDT, J. (1995) Shell directions as a tool in palaeocurrent analysis. *Sedimentary Geology*, **95**, 161-186.

WENDT, J. & BELKA, Z. (1991) Age and depositional environment of Upper Devonian (early Frasnian to early Famennian) black shales and limestones (Kellwasser facies) in the eastern Anti-Atlas, Morocco. *Facies*, **25,** 51-90.

WENDT, J., KAUFMANN, B. & BELKA**,** Z**.** (2001) An exhumed Palaeozoic underwater scenery: the Visean mud mounds of the eastern Anti-Atlas (Morocco). *Sedimentary Geology*, **145**, 215-233.

WENZEL, B., LÈCUYER, C. & JOACHIMSKI, M.M. (2000) Comparing oxygen isotope record of Silurian calcite and phosphate - $\delta^{18}O$ compositions of brachiopods and conodonts. *Geochimica et Cosmochimica Acta*, **64**, 1859-1872.

WHITE, W.M. & PATCHETT, P.J. (1984) Hf-Nd-Sr and incompatible-element abundances in island arcs: implications for magma origins and crust-mantle evolution. *Earth and Planetary Science Letters*, **67**, 167-185.

WIEDERER, U., KÖNIGSHOF, P., FEIST, R., FRANKE, W. & DOUBLIER, M.P. (2002) Low-grade metamorphism in the Montagne Noire (S-France): Conodont Alteration Index (CAI) in Palaeozoic carbonates and implications for the exhumation of a hot metamorphic core complex. *Schweizerische Mineralogische, Petrographische Mitteilungen*, **82**, 393-407.

WIRTH, M. (1967) Zur Gliederung des höheren Paläozoikums (Givet-Namur) im Gebiet des Quinto-Real (West Pyrenäen) mit Hilfe von Conodonten. *Neues Jarbuch für Geologie und Paläontologie, Abhandlungen*, **127 (2)**, 179-224.

WITZKE, B.J. & HECKEL, P.H. (1988) Paleoclimatic indicators and inferred Devonian paleolatitudes of Euramerica. In: MCMILLAN, N.J., EMBRY, A.F. & GLASS, D.J.(eds), Devonian of the World, vol. I: Regional Syntheses. *Canadian Society of Petroleum Geologist, Memoir*, **14**, 49-63.

WICKMAN, F.E. (1948) Isotope ratios: a clue to the age of certain marine sediments. Journal of *Geology*, **56**, 61-66.

WRIGHT, J. (1990) Conodont geochemistry: A key to the Paleozoic. *Courier Forschungsinstitut Senckenberg*, **118**, 277-305.

WRIGHT, J., SEYMOUR, R.S. & SHAW, H.F. (1984) REE and Nd isotopes in conodont apatites: Variation with geological age and depositional environment. In: CLARCK, D. L.(ed.), Conodont Biofacies and Provincialism. *Geological Society of America, Special Papers*, **196**, 325-340

WRIGHT, J., SCHRADER, H. & HOLSER, W.T. (1987) Paleoredox variations in ancient oceans recorded by rare earth elements in fossil apatite. *Geochimica et Cosmochimica Acta*, **51**, 631-644.

Appendix

Table. 1. Register of localities.

Locality code	Locality	Coordinates	Conodont CAI	Country
AA	Afrou n'Akhou	N 30˚38'886 / W 5˚05'079	4	Morocco
AN	Ait ou Nebgui	N 30˚45'294 / W 4˚54'958	3.5-4	Morocco
AS	Jebel Amessoui	N 31˚01'359 / W 4˚17'238	4.5	Morocco
AZ	Azzel Matti	N 25˚37'735 / E 0˚55'915	1	Algeria
BF	Bou Ifarherioun W	N 31˚07'568 / W 4˚18'889	4	Morocco
BI	Bou Ifarherioun E	N 31˚07'738 / W 4˚17'555	4	Morocco
BK	Klucze	N 50˚20'000 / E 19˚33'750	2.5	Poland
BO	Boleslaw	N 50˚14'000 / E 19˚16'000	1	Poland
CO	Coumiac	N 43˚28'306 / E 3˚03'643	2.5	France
DU	Dule	N 50˚46'865 / E 21˚05'234	2	Poland
DZ	Dzikowiec	N 50˚34'253 / E 16˚34'830	2.5	Poland
EL	El Kahla	N 31˚08'162 / W 4˚13'873	4	Morocco
ER	Erfoud	N 31˚25'886 / W 4˚13'175	4	Morocco
GA	Galezice	N 50˚50'811 / E 20˚23'426	1.5	Poland
HB	Hassi Boulmane	N 30˚41'766 / W 4˚43'238	4	Morocco
HL	Hamar Laghdad	N 31˚22'663 / W 4˚02'952	4	Morocco
IH	Jebel Irhs 1	N 31˚15'706 / W 4˚22'349	4	Morocco
IN	Injar	N 31˚22'098 / W 3˚51'714	4-4.5	Morocco
IS	Jebel Irhs 2	N 31˚14'891 / W 4˚22'095	4	Morocco
IT	Irht n'Teslit	N 30˚54'293 / W4˚58'254	4.5	Morocco
JR	Jebel Rheris	N 31˚16'359 / W 4˚43'365	4.5-5	Morocco
JT	Jebel Tamamate	N 26˚14'886 / E 0˚46'934	1.5	Algeria
KA	Kadzielnia	N 50˚51'751 / E 20˚37'103	1.5	Poland
KO	Kowala	N 50˚47'257 / E 20˚33'783	1.5	Poland
LH	Lahmida	N 31˚30'670 / W 4˚19'262	3.5-4	Morocco
MI	Mech Irdane	N 31˚13'622 / W 4˚21'187	4	Morocco
MM	Madene el Mrakib	N 30˚44'158 / W 4˚42'794	4	Morocco
MR	Gara de Mrirt	N 33˚08'831 / W 5˚31'391	4.5-5	Morocco
MS	Mimsmarn	N 30˚53'614 / W 4˚58'190	4.5	Morocco
OC	Ouidane Chebbi	N 31˚14'324 / W 3˚48'254	4	Morocco
OJ	Oum el Jerane	N 30˚59'402 / W 4˚08'286	3.5	Morocco
OT	Otara	N 31˚08'288 / W 4˚22'317	4	Morocco
PO	Pomorzany	N 50˚17'330 / E 19˚20'000	2.5	Poland
RH	Rich Haroun	N 31˚19'864 / W 4˚10'825	4	Morocco
SO	Sosnowiec	N 50˚17'500 / E 19˚09'500	3-4	Poland
ST	Stokowka	N 50˚49'932 / E 20˚25'652	1.5	Poland
TA	Oued Talilit	N 31˚00'598 / W 4˚16'095	4.5	Morocco
TD	Tisserdimine	N 31˚16'929 / W 3˚58'825	4	Morocco
TG	Todowa Grzaba	N 50˚50'662 / E 20˚23'936	1.5	Poland

Locality code	Locality	Coordinates	Conodont CAI	Country
TH	Takkat ou el Heyene	N 31˚00'714 / W 4˚07'696	4	Morocco
TM	Taourirt Mouchane	N 30˚37'989 / W 4˚48'127	4	Morocco
TT	Tiouririne Toungaline	N 30˚37'826 / W 5˚01'397	4	Morocco
WB	Wolbrom	N 50˚23'000 / E 19˚45'000	2.5	Poland

Table 2. Taxonomic content and age of the samples.

Sample	Fossils	Taxonomic content	Age	Area
MI-0/1	conodonts	palmatolepids, ancyrodellids	Zone 8	Anti-Atlas
MI-1B	conodonts	ancyrodellids	Zone 8 - 11	Anti-Atlas
MI-1T	conodonts	bulk	Zone 11	Anti-Atlas
MI-2B	conodonts	ancyrodellids	Zone 11	Anti-Atlas
MI-3B	conodonts	ancyrodellids	Zone 11	Anti-Atlas
MI-3T	conodonts	ancyrodellids	Zone 11	Anti-Atlas
MI-4B	conodonts	bulk	Zone 13	Anti-Atlas
MI-4T	conodonts	ancyrodellids	Zone 13	Anti-Atlas
MI-5T	conodonts	bulk	Zone 13	Anti-Atlas
MI-7B	conodonts	bulk	Middle triangularis	Anti-Atlas
MI-7T	conodonts	palmatolepids, icriodids	Middle triangularis	Anti-Atlas
MI-8M	conodonts	palmatolepids	Middle triangularis	Anti-Atlas
MI-9B	conodonts	palmatolepids, ramiforms	Middle triangularis	Anti-Atlas
MI-9M	conodonts	palmatolepids, ramiforms	Upper triangularis	Anti-Atlas
MI- 9T	conodonts	palmatolepids	Upper triangularis	Anti-Atlas
MI-10B	conodonts	palmatolepids, ramiforms	Upper triangularis	Anti-Atlas
MI-10T	conodonts	palamatolepids	Lower crepida	Anti-Atlas
MI-11B	conodonts	palmatolepids	Uppermost crepida	Anti-Atlas
MI-11T	conodonts	palmatolepids	rhomboidea	Anti-Atlas
MI-12	conodonts	palmatolepids	rhomboidea	Anti-Atlas
MI-13	conodonts	palmatolepids	Lower marginifera	Anti-Atlas
MI-14	conodonts	bulk	Lower marginifera	Anti-Atlas
MI-15	conodonts	palmatolepids	Lower trachytera	Anti-Atlas
MI-16	conodonts	bulk	Lower - Upper trachytera	Anti-Atlas
MI-18	conodonts	bulk	postera - expansa	Anti-Atlas
AN-1	conodonts	bulk	Zone 7 - 11	Anti-Atlas
AN-2	conodonts	ancyrodellids	Zone 7 - 11	Anti-Atlas
AN-3	conodonts	bulk	Zone 11	Anti-Atlas
AN-4B	conodonts	ramiforms	Zone 11	Anti-Atlas
AN-4M	conodonts	ancyrodellids	Zone 11	Anti-Atlas
AN-4T	conodonts	bulk	Zone 11	Anti-Atlas
AN-5	conodonts	bulk	Zone 11	Anti-Atlas
AN-6	conodonts	bulk	Zone 11	Anti-Atlas

Sample	Fossils	Taxonomic content	Age	Area
AN-8	conodonts	ancyrodellids	Zone 11	Anti-Atlas
AN-8a	conodonts	ancyrodellids	Zone 11	Anti-Atlas
AN-9T	conodonts	ramiforms	Zone 11	Anti-Atlas
AN-10	conodonts	bulk	Zone 13	Anti-Atlas
AN-11	conodonts	ancyrodellids	Zone 13	Anti-Atlas
AN-12B	conodonts	ancyrodellids	Upper triangularis	Anti-Atlas
AN-12T	conodonts	palamtolepids	Uppermost crepida - rhomboidea	Anti-Atlas
AN-12T-1	conodonts	palmatolepids	Upper crepida	Anti-Atlas
AN-12T-2	conodonts	palmatolepids	Lower - Middle crepida	Anti-Atlas
AN-13B	conodonts	palmatolepids,some basal bodies	rhomboidea	Anti-Atlas
AN-14	conodonts	palmatolepids	rhomboidea	Anti-Atlas
LH-5	conodonts	bulk	Zone 6	Anti-Atlas
LH-6	conodonts	polignathids	Zone 11	Anti-Atlas
LH-7	conodonts	bulk	Zone 11	Anti-Atlas
LH-8	conodonts	bulk	Zone 11	Anti-Atlas
LH-9	conodonts	polignathids	Zone 11	Anti-Atlas
LH-10	conodonts	bulk	Zone 11	Anti-Atlas
LH-11	conodonts	bulk	Zone 11	Anti-Atlas
LH-12	conodonts	bulk	Zone 11	Anti-Atlas
LH-13	conodonts	bulk	Zone 11	Anti-Atlas
LH-14	conodonts	bulk	Zone 11	Anti-Atlas
LH-18	conodonts	bulk	Zone 13	Anti-Atlas
LH-19	conodonts	bulk	Zone 13	Anti-Atlas
LH-20	conodonts	bulk	Zone 13	Anti-Atlas
LH-21	conodonts	palmatolepids	Zone 13	Anti-Atlas
LH-22	conodonts	bulk	Zone 13	Anti-Atlas
LH-23	conodonts	ancyrodellids	Zone 13	Anti-Atlas
LH-24	conodonts	bulk	Zone 13	Anti-Atlas
LH-25	conodonts	palmatolepids	triangularis	Anti-Atlas
LH-26	conodonts	palmatolepids	triangularis	Anti-Atlas
LH-34	conodonts	bulk	crepida	Anti-Atlas
LH-38	conodonts	palmatolepids	Uppermost crepida	Anti-Atlas
LH-39	conodonts	icriodids, palmatolepids	Uppermost crepida	Anti-Atlas
LH-40	conodonts	palmatolepids	rhomboidea	Anti-Atlas
LH-43	conodonts	bulk	rhomboidea	Anti-Atlas
LH-44	conodonts	palmatolepids	rhomboidea	Anti-Atlas
LH-47	conodonts	ramiforms	rhomboidea	Anti-Atlas
LH-48	conodonts	polignathids	rhomboidea	Anti-Atlas
LH-49	conodonts	bulk	rhomboidea	Anti-Atlas
LH-50	conodonts	bulk	Lower marginifera	Anti-Atlas
LH-51	conodonts	bulk	Lower marginifera	Anti-Atlas
LH-52	conodonts	palmatolepids	Upper marginifera	Anti-Atlas
LH-56	conodonts	palmatolepids	expansa	Anti-Atlas
AA-3B	conodonts	bulk	Zone 11	Anti-Atlas
AS-2	conodonts	bulk	Zone 11	Anti-Atlas

Sample	Fossils	Taxonomic content	Age	Area
AS-3	conodonts	bulk	rhomboidea	Anti-Atlas
AZ-12	conodonts	polignathids	Zone 1 - 4	Algeria
BF-1	conodonts	bispathodids	expansa	Anti-Atlas
BF-2	conodonts	polignathids, icriodids	expansa	Anti-Atlas
BF-3	conodonts	bispathodids	expansa	Anti-Atlas
BI-1T	conodonts	bulk	Zone 11	Anti-Atlas
BI-2B	conodonts	bulk	Zone 11	Anti-Atlas
BI-2T	conodonts	palmatolepids	Uppermost crepida	Anti-Atlas
BI-B/3	conodonts	bulk	Lower marginifera	Anti-Atlas
EL-01	conodonts	ancyrodellids	Zone 10 - 11	Anti-Atlas
ER-1T	conodonts	bulk	Zone 11	Anti-Atlas
ER-2B	conodonts	bulk	Zone 11	Anti-Atlas
ER-2T	conodonts	bulk	Uppermost crepida	Anti-Atlas
ER-3B	conodonts	bulk	rhomboidea	Anti-Atlas
HL-2B	conodonts	ancyrodellids	Zone 11	Anti-Atlas
HL-2T	conodonts	palmatolepids, some basal bodies	Uppermost crepida	Anti-Atlas
IH-1B	conodonts	ancyrodellids	Zone 11	Anti-Atlas
IH-2B	conodonts	palmatolepids, icriodids	Uppermost crepida	Anti-Atlas
IN-8	conodonts	bulk	Zone 11	Anti-Atlas
IT-4B	conodonts	bulk	Zone 11	Anti-Atlas
JR-1	conodonts	bulk	Zone 11	Anti-Atlas
JT-20	conodonts	gnathodids	Visean	Algeria
MM-4B	conodonts	ramiforms	Zone 11	Anti-Atlas
OC-II-39	conodonts	bulk	Zone 6	Anti-Atlas
OJ-A	conodonts	bispathodids	expansa	Anti-Atlas
OJ-B	conodonts	bispathodids	expansa	Anti-Atlas
OJ-C	conodonts	bulk	expansa	Anti-Atlas
OH-1	conodonts	bulk	Zone 11	Anti-Atlas
OT-19	conodonts	bulk	Zone 13	Anti-Atlas
OT-23	conodonts	palmatolepids	Middle triangularis	Anti-Atlas
RH-5B	conodonts	bulk	Zone 11	Anti-Atlas
RH-5et	conodonts	palmatolepids	rhomboidea	Anti-Atlas
TH-2	conodonts	bulk	Zone 11	Anti-Atlas
TH-4	conodonts	palmatolepids	Uppermost crepida	Anti-Atlas
TM-7T	conodonts	bulk	Uppermost crepida	Anti-Atlas
MR-96	conodonts	palmatolepids	Zone 9 - 10	Moroccan Meseta
MR-97	conodonts	bulk	Zone 11	Moroccan Meseta
MR-98	conodonts	palmatolepids	Zone 11	Moroccan Meseta
MR-99	conodonts	bulk	Zone 11	Moroccan Meseta
MR-0	conodonts	bulk	Zone 11	Moroccan Meseta
MR-1T	conodonts	bulk	Zone 12	Moroccan Meseta
MR-2B	conodonts	bulk	Zone 12	Moroccan Meseta
MR-2T	conodonts	bulk	Zone 12	Moroccan Meseta
MR-3B	conodonts	bulk	Zone 13	Moroccan Meseta
MR-3M	conodonts	palmatolepids	Zone 13	Moroccan Meseta

Sample	Fossils	Taxonomic content	Age	Area
MR-3T	conodonts	bulk	Zone 13	Moroccan Meseta
MR-4A	conodonts	bulk	Zone 13	Moroccan Meseta
MR-4B	conodonts	bulk	Zone 13	Moroccan Meseta
MR-4C	conodonts	bulk	Lower triangularis	Moroccan Meseta
MR-5B	conodonts	palmatolepids	Lower triangularis	Moroccan Meseta
MR-5B2	conodonts	palmatolepids, icriodids	Lower triangularis	Moroccan Meseta
MR-5T	conodonts	bulk	Middle triangularis	Moroccan Meseta
DZ-2B	conodonts	bispathodids	Upper expansa - Lower praesulcata	southern Poland
DZ-22	conodonts	polignathids	Upper expansa - Lower praesulcata	southern Poland
KA-1	conodonts	bulk, basal bodies	Lower crepida	southern Poland
KA-2	conodonts	polignathids, palmatolepids, basal	Lower marginifera	southern Poland
KA-5	conodonts	palmatolepids, basal bodies	Lower marginifera	southern Poland
KA-6	conodonts	bulk, basal bodies	Lower marginifera	southern Poland
KA-7	conodonts	bulk, basal bodies	Lower marginifera	southern Poland
KA-8	conodonts	bulk, baal bodies	Lower marginifera	southern Poland
KO-3	conodonts	bulk	Lower marginifera	southern Poland
CO-21	conodonts	bulk	Zone 12	Montagne Noire
CO-23d	conodonts	bulk	Zone 12	Montagne Noire
CO-23e	conodonts	bulk	Zone 12	Montagne Noire
CO-24a	conodonts	ancyrodellids, ramiforms	Zone 12	Montagne Noire
CO-24b	conodonts	icriodids	Zone 13	Montagne Noire
CO-24d	conodonts	bulk	Zone 13	Montagne Noire
CO-24e	conodonts	bulk	Zone 13	Montagne Noire
CO-25a	conodonts	bulk	Zone 13	Montagne Noire
CO-25b	conodonts	palmatolepids	Zone 13	Montagne Noire
CO-26c	conodonts	palmatolepids	Zone 13	Montagne Noire
CO-27	conodonts	bulk	Zone 13	Montagne Noire
CO-28a	conodonts	bulk	Zone 13	Montagne Noire
CO-29a	conodonts	bulk	Zone 13	Montagne Noire
CO-29d	conodonts	bulk	Zone 13	Montagne Noire
CO-30a	conodonts	bulk	Zone 13	Montagne Noire
CO-31a	conodonts	bulk	Zone 13	Montagne Noire
CO-31c	conodonts	palmatolepids, ancyrodellids	Zone 13	Montagne Noire
CO-31e2	conodonts	ancyrodellids	Zone 13	Montagne Noire
CO-31f	conodonts	bulk	Zone 13	Montagne Noire
CO-31g	conodonts	bulk	Zone 13	Montagne Noire
CO-32a	conodonts	bulk	Lower triangularis	Montagne Noire
CO-32b	conodonts	bulk	Lower triangularis	Montagne Noire
CO-32d	conodonts	palmatolepids	Middle triangularis	Montagne Noire
CO-32f	conodonts	palmatolepids	Middle triangularis	Montagne Noire
CO34a	conodonts	bulk	Upper triangularis	Montagne Noire
CO-35b	conodonts	bulk	Upper triangularis	Montagne Noire
CO-35e	conodonts	palmatolepids	Upper triangularis	Montagne Noire
CO-36B	conodonts	palmatolepids	Upper triangularis	Montagne Noire
CO-36T	conodonts	palmatolepids	Upper triangularis	Montagne Noire

Sample	Fossils	Taxonomic content	Age	Area
CO-37aB	conodonts	bulk	Upper triangularis	Montagne Noire
CO-37bB	conodonts	bulk	Lower crepida	Montagne Noire
CO-37bT	conodonts	bulk	Lower crepida	Montagne Noire
CO-38B	conodonts	bulk	Middle crepida	Montagne Noire
CO-39T	conodonts	palmatolepids	Middle crepida	Montagne Noire
CO-40T	conodonts	palmatolepids	Upper crepida	Montagne Noire
CO-41	conodonts	palmatolepids	Upper crepida	Montagne Noire
CO-43B	conodonts	bulk	Upper crepida	Montagne Noire
CO-44	conodonts	bulk	Upper crepida	Montagne Noire
CO-46	conodonts	bulk	Upper crepida	Montagne Noire
CO-47	conodonts	bulk	Upper crepida	Montagne Noire
CO-49T	conodonts	bulk	Upper crepida	Montagne Noire
CO-51B	conodonts	palmatolepids	Uppermost crepida	Montagne Noire
CO-51T	conodonts	bulk	Uppermost crepida	Montagne Noire
CO-52	conodonts	palmatolepids	rhomboidea	Montagne Noire
CO-53	conodonts	bulk	rhomboidea	Montagne Noire
CO-56	conodonts	palmatolepids	rhomboidea	Montagne Noire
CO-24a	placoderms	----------	Zone 12	Montagne Noire
CO-35b	shark teeth	----------	Upper triangularis	Montagne Noire
CO-37aB	shark teeth	----------	Upper triangularis	Montagne Noire
CO-37bT	shark teeth	----------	Lower crepida	Montagne Noire
CO-38B	shark teeth	----------	Middle crepida	Montagne Noire
CO-39T	shark teeth	----------	Middle crepida	Montagne Noire
CO-40T	shark teeth	----------	Upper crepida	Montagne Noire
CO-41	shark teeth	----------	Upper crepida	Montagne Noire
CO-43B	shark teeth	----------	Upper crepida	Montagne Noire
CO-44	shark teeth	----------	Upper crepida	Montagne Noire
CO-47	shark teeth	----------	Upper crepida	Montagne Noire
CO-49T	shark teeth	----------	Upper crepida	Montagne Noire
CO-51T	shark teeth	----------	Uppermost crepida	Montagne Noire
MI-4B	placoderms	----------	Zone 13	Montagne Noire
KA-2	shark teeth	----------	Lower marginifera	southern Poland
KA-2	placoderms	----------	Lower marginifera	southern Poland
KA-5	shark teeth	----------	Lower marginifera	southern Poland
JT-20	shark teeth	----------	Visean	Algeria
EL-01	placoderms	----------	Zone 10 - 11	Anti-Atlas
BF-1	shark teeth	----------	expansa	Anti-Atlas
BF-2	placoderms	----------	expansa	Anti-Atlas

Table 3. Sm-Nd isotopic data of conodont samples from the Anti-Atlas, Moroccan Meseta and southern Poland.

Sample	Weight (mg)	Sm (ppm)	Nd (ppm)	$^{147}Sm/^{144}Nd$	$^{143}Nd/^{144}Nd$	$^{143}Nd/^{144}Nd$ (365 Ma)	ε_{Nd} (365 Ma)
Mech Irdane section							
MI-0/1*	5.94	42.9	137.8	0.1881	0.512153 ± 9	0.511704	-9.1
MI-1B	2.31	15.4	52.0	0.1794	0.512072 ± 10	0.511643	-10.2
MI-1T	1.60	16.2	45.6	0.2143	0.512165 ± 10	0.511656	-10.0
MI-2B	1.66	21.9	55.4	0.2388	0.512195 ± 10	0.511624	-10.6
MI-3B*	6.00	50.1	147.0	0.2059	0.512225 ± 8	0.511733	-8.5
MI-3T	2.87	9.8	31.1	0.1899	0.512124 ± 9	0.511670	-9.7
MI-4B	1.72	32.1	100.4	0.1932	0.512186 ± 10	0.511724	-8.7
MI-4T	1.93	15.1	57.5	0.1591	0.512078 ± 10	0.511698	-9.2
MI-5T	1.91	9.2	30.6	0.1823	0.512071 ± 10	0.511635	-10.4
MI-7B*	3.60	47.5	184.4	0.1557	0.512088 ± 11	0.511716	-8.8
MI-7T	2.07	34.0	114.0	0.1804	0.512129 ± 10	0.511697	-9.2
MI-8M	1.37	53.5	179.7	0.1799	0.512124 ± 8	0.511694	-9.2
MI-9B	1.41	48.9	159.2	0.1856	0.512122 ± 10	0.511678	-9.6
MI-9M	1.57	34.5	115.1	0.1813	0.512137 ± 9	0.511704	-9.1
MI- 9T*	3.08	75.9	286.4	0.1603	0.512094 ± 6	0.511711	-8.9
MI-10B	1.55	26.7	86.8	0.1860	0.512156 ± 10	0.511711	-8.9
MI-10T*	4.99	36.0	116.0	0.1874	0.512136 ± 8	0.511688	-9.4
MI-11B*	3.11	24.7	91.3	0.1635	0.512138 ± 8	0.511747	-8.2
MI-11T	6.39	19.1	64.9	0.1777	0.512168 ± 8	0.511743	-8.3
MI-12*	3.96	34.8	102.9	0.2044	0.512232 ± 8	0.511744	-8.3
MI-13*	5.06	15.0	45.9	0.1976	0.512220 ± 15	0.511748	-8.2
MI-14*	9.36	25.8	75.4	0.2069	0.512253 ± 8	0.511759	-8.0
MI-15*	3.05	32.6	79.1	0.2492	0.512264 ± 8	0.511669	-9.7
MI-16*	11.03	25.9	80.0	0.1957	0.512189 ± 7	0.511721	-8.7
MI-18	1.45	53.5	140.5	0.2230	0.512285 ± 10	0.511736	-8.4
Ait ou Nebgui section							
AN-1*	8.64	32.7	97.7	0.2025	0.512182 ± 7	0.511697	-9.2
AN-2 *	6.23	26.8	88.1	0.1839	0.512252 ± 10	0.511813	-6.9
AN-3	3.59	45.7	110.3	0.2506	0.512401 ± 12	0.511802	-7.1
AN-4B	2.36	28.5	102.7	0.1679	0.512205 ± 9	0.511804	-7.1
AN-4M*	6.39	27.9	106.2	0.1589	0.512132 ± 6	0.511752	-8.1
AN-4T	3.98	26.3	68.5	0.2318	0.512401 ± 11	0.511847	-6.3
AN-5*	2.23	37.4	72.8	0.3103	0.512772 ± 10	0.512031	-2.7
AN-6*	8.53	33.1	78.1	0.2558	0.512543 ± 9	0.511931	-4.6
AN-8*	7.01	23.4	73.0	0.1941	0.512366 ± 10	0.511902	-5.2
AN-8a*	6.01	23.6	81.1	0.1761	0.512148 ± 7	0.511727	-8.6
AN-9T	2.05	28.9	86.6	0.2015	0.512229 ± 10	0.511748	-8.2
AN-10*	8.10	30.5	90.2	0.2044	0.512203 ± 8	0.511715	-8.8

Sample	Weight (mg)	Sm (ppm)	Nd (ppm)	$^{147}Sm/^{144}Nd$	$^{143}Nd/^{144}Nd$	$^{143}Nd/^{144}Nd$ (365 Ma)	ε_{Nd} (365 Ma)
AN-11	3.80	26.3	97.5	0.1629	0.512138 ± 10	0.511749	-8.2
AN-12B*	3.44	20.9	96.9	0.1307	0.512050 ± 9	0.511738	-8.4
AN-12T*	3.62	37.5	115.2	0.1970	0.512221 ± 10	0.511750	-8.2
AN-12T-1	1.13	45.9	173.4	0.1598	0.512111 ± 10	0.511729	-8.6
AN-12T-2*	1.61	41.2	153.9	0.1618	0.512140 ± 9	0.511754	-8.1
AN-13B	1.90	154.7	501.0	0.1867	0.512181 ± 10	0.511735	-8.5
AN-14	1.86	78.9	272.0	0.1753	0.512137 ± 10	0.511718	-8.8
Lahmida section							
LH-5*	8.43	18.9	44.2	0.2588	0.512313 ± 12	0.511694	-9.2
LH-6*	9.15	24.3	83.3	0.1760	0.512134 ± 8	0.511714	-8.9
LH-7*	12.41	31.7	65.9	0.2906	0.512422 ± 9	0.511727	-8.6
LH-8*	1.03	34.3	78.1	0.2655	0.512481 ± 17	0.511846	-6.3
LH-9*	6.08	37.6	74.7	0.3041	0.512586 ± 10	0.511859	-6.0
LH-10*	11.46	24.2	55.1	0.2650	0.512335 ± 8	0.511701	-9.1
LH-11	3.11	33.7	43.5	0.4683	0.512806 ± 10	0.511687	-9.4
LH-12*	2.71	27.0	31.7	0.5153	0.512927 ± 9	0.511695	-9.2
LH-13*	9.02	29.4	86.4	0.2058	0.512281 ± 10	0.511789	-7.4
LH-14	6.80	24.1	28.9	0.5051	0.512898 ± 9	0.511691	-9.3
LH-18	1.14	59.2	143.9	0.2485	0.512226 ± 10	0.511632	-10.5
LH-19	1.20	49.1	77.4	0.3838	0.512659 ± 10	0.511741	-8.3
LH-20	2.25	24.1	32.5	0.4494	0.512648 ± 11	0.511574	-11.6
LH-21	2.12	17.7	25.5	0.4205	0.512619 ± 11	0.511614	-10.8
LH-22	2.00	18.3	37.5	0.2947	0.512403 ± 11	0.511698	-9.2
LH-23	3.68	19.4	59.6	0.1972	0.512274 ± 11	0.511803	-7.1
LH-24	3.89	25.0	59.6	0.2531	0.512219 ± 11	0.511614	-10.8
LH-25	2.36	41.9	83.1	0.3050	0.512411 ± 10	0.511682	-9.5
LH-26	2.86	23.3	57.9	0.2429	0.512308 ± 10	0.511728	-8.6
LH-34*	4.38	37.6	69.1	0.3294	0.512473 ± 8	0.511685	-9.4
LH-38	11.51	66.1	139.8	0.2856	0.512422 ± 12	0.511740	-8.4
LH-39*	5.91	27.7	34.7	0.4821	0.512813 ± 8	0.511661	-9.9
LH-40*	3.79	75.5	225.9	0.2021	0.512256 ± 6	0.511773	-7.7
LH-43	6.26	55.6	143.0	0.2348	0.512303 ± 11	0.511742	-8.3
LH-44	4.75	33.1	79.4	0.2518	0.512317 ± 13	0.511716	-8.8
LH-47	6.60	38.8	91.4	0.2566	0.512294 ± 10	0.511681	-9.5
LH-48*	2.68	28.7	50.6	0.3428	0.512531 ± 13	0.511712	-8.9
LH-49	4.69	38.8	63.1	0.3718	0.512539 ± 10	0.511650	-10.1
LH-50	1.76	23.7	40.2	0.3562	0.512494 ± 11	0.511643	-10.3
LH-51	1.85	26.5	50.8	0.3156	0.512413 ± 11	0.511659	-9.9
LH-52	7.40	37.6	74.3	0.3056	0.512387 ± 10	0.511657	-10.0
LH-56*	7.53	67.7	162.0	0.2528	0.512344 ± 9	0.511740	-8.4
other locations in the Anti-Atlas and Algeria							
AA-3B	6.29	9.0	31.2	0.1753	0.512091 ± 10	0.511672	-9.7
AS-2*	7.19	76.1	221.4	0.2079	0.512119 ± 9	0.511623	-10.6

Sample	Weight (mg)	Sm (ppm)	Nd (ppm)	$^{147}Sm/^{144}Nd$	$^{143}Nd/^{144}Nd$	$^{143}Nd/^{144}Nd$ (365 Ma)	ε_{Nd} (365 Ma)
AS-3*	10.64	26.1	91.2	0.1733	0.512119 ± 7	0.511705	-9.0
AZ-12	3.20	12.1	29.9	0.2440	0.512251 ± 10	0.511668	-9.8
BF-1	2.18	48.0	114.9	0.2525	0.512296 ± 9	0.511692	-9.3
BF-2*	6.45	29.6	81.0	0.2211	0.512220 ± 9	0.511691	-9.3
BF-3	2.62	42.3	94.6	0.2701	0.512197 ± 15	0.511552	-12.0
BI-1T	2.72	41.0	76.1	0.3255	0.512526 ± 11	0.511748	-8.2
BI-2B*	8.13	39.8	101.8	0.2363	0.512286 ± 10	0.511721	-8.7
BI-2T*	4.91	47.4	138.9	0.2065	0.512256 ± 7	0.511762	-7.9
BI-B/3	3.53	26.1	49.5	0.3185	0.512411 ± 22	0.511650	-10.1
EL-01*	4.82	42.3	123.8	0.2065	0.512176 ± 9	0.511682	-9.5
ER-1T*	8.19	22.6	43.3	0.3151	0.512508 ± 10	0.511755	-8.1
ER-2B*	6.15	30.3	77.9	0.2355	0.512316 ± 9	0.511753	-8.1
ER-2T	2.25	30.6	46.8	0.3948	0.512582 ± 13	0.511639	-10.3
ER-3B*	4.09	51.3	105.4	0.2944	0.512395 ± 11	0.511691	-9.3
HL-2B*	9.01	8.3	24.8	0.2033	0.512120 ± 9	0.511634	-10.4
HL-2T*	2.74	58.1	176.7	0.1987	0.512235 ± 8	0.511760	-8.0
IH-1B	6.55	26.2	73.5	0.2155	0.512231 ± 11	0.511715	-8.8
IH-2B*	5.32	18.1	57.0	0.1919	0.512225 ± 8	0.511766	-7.8
IN-8	2.94	38.6	65.0	0.3594	0.512644 ± 12	0.511785	-7.5
IT-4B	4.45	24.0	79.2	0.1836	0.512222 ± 11	0.511783	-7.5
JR-1*	7.80	24.8	83.8	0.1791	0.512069 ± 6	0.511641	-10.3
JT-20	3.18	41.4	131.1	0.1908	0.512134 ± 10	0.511678	-9.6
MM-4B	3.62	27.2	70.8	0.2327	0.512257 ± 12	0.511701	-9.1
OC-II-39	2.16	26.7	49.8	0.3240	0.512426 ± 10	0.511651	-10.1
OJ-A	3.55	24.3	57.4	0.2562	0.512231 ± 10	0.511618	-10.7
OJ-B	2.30	25.2	61.1	0.2495	0.512251 ± 10	0.511654	-10.0
OJ-C	2.77	19.5	49.4	0.2387	0.512246 ± 10	0.511675	-9.6
OH-1	5.89	16.6	40.5	0.2476	0.512241 ± 11	0.511649	-10.1
OT-19	1.41	36.3	131.0	0.1675	0.512115 ± 10	0.511715	-8.8
OT-23	0.90	60.9	165.7	0.2222	0.512220 ± 10	0.511689	-9.4
RH-5B	3.20	24.1	40.4	0.3614	0.512537 ± 13	0.511674	-9.6
RH-5et*	5.16	25.1	45.6	0.3332	0.512495 ± 8	0.511699	-9.2
TH-2*	7.13	34.7	70.5	0.2977	0.512309 ± 7	0.511598	-11.1
TH-4*	7.45	40.3	137.5	0.1770	0.512148 ± 8	0.511725	-8.6
TM-7T*	2.87	38.9	76.2	0.3085	0.512421 ± 9	0.511684	-9.4
Mrirt section							
MR-96*	5.08	38.1	133.0	0.1733	0.512303 ± 7	0.511889	-5.4
MR-97*	9.10	33.0	132.7	0.1504	0.512326 ± 8	0.511967	-3.9
MR-98*	7.94	48.1	153.0	0.1899	0.512491 ± 8	0.512037	-2.6
MR-99*	7.41	32.6	112.6	0.1751	0.512130 ± 12	0.511675	-8.9
MR-0*	6.62	33.8	115.9	0.1760	0.512128 ± 7	0.511708	-9.0
MR-1T	2.61	23.7	96.8	0.1480	0.512085 ± 10	0.511731	-8.5
MR-2B	1.79	40.6	131.5	0.1866	0.512137 ± 15	0.511691	-9.3
MR-2T	2.27	11.9	57.8	0.1242	0.512024 ± 10	0.511727	-8.6

Sample	Weight (mg)	Sm (ppm)	Nd (ppm)	$^{147}Sm/^{144}Nd$	$^{143}Nd/^{144}Nd$	$^{143}Nd/^{144}Nd$ (365 Ma)	ε_{Nd} (365 Ma)
MR-3B*	8.28	27.1	102.4	0.1598	0.512110 ± 8	0.511728	-8.6
MR-3M*	3.89	29.4	120.7	0.1475	0.512084 ± 12	0.511731	-8.5
MR-3T*	9.12	41.9	124.6	0.2034	0.512217 ± 8	0.511731	-8.5
MR-4A*	8.67	68.5	158.9	0.2606	0.512311 ± 9	0.511688	-9.4
MR-4B*	4.36	55.5	136.3	0.2459	0.512300 ± 7	0.511713	-8.9
MR-4C*	8.27	41.6	122.9	0.2046	0.512216 ± 8	0.511727	-8.6
MR-5B*	5.78	50.5	198.4	0.1534	0.512079 ± 9	0.511712	-8.9
MR-5B2*	5.37	59.8	235.2	0.1539	0.512073 ± 12	0.511705	-9.0
MR-5T*	6.06	33.6	140.6	0.1444	0.512053 ± 9	0.511708	-9.0
southern Poland							
DZ-2B	6.19	31.4	112.3	0.1689	0.512417 ± 12	0.512013	-3.0
DZ-22	9.93	35.6	135.4	0.1592	0.512293 ± 11	0.512290	-5.0
KA-1	1.48	55.1	234.4	0.1422	0.512103 ± 9	0.511763	-7.9
KA-2	1.57	61.8	273.4	0.1366	0.512090 ± 10	0.511764	-7.9
KA-5	1.55	77.1	313.8	0.1485	0.512072 ± 10	0.511992	-8.8
KA-6	1.65	70.0	283.6	0.1492	0.512117 ± 9	0.512037	-7.9
KA-7	1.45	77.8	295.7	0.1591	0.512160 ± 10	0.512183	-7.6
KA-8	4.15	80.6	317.6	0.1534	0.512153 ± 12	0.512150	-7.4
KO-3	1.66	46.2	198.2	0.1410	0.512082 ± 11	0.512074	-8.2

Errors:

For samples measured in Munich: $^{143}Nd/^{144}Nd < 1.1\times10^{-5}$ ($2\sigma_m$, within-run error), external precision $< 1.9\times10^{-5}$;

* For samples measured in Giessen: $^{143}Nd/^{144}Nd < 0.8\times10^{-5}$ ($2\sigma_m$, within-run error), external precision $< 1.6\times10^{-5}$

Table 4. Sm-Nd and Sr isotopic data of conodont samples from the Coumiac section.

Sample	Weight (mg)	Sm (ppm)	Nd (ppm)	$^{147}Sm/^{144}Nd$	$^{143}Nd/^{144}Nd$	$^{143}Nd/^{144}Nd$ (365 Ma)	ε_{Nd} (365 Ma)	$^{87}Sr/^{86}Sr$
CO-21*	12.78	20.0	65.1	0.1858	0.512172 ± 8	0.511728	-8.6	---
CO-23d*	7.43	15.8	45.5	0.2098	0.512224 ± 10	0.511723	-8.7	0.708094 ± 11
CO-23e*	7.30	12.6	45.3	0.1682	0.512162 ± 10	0.511760	-8.0	0.708896 ± 14
CO-24a*	6.64	40.3	140.1	0.1739	0.512150 ± 11	0.511734	-8.5	0.708111 ± 8
CO-24b*	7.38	78.7	222.1	0.2143	0.512209 ± 10	0.511697	-9.2	0.708146 ± 10
CO-24d*	5.31	24.4	64.5	0.2285	0.512230 ± 11	0.511684	-9.5	0.708130 ± 12
CO-24e*	3.98	21.6	51.9	0.2517	0.512273 ± 10	0.511671	-9.7	0.708102 ± 19
CO-25a*	3.85	13.8	47.0	0.1779	0.512166 ± 11	0.511741	-8.3	0.708101 ± 10
CO-25b*	4.55	17.1	57.2	0.1804	0.512176 ± 8	0.511745	-8.3	0.708199 ± 33
CO-26c*	7.92	13.3	38.9	0.2074	0.512219 ± 8	0.511724	-8.7	---
CO-27	9.86	15.3	45.7	0.2026	0.512271 ± 11	0.511787	-7.4	0.708170 ± 12
CO-28a	7.18	10.6	36.9	0.1742	0.512198 ± 13	0.511782	-7.5	0.708134 ± 13

Sample	Weight (mg)	Sm (ppm)	Nd (ppm)	$^{147}Sm/^{144}Nd$	$^{143}Nd/^{144}Nd$	$^{143}Nd/^{144}Nd$ (365 Ma)	ε_{Nd} (365 Ma)	$^{87}Sr/^{86}Sr$
CO-29a*	6.04	13.7	44.6	0.1852	0.512208 ± 9	0.511766	-7.9	0.708077 ± 9
CO-29d*	5.45	23.0	78.8	0.1762	0.512189 ± 6	0.511768	-7.8	0.708138 ± 11
CO-30a	3.52	18.8	62.2	0.1830	0.512178 ± 11	0.511740	-8.3	0.708082 ± 10
CO-31a	7.91	19.5	57.4	0.2052	0.512260 ± 10	0.511769	-7.8	0.708130 ± 10
CO-31c	6.94	18.8	56.0	0.2032	0.512267 ± 11	0.511781	-7.5	0.708106 ± 11
CO-31e2	8.46	19.7	58.0	0.2052	0.512281 ± 10	0.511790	-7.4	0.708133 ± 10
CO-31f*	7.05	28.5	93.2	0.1847	0.512153 ± 7	0.511711	-8.9	0.708117 ± 9
CO-31g*	3.29	30.0	72.6	0.2497	0.512300 ± 8	0.511703	-9.1	0.708107 ± 10
CO-32a*	1.49	40.0	131.7	0.1837	0.512185 ± 9	0.511746	-8.2	0.708155 ± 9
CO-32b*	3.60	24.0	85.2	0.1705	0.512124 ± 7	0.511717	-8.8	0.708142 ± 19
CO-32d*	7.34	54.2	154.5	0.2122	0.512205 ± 7	0.511697	-9.2	0.708175 ± 7
CO-32f*	3.11	49.4	121.0	0.2466	0.512251 ± 7	0.511661	-9.9	0.708178 ± 10
CO34a*	1.96	32.1	79.3	0.2445	0.512278 ± 10	0.511694	-9.3	0.708150 ± 9
CO-35b	4.22	49.2	129.8	0.2291	0.512233 ± 13	0.511685	-9.4	0.708174 ± 14
CO-35e*	4.16	50.4	114.5	0.2662	0.512314 ± 9	0.511678	-9.6	0.708186 ± 16
CO-36B*	4.00	53.9	119.6	0.2726	0.512318 ± 8	0.511666	-9.8	0.708180 ± 10
CO-36T*	3.14	64.3	151.4	0.2568	0.512289 ± 8	0.511676	-9.6	0.708200 ± 8
CO-37aB	3.54	85.8	202.6	0.2560	0.512291 ± 15	0.511679	-9.5	0.708238 ± 11
CO-37bB*	3.53	27.1	57.6	0.2839	0.512347 ± 9	0.511668	-9.8	0.708161 ± 9
CO-37bT	3.87	47.8	124.6	0.2318	0.512268 ± 16	0.511714	-8.9	0.708176 ± 10
CO-38B*	3.06	41.9	112.1	0.2258	0.512251 ± 9	0.511711	-8.9	0.708161 ± 20
CO-39T*	4.77	90.6	209.0	0.2621	0.512275 ± 8	0.511648	-10.1	0.708197 ± 8
CO-40T	2.18	63.0	153.9	0.2473	0.512282 ± 20	0.511691	-9.2	---
CO-41	4.48	53.3	123.9	0.2600	0.512340 ± 10	0.511719	-8.8	0.708226 ± 11
CO-43B	3.34	41.8	109.5	0.2308	0.512277 ± 18	0.511725	-8.6	0.708217 ± 10
CO-44*	3.87	44.4	105.9	0.2533	0.512275 ± 8	0.511669	-9.7	0.708191 ± 10
CO-46*	4.48	40.6	98.1	0.2502	0.512275 ± 8	0.511677	-9.6	0.708169 ± 8
CO-47	4.27	45.3	125.4	0.2185	0.512271 ± 10	0.511749	-8.2	0.708210 ± 11
CO-49T	1.73	36.6	91.1	0.2432	0.512255 ± 11	0.511674	-9.6	0.708217 ± 24
CO-51B	3.25	73.5	196.8	0.2258	0.512223 ± 10	0.511683	-9.5	0.708251 ± 21
CO-51T	3.94	30.4	79.0	0.2325	0.512287 ± 10	0.511732	-8.5	0.708230 ± 25
CO-52*	6.67	29.3	70.4	0.2522	0.512321 ± 7	0.511718	-8.8	---
CO-53*	5.08	35.6	98.3	0.2191	0.512262 ± 8	0.511739	-8.4	---
CO-56	3.60	49.6	138.6	0.2166	0.512218 ± 10	0.511700	-9.1	0.708260 ± 22

Errors:

For samples measured in Munich: $^{143}Nd/^{144}Nd < 1.1\times10^{-5}$ ($2\sigma_m$, within-run error), external precision $<1.9\times10^{-5}$;

* For samples measured in Giessen: $^{143}Nd/^{144}Nd < 0.8\times10^{-5}$ ($2\sigma_m$, within-run error), external precision $<1.6\times10^{-5}$ and $^{87}Sr/^{86}Sr < 1.6\times10^{-5}$ ($2\sigma_m$, within-run error), external precision 2.8×10^{-5}

Table 5. Sm-Nd and Sr isotopic data of fish remains (shark teeth, placoderms). Placoderm samples are marked (p).

Sample	Weight (mg)	Sm (ppm)	Nd (ppm)	$^{147}Sm/^{144}Nd$	$^{143}Nd/^{144}Nd$	$^{143}Nd/^{144}Nd$ (365 Ma)	ε_{Nd} (365 Ma)	$^{87}Sr/^{86}Sr$
CO-24a (p)*	0.90	616.8	2230.0	0.1672	0.512165 ± 8	0.511765	-7.9	----
CO-35b	0.39	527.4	1288.7	0.2474	0.512206 ± 12	0.511615	-10.8	0.708958 ± 74
CO-37aB	0.62	735.9	1654.2	0.2689	0.512308 ± 12	0.511665	-9.8	----
CO-37bT	0.48	546.5	1442.3	0.2291	0.512246 ± 16	0.511699	-9.2	0.709499 ± 10
CO-38B*	0.32	638.3	1824.5	0.2115	0.512179 ± 8	0.511673	-9.7	0.709348 ± 16
CO-39T*	0.27	822.5	1957.5	0.2540	0.512258 ± 8	0.511651	-10.1	----
CO-40T	0.24	876.8	2142.1	0.2475	0.512268 ± 10	0.511676	-9.4	0.709146 ± 25
CO-41	0.50	801.7	1885.9	0.2570	0.512305 ± 11	0.511691	-9.3	0.709128 ± 11
CO-43B	0.56	686.6	1762.9	0.2355	0.512219 ± 19	0.511656	-10.0	0.709085 ± 10
CO-44*	0.30	667.2	1752.6	0.2302	0.512189 ± 8	0.511639	-10.3	0.708859 ± 42
CO-47	0.27	520.0	1312.6	0.2395	0.512229 ± 11	0.511656	-10.0	0.708990 ± 14
CO-49T	0.55	588.3	1464.5	0.2428	0.512223 ± 11	0.511642	-10.3	0.709036 ± 54
CO-51T	0.58	461.6	1234.9	0.2260	0.512215 ± 10	0.511675	-9.6	0.709062 ± 42
MI-4B (p)	6.35	131.4	444.7	0.1787	0.512103 ± 13	0.511676	-9.6	----
KA-2	0.39	510.1	2320.2	0.1329	0.512073 ± 10	0.511755	-8.1	----
KA-2 (p)	1.79	419.5	1852.6	0.1369	0.512057 ± 9	0.511729	-8.6	----
KA-5	1.74	709.3	3016.8	0.1421	0.512055 ± 8	0.511715	-8.8	----
JT-20	0.56	590.9	1966.9	0.1816	0.512084 ± 11	0.511650	-10.1	----
EL-01(p)	1.26	160.4	618.0	0.1569	0.512123 ± 15	0.511748	-8.2	----
BF-1	0.41	492.9	1474.1	0.2022	0.512236 ± 9	0.511753	-8.1	----
BF-2 (p)	11.58	50.0	128.3	0.2356	0.512276 ± 10	0.512286	-8.9	----

Errors:

For samples measured in Munich: $^{143}Nd/^{144}Nd < 1.1\times10^{-5}$ ($2\sigma_m$, within-run error), external precision $<1.9\times10^{-5}$;

* For samples measured in Giessen: $^{143}Nd/^{144}Nd < 0.8\times10^{-5}$ ($2\sigma_m$, within-run error), external precision $<1.6\times10^{-5}$ and $^{87}Sr/^{86}Sr < 1.6\times10^{-5}$ ($2\sigma_m$, within-run error), external precision 2.8×10^{-5}

Table 6. Additional taxonomic, stratigraphic and isotopic (Sm-Nd) data of conodont samples from southern Poland and Anti-Atlas provided by Z. Belka, University of Halle.

Sample	Age	Taxonomic content	Conodont CAI	Sm (ppm)	Nd (ppm)	ε_{Nd} (360 Ma)
BK-1	Lower praesulcata	bulk	25	12.3	54.5	-3.7
BK-2	Lower expansa	bulk	25	15.1	65.1	-7.2
BO-1	anchoralis	bulk	1	8.5	38.0	-2.0
BO-2	crenulata	bulk	1	15.6	64.2	-4.2
BO-3	crenulata	bulk	1	11.4	47.2	-5.2

Sample	Age	Taxonomic content	Conodont CAI	Sm (ppm)	Nd (ppm)	ε_{Nd} (360 Ma)
BO-4	anchoralis	bulk	2	25.0	101.5	-1.8
DU-1	Upper marginifera	bulk	2	20.2	90.7	-7.1
GA-1	Lower postera/Upper postera	bulk	15	21.2	132.6	-4.4
GA-2/1	Middle expansa	palmatolepids	2	10.2	48.1	-5.1
GA-2/2	Middle expansa	polignathids	2	14.0	66.3	-5.0
GA-2/3	Middle expansa	bispathodids	2	11.4	53.0	-5.4
GA-2/4	Middle expansa	bulk	2	9.1	42.4	-5.1
GA-3/1	Lower expansa	polignathids	2	40.2	141.0	-4.1
GA-3/2	Lower expansa	bulk	2	60.3	220.0	-4.0
HB-3B/1	jamieae	ramiforms	4	22.3	70.1	-9.1
HB-3B/2	jamieae	icriodids	4	21.2	68.0	-8.9
IS-4B	Middle expansa	bulk	4	19.3	41.2	-10.8
KA-3/1	Upper crepida	palmatolepids	15	57.6	234.2	-9.2
KA-3/2	Upper crepida	palmatolepids	15	41.9	170.0	-9.5
KA-4/1	rhomboidea	polignathids	15	5.8	25.3	-8.1
KA-4/2	rhomboidea	palmatolepids	15	43.8	197.1	-8.2
MI-2B	winchelli	ancyrodellids	4	185	45.5	-10.1
MI-2B	winchelli	ramiforms	4	17.3	45.9	-10.2
MS-5B/1	jamieae	ramiforms	4	18.6	67.3	-8.6
MS-5B/2	jamieae	ramiforms	4	12.4	32.4	-1.0
MS-5B/3	jamieae	ancyrodellids	4	22.0	80.9	-8.4
MS-5B/4	jamieae	icriodids	4	26.7	97.1	-8.2
OT-29	Upper crepida	palmatolepids	4	90.9	245.5	-9.2
PO-1	Upper expansa	bulk, basal bodies	25	19.6	954	-3.3
PO-2/1	Lower expansa	bulk	25	8.6	34.9	-7.4
PO-2/2	Lower expansa	polignathids	25	12.7	49.9	-7.7
PO-2/3	Lower expansa	palmatolepids, basal bodies	25	179.0	690.0	-7.5
SO-1	anchoralis	bulk	35	66.0	265.1	-3.9
SO-2	anchoralis	bulk	35	16.8	72.8	-5.3
ST-1/1	Lower marginifera	bulk	2	26.2	95.3	-3.7
ST-1/2	Lower marginifera	palmatolepids, basal bodies	2	131.8	466.7	-3.8
ST-1/3	Lower marginifera	palmatolepids, basal bodies	2	57.5	213.6	-3.8
TA-8	Upper expansa/Lower praesulcata	bispathodids	45	17.2	37.7	-10.1
TG-1	Upper/Uppermost marginifera	palmatolepids, basal bodies	1.5-2	107.0	464.7	-7.6
TG-1M	Lower trachytera	bulk, basal bodies	1.5-2	184.4	816.0	-6.9
TG-2	Lower trachytera	palmatolepids, basal bodies	1.5-2	92.2	408.0	-7.6
TG-4	Lower trachytera	palmatolepids, basal bodies	1.5-2	67.4	290.4	-7.2
TG-5T	Lower trachytera	palmatolepids, basal bodies	1.5-2	106.2	464.8	-7.1
TG-6B	Upper trachytera	bulk, basal bodies	1.5-2	71.8	293.2	-4.6
TG-7	Upper trachytera/Lower postera	palmatolepids, basal bodies	1.5-2	84.5	378.2	-6.8
TG-9	Lower expansa	bulk, basal bodies	1.5-2	97.8	437.7	-6.2
TG-10	Lower expansa	palmatolepids, basal bodies	1.5-2	175.3	764.0	-6.8
TG-11	Lower expansa	palmatolepids, basal bodies	1.5-2	162.7	704.1	-6.3
TG-13	Lower/Middle expansa	bulk, basal bodies	1.5-2	75.5	329.6	-6.3
TG-25/1	anchoralis (?)	scaliognathids	15	35.0	138.6	-1.6
TG-25/2	anchoralis (?)	polignathids	15	24.7	97.2	-1.8

Sample	Age	Taxonomic content	Conodont CAI	Sm (ppm)	Nd (ppm)	ε_{Nd} (360 Ma)
TG-25/3	anchoralis (?)	polignathids	15	31.3	125.3	-1.6
TG-26/1	Lower praesulcata	palmatolepids	1.5-2	25.3	103.2	-3.3
TG-26/2	Lower praesulcata	bulk	1.5-2	13.6	56.7	-3.5
TG-26/3	Lower praesulcata	bispathodids	1.5-2	15.6	62.7	-3.3
TG-26/4	Lower praesulcata	bispathodids	1.5-2	16.0	63.7	-3.0
TM-7B/1	winchelli	icriodids	4	24.2	62.1	-6.1
TM-7B/2	winchelli	ancyrodellids	4	31.9	100.3	-5.6
TT-4T	Lower expansa	bispathodids	4	14.0	26.3	-10.5
WB-1	Middle expansa	bulk	25	6.6	27.1	-7.1

Table 7. Results of ICP-MS analysis of selected conodont samples. Concentrations are given in ppm.

Sample / Element	AN-8a	AN-12T-1	Coum 28a	Coum 31e2	K-M-Base	MI-3T	MI–12	MI-18	525-27	525-41
Na	5604	4823	5629	3711	10264	4350	5144	6737	7287	7750
Mg	369	461	471	149	431	463	501	390	390	638
Al	2152	1958	953	1502	744	3543	765	770	713	1393
K	260	230	278	733	195	242	82	166	176	145
Sc	<0.00	<0.001	0.07	<0.001	3	0.09	0.20	0.35	0.07	0.69
Cr	3	3	3	1	1	2	2	2	3	9
Mn	9	15	29	27	8	37	566	1771	37	352
Fe	3145	4055	2855	2784	1502	2477	2349	3138	1676	3129
Co	0.33	0.67	0.98	0.40	1	3	3	3	<0.001	1
Ni	14	8	9	<0.001	1	81	<0.001	24	<0.001	<0.001
Cu	<0.00	<0.001	<0.001	<0.001	<0.001	<0.001	<0.001	<0.001	<0.001	<0.001
Zn	785	<0.001	<0.001	<0.001	<0.001	82	<0.001	<0.001	<0.001	<0.001
As	30	35	46	12	3	14	3	8	<0.001	8
Sr	5106	5568	4714	3494	5850	4544	5842	5615	6313	5912
Y	57	64	80	73	217	52	54	130	204	174
Cd	7	<0.001	0.53	<0.001	0.69	0.55	0.47	0.14	<0.001	<0.001
Ba	<0.00	304	<0.001	<0.001	136	742	294	<0.001	2412	401
La	17	25	18	13	82	16	17	48	19	23
Ce	63	91	44	30	185	59	65	813	63	154
Pr	13	22	11	8	50	12	14	26	16	18
Nd	72	130	58	48	242	65	80	145	94	98
Sm	21	34	17	16	58	19	22	57	54	46
Eu	4	7	4	4	12	5	5	16	17	13
Gd	21	31	18	20	56	18	19	68	87	61
Tb	3	4	2	3	7	2	2	7	12	8
Dy	11	16	13	13	36	10	10	30	50	40
Ho	2	2	2	2	6	2	2	4	7	6
Er	3	4	5	4	13	3	3	7	13	11

Sample / Element	AN-8a	AN-12T-1	Coum 28a	Coum 31e2	K-M-Base	MI-3T	MI–12	MI-18	525-27	525-41
Tm	0.30	0.32	0.45	0.44	1	0.27	0.31	0.59	1	1
Yb	1	1	2	2	6	1	1	2	5	4
Lu	0.11	0.11	0.21	0.20	0.69	0.12	0.14	0.25	0.44	0.41
Pb	23	21	<0.001	<0.001	10	<0.001	<0.001	<0.001	<0.001	<0.001
Th	6	16	2	1	6	4	6	9	7	15
U	15	61	2	2	7	36	4	2	6	2